UiT The Arctic University of Norway

Faculty of Science and Technology

Department of Geosciences

The Mjølnir Impact Crater in the central Barents Sea – a potential hydrocarbon system?

Sindre A. Rein

Master thesis in geology, GEO-3900, May 2020

Abstract

A meteor impact event on the Bjameland Platform in the Norwegian Barents Sea about 142 ± 2.6 million years ago formed the Mjølnir Impact Crater. The structure has diameter of 40 km impacting the Mesozoic stratigraphy, and has previously been investigated with emphasis on the dynamics of the impact, the structure formation, sedimentation and post-impact tectonics. Impact structures have proven to be petroliferous elsewhere in the world. By applying new seismic 2D- and P-cable data and integrating prior studies, this thesis focuses on how the structure of the Mjølnir Impact Crater might represent a petroleum system in the Barents Sea.

The structural setting of the Mjølnir impact Crater shows several potential structural traps, including horst and graben structures within the crater, and listric rim faults at the periphery. A simplified 1D maturation model of potential source rocks in the area, indicate that the Hekkingen and Steinkobbe formations are sufficiently matured and have generated oil, while the Lower Triassic formations have generated gas. These source rocks may potentially charge the Mjølnir Impact Crater by petroleum migration vertically along deep-seated faults and laterally in the southward dipping stratigraphy, from the Nordkapp Basin area. The southern section of the Mjølnir Impact Crater is considered have the highest hydrocarbon potential, due to a thicker overburden and favorable migration pathways. Five seismic anomalies of high amplitude have been identified in the southern Mjølnir Impact Crater. These are interpreted to represent hydrocarbon accumulations, structurally trapped in horsts and by listric rim faults, and overlain by Upper Jurassic shales with sealing properties. Volumetric calculations for one of the amplitude anomalies suggest that 24,4 MMSm^3 of oil may be accumulated at the southern boundary of the crater.

In conclusion, presence of source rocks, migration pathways, reservoir and traps supported by observations of seismic amplitude anomalies suggests that the Mjølnir Impact Crater represents a potential hydrocarbon system.

Acknowledgements

Jeg ønsker først og fremst må jeg takke min hovelveileder Stig-Morten Knutsen og bi-veiledere Amando Lasabuda og Sondre Krogh Johansen for en veldig interresant oppgave som kombinerer både petroleum og meteorer. Jeg setter også stor pris på oppfølgingen jeg har fått underveis i prosessen, det hadde ikke gått uten!

Kjære studiekamerater, takk for at dere har klart å holde ut med meg i 5 år, det skal godt gjøres! Tusen takk for fine stunder og eksamensperioder, jeg har stortrivdes med dere, og vi holder selvsagt kontakten.

Contents

1 . Introduction

The Mjølnir Impact Crater is a large, semi-circular structural element on the Bjarmeland Platform in the central parts of the Norwegian Barents Sea. The crater has previously been investigated with focus on the morphology and modelling of the impact structure, especially in terms of dynamics of the impact, structure forming, sedimentation, and post-impact tectonics (e.g. Gudlaugsson, 1993; Dypvik et al., 1996; Dypvik et al., 2004; Dypvik et al., 2010d; Corseri et al., 2020). Globally, impact craters have been proven as successful hydrocarbon plays (Donofrio, 1998; Barton et al., 2009). The relationship between impact and associated structuring, and potential hydrocarbon systems is however complex and needs further investigations. During recent years the Mjølnir Impact Crater has been covered with a denser 2D seismic grid (chapter 4.1), with better quality than previous vintages. The crater was offered to the industry as acreage for the 24th concession round, and several oil and gas discoveries in the Barents Sea are found in the same stratigraphic units as influenced by the impact that caused the Mjølnir Impact Crater.

1.1 Objectives

The main objective of this thesis is to map the structural components, investigate the relationship between the structure of the crater and impact factors on a potential hydrocarbon system in the area around the Mjølnir Impact Crater. Integration with previous work will be an important part of the thesis.

2 Theoretical framework

2.1 The Mjølnir Impact Crater

The Mjølnir Impact Crater is a 40 km in diameter semi-circular complex structure hosted by the Bjarmeland Platform in the central Barents Sea at 73º48' N, 29º40' (Fig. 2.1). E. Gudlaugsson (1993) was the first to describe the structure and suggest that it was of impact-related origin. According to the Earth Impact Database (EID, 2019), the Mjølnir Impact Crater represents one of total 190 confirmed impact structures on Earth. The Mjølnir Impact Crater was first recognized in 1993, and later included in the Earth Impact Database of 1996, based on several impact-related characteristics (EID, 2019). Stratigraphically, the Mjølnir structure cuts into the Early Triassic to Earliest Cretaceous sedimentary strata. The timing of impact has been dated to coincide with the Volgian-Ryazanian boundary (i.e. 142 ± 2.6 Ma) in a marine shelf environment (300-400 m water depth). The impact crater is a cavity left by a 0.9-3 km in diameter bolide, weighing upwards of $10*10^{12}$ kg (Dypvik et al., 2010b). Previous studies of the Mjølnir structure include two shallow boreholes; one drilled ~30 km from the crater edge (7430/10-U-01) and one near the center (7329/03-U-01) (Fig. 2.1). From these shallow boreholes, the impact-related Ragnarok Formation and Sindre Bed were identified, and the timing of the impact was constrained (Dypvik et al., 2010c).

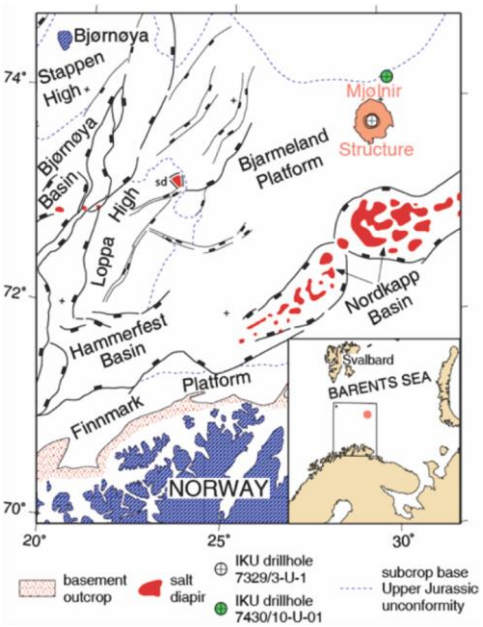

Figure 2.1: Location map of the Mjølnir Impact Crater. Also displays the location of well 7329/3-U-1 on the central peak and 7430/10-U-01 positioned 30-km northeast of the crater. Figure from Dypvik et al. (2010b)

2.2 Impact Craters

Impact craters are important phenomena when it comes to shaping the lithosphere of Earth and other planets (Dypvik et al., 2010b). The upper crust of Earth is a very dynamic system, which includes several processes that drastically changes its exterior on a geological timescale. These processes include weathering, erosion, volcanism and plate tectonics. The continuous changes these processes cause also apply to impact crater structures and subsequently, only few crater structures are preserved and discovered on Earth. If the crater density on the Earth surface is compared to that of the less disturbed Moon and Mars, it is significantly lower (Dypvik et al., 2010b).

2.2.1 The formation of impact craters

The impact of a bolide, moving many kilometers per second, on the surface of the earth initiates an orderly sequence of events that results in an impact crater (Melosh, 2013). Even though this is a continuous process, Melosh (2013) suggests that the creation of impact craters may be divided into three distinct stages, based on the dominating physical process; an initial contact and compression stage, a second stage characterized by excavation of the transient crater and lastly, a third stage involving modification of the crater itself. The three stages are however somewhat overlapping, and a clear distinction is hard to make.

2.2.1.1 The contact and compression stage

The initial contact and compression stage is the briefest of the three, lasting only a split second. During this stage, the incoming projectile first contacts the target surface, subsequently transferring its immense energy and momentum to the target rock. The projectile only travels a finite distance into the target before it decelerates completely and is destroyed primarily by melting and vaporization. The vast amount of energy transferred creates compressional shockwaves that propagate and attenuate in the target material and the projectile. As the shockwave moves upwards in the projectile, eventually reaching its top surface, pressure relief waves propagate downwards reaching the projectile-target interface, initiating the excavation stage. As the contact and compression stage terminates, vaporized and melted projectile and target material expands violently in a rising vapor plume. Condensates from the plume produces one of the most extensive sedimentary deposits linked to impact events (Melosh, 2013).

2.2.1.2 The excavation stage

The second excavation stage (Fig. 2.4) encompasses further opening and widening of the bowl-shaped cavity (transient cavity) from the initial contact and compression stage, through complex interaction between the created shockwave and the original ground surface. The shockwave expands with a roughly hemispherical wave front. As it propagates the energy attenuates and is spread over a larger volume of rock, degrading the shockwave into a plastic wave and subsequently an elastic wave. The shockwaves that initially travel upwards, intersect the surface, creating downwards-moving rarefaction waves. These rarefaction waves interfere with the shockwaves in the near-surface regions, creating an interference zone. The interaction between these two types of waves produce an excavation flow (Fig. 2.2), based on particle movement induced by the two waves. The effects of the excavation flow promote further partitioning of the target material: namely, an upper excavated zone and a lower displaced zone (Fig. 2.2). Material in the former zone is excavated from the cavity and ejected beyond the crater-rim and dumped as ejecta deposits (Osinski et al., 2013). The material in the lower displaced zone is accelerated downwards and outwards, along curved paths, establishing the base of the expanding cavity. The shockwave compression and the amplitude of excursion decreases with distance travelled in the target rock, and since the compression is irreversible it causes a net rise in temperature and particle velocity in the rocks (Kenkmann et al., 2013). The growth of the transient cavity also leads to a structural uplift of the crater rim (complex craters) and formation of interthrust wedges, due to horizontal compressive forces (Melosh, 2013). As the excavation stage terminates, the resulting transient cavity is typically 10 to 20 times the size of the projectile in diameter, as shown in Figure 2.4 (Kenkmann et al., 2013)**.** It is worth mentioning that the sub-surface flow-fields changes with the angle of impact and in this section only an ideal case scenario of a vertical impact is considered and discussed (Melosh, 2013).

It is during the excavation stage that one of the most characteristic impact depositional features is formed, namely the ejecta deposits. Ejecta deposits include all material that has been transported from the central transient cavity and beyond the rim of the impact structure. The ejecta deposits may either be classified as proximal or distal. The proximal ejecta deposits are deposited found in a radius of five crater radii from the impact point. The distal deposits are found outside this radius and may be spread globally, depending on the scale of the impact (Osinski et al., 2013). Melosh (2013) introduces another subcategory of the

proximal ejecta deposits, which he terms as continuous ejecta blanket. These deposits usually extend about one or two crater radii beyond the rim of the crater. The thickness of deposits is typically largest at the crater rim, and it decreases laterally.

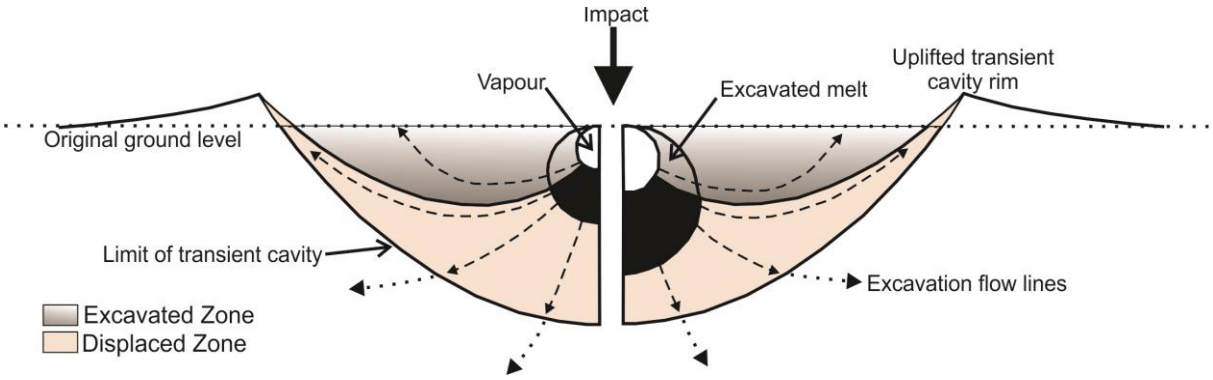

Figure 2.2: The figure shows a cross-section through a transient cavity in the excavation stage. Modified from Kenkmann et al. (2013)

2.2.1.3 The modification stage

The third modification stage encompasses processes that transform the transient cavity created in the excavation stage into the final crater form (Fig. 2.4). As opposed to the excavation flow, describing the target materials motion and deposition away from the point of impact, the modification flow is reversed, principally driven by gravitational effects, consequently closing the transient cavity to some degree. The onset of the modification stage is said to be when the transient cavity reaches its maximum horizontal extent at the target surface, and the flow direction reverses (Kenkmann et al., 2013). The extent to which the transient cavity is altered during this stage depends on its initial size, and the environment and properties of the target area. These variables open for a morphological subdivision of craters as either (1) simple or (2) complex. (1) Simple craters are simple bowl-shaped depressions with a well-defined raised crater rim. On Earth, simple craters reach a maximum diameter of 4 km in crystalline targets and 2-3 km in sedimentary targets. These ranges in maximum diameters thus represent the transition diameter from simple- to complex craters (Dypvik et al., 2010b). The alteration of these relatively small craters chiefly transpires through collapse of the crater walls (Kenkmann et al., 2013). (2) Craters of larger diameter display a more

complicated form and are known as complex craters (Fig 2.3). The most noteworthy difference between complex and simple impact craters is the characteristic uplifted crater floor found in complex craters. This may form a central uplift, a patchy distribution of hills and hummocks, a peak ring or a pan flat crater floor. These features are consequences of extensive gravity-driven collapse, originating from the deepest point of the transient cavity. The processes forming the central high in complex craters involves rebound of the crater floor and elevation of denser underlying strata (Tsikalas et al., 2010b). In large impact craters, the central uplift may grow large enough so that it becomes gravitationally unstable and subsequently collapse downward and outward, under its own weight (Kenkmann et al., 2013). During crater collapse, an outer concentric fault zone form. The faults in the fault zone often develop a listric shape, and possibly merge into low-angle detachments with depth in stratified targets (Kenkmann et al., 2013). The concentric faulting typically result in step-like terraces at the periphery of the crater (Tsikalas et al., 2010b).

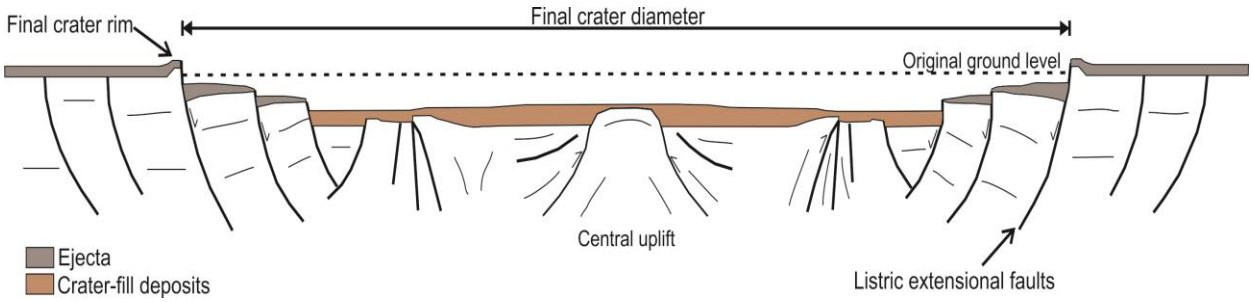

Figure 2.3: The figure shows a schematic cross-section of a complex crater. Modified from Kenkmann et al. (2013)

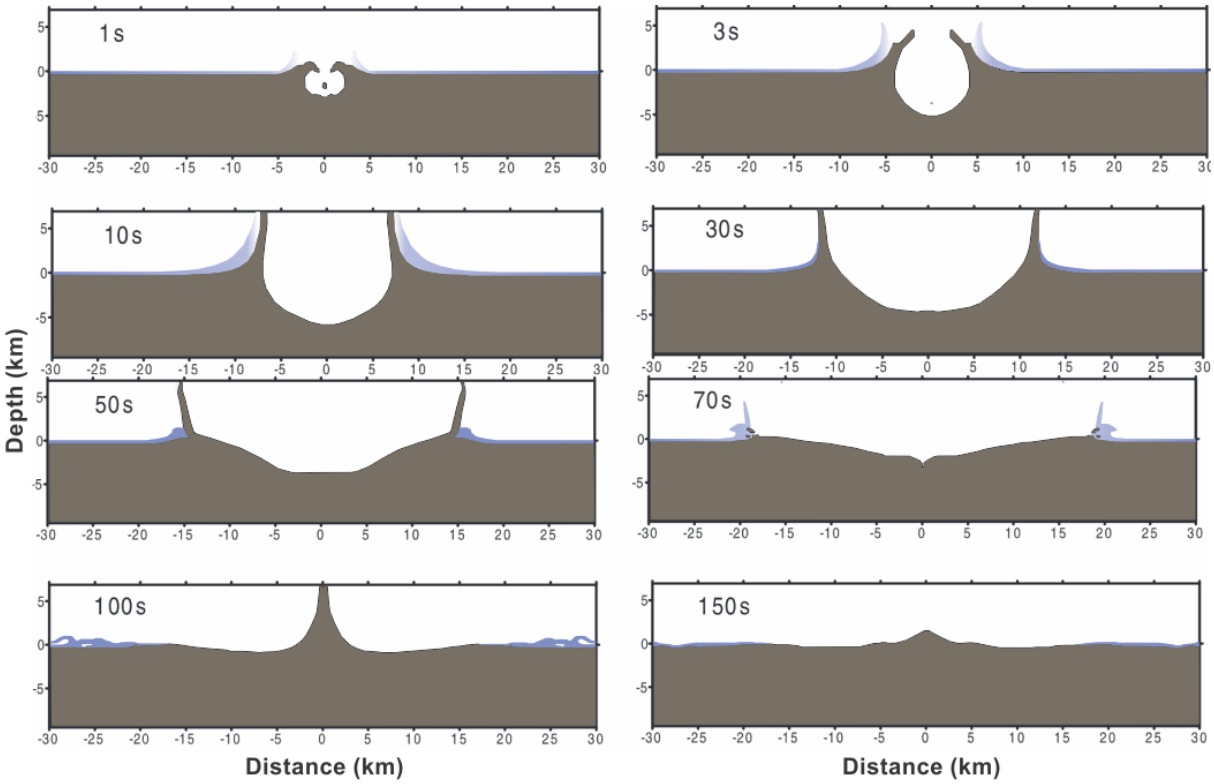

Figure 2.4: Hydrocode simulation of a vertical, marine impact. Illustrating the excavation stage (1-30s) and modification stage (30-150s) roughly, and the subsequent resurge of water. The model is based on a 1.6-km-diameter stony asteroid into a 400-metres-deep marine environment. Modified from Shuvalov et al. (2002)

2.2.2 Marine impacts

The three stages suggested by Melosh (2013) formerly described primarily include mechanisms involved in a subaerial impact. Previous studies have however showed that there are significant differences between impact craters formed on land and those formed in a marine environment (e.g Okeefe & Ahrens, 1982; Jansa, 1993; Dypvik et al., 2010c). The presence of water will influence the cratering processes significantly, based on the water depth in the target area, but also the water content in the sediments themselves. According to Shuvalov et al. (2010), numerical and experimental studies have shown that no underwater crater is formed if the ratio (d/h) between bolide diameter (d) the water depth (h) is below 0.1. If the d/h > 1 (i.e. the bolide diameter is larger than the water depth), the water column will have minor influence on the cratering process. The pore water content in target area sediments and rocks influence their rheological properties and consequently the formation of an impact crater. Lastly, the water will affect the final crater morphology and deposition of ejecta through post-impact effects (Shuvalov et al., 2010). Impacts in unconsolidated, water-covered sedimentary targets have shown a larger degree of collapse. During marine impacts a water cavity is formed, eventually leading to a backwash of water as the sea level is brought back to normal conditions. The backwash may lead to extensive infilling of the crater interior and erosion of the raised crater rim, and the creation of erosional features such as gullies (Dypvik et al., 2010c). Marine impact craters have higher preservation potential than their terrestrial equivalents, as post-impact sedimentation commence shortly after, covering the structure. The thickness of these post-impact sediments may eventually become substantial, leading to significant modification of the crater, both structurally and through deformation (Tsikalas et al., 2010b).

2.3 The petroleum system

The petroleum system is a unifying concept that includes all the essential elements, timing and processes required for accumulations of hydrocarbon to occur. The essential elements and processes include the following; (1) A pod of active source rock generating hydrocarbons, (2) a migration pathway through permeable layers and faults, (3) a reservoir rock with sufficient permeability and pore volumes for storing hydrocarbons, (4) a trap, (5) an impermeable sealing lithology and (6) overburden rock providing sufficient subsidence of the system (i.e. increased temperature and pressure). These elements and processes need to occur in a certain order in both time and space for there to be an accumulation of hydrocarbons (Magoon & Dow, 1994). Figure 2.5 summarizes the essential elements and processes in a petroleum system event chart. The chart provides a timeline and an ideal timely coincidence and fortuitous arrangement of the elements and processes.

A petroleum system is limited by its geographic, stratigraphic and temporal extent. The temporal aspect primarily includes the age, critical moment and preservation time of the petroleum system. The age of a system is the time it takes for the process of generation-migration-accumulation of hydrocarbons. The critical moment is the time that best portrays the process of generation-migration-accumulation of hydrocarbons in the given petroleum system. The preservation time stretches from the earliest generation of hydrocarbons and extends to the present day (Magoon & Dow, 1994). The lithological units encompassing essential elements for the petroleum system delimit its stratigraphic extent. Lastly, the geographic extent is determined at the critical moment and is defined by an outline of the active source rock, all hydrocarbon seeps, shows and accumulations (Magoon & Dow, 1994).

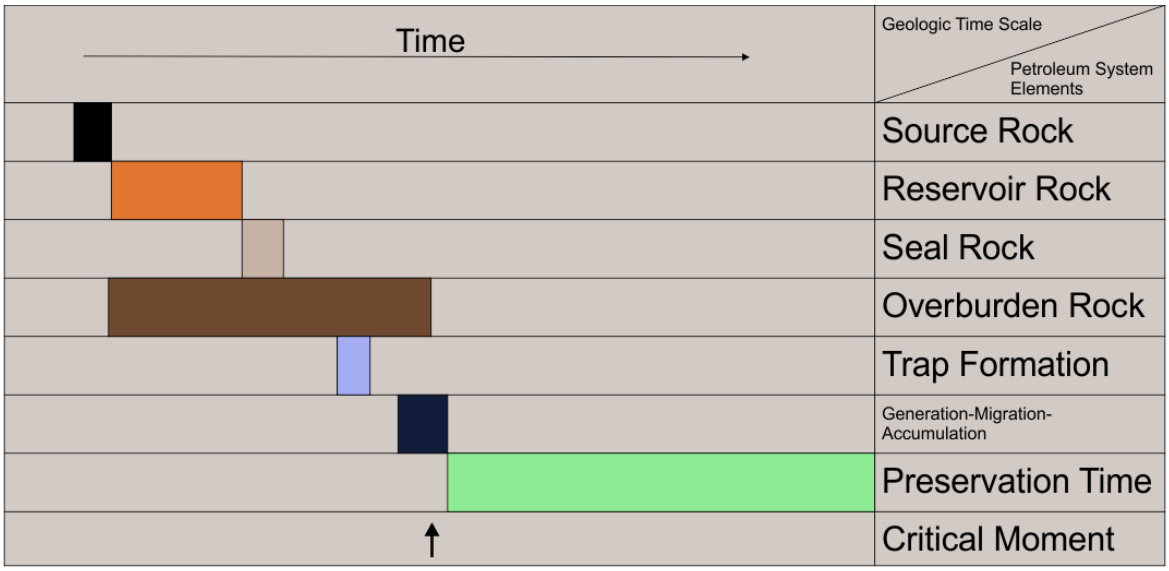

Figure 2.5: Petroleum system event chart showing when the essential elements and processes were deposited and occurred on a geologic time scale. Modified from Magoon and Dow (1994)

2.3.1 Source rock and generation of hydrocarbons

A petroleum source rock constitutes a high content of organic matter, capable of generating hydrocarbons, given the right conditions. When initially deposited the preservation of organic content in sediment is highly dependent on anaerobic bottom conditions and a rapid sedimentation rate. As the organic-rich sediment is buried with time, e.g. through basin infill, it is exposed to increased temperature and pressure. In the shallow subsurface, diagenesis occurs and the organic content transforms into kerogen, an insoluble organic matter. There are different types of kerogen, dependent on their depositional origin. The different types of kerogen are prone to generate oil, condensate or gas (Selley & Sonnenberg, 2015). Consecutive deposition of sediments in the basin leads to deep burial reaching depths of several thousand meters, exposing the kerogen to higher pressures and temperatures depending on the geothermal gradient in the basin. Eventually, the kerogen enters a phase called catagenesis, expelling petroleum as the kerogen is “cooked”. During catagnesis the kerogen generates oil first, at temperatures between 60 ^{o}C and 120 ^{o}C, and subsequently gas from 120 ^{o}C to 225 ^{o}C (Selley & Sonnenberg, 2015)

2.3.2 Migration

Migration may be subdivided into three types; primary, secondary and tertiary. Primary migration is understood as the emigration of petroleum from low permeability source rock into adjacent permeable beds, referred to as carrier beds. The mechanisms behind primary migration are considered to be one of the last mysteries within petroleum geology, and there is a lack of consensus to how it actually works (Bjørlykke, 2010; Selley & Sonnenberg, 2015). Secondary migration refers to subsequent movement of hydrocarbons through sufficiently permeable carrier beds and reservoirs. When oil and gas have accumulated in a given trap, it may leak and migrate into a higher trap or to the surface, this is termed tertiary migration (Bjørlykke, 2010).

2.3.3 Reservoir

One of the essentials prerequisites for a commercial accumulation of hydrocarbons to occur is the existence of a reservoir. In theory, any type of lithology may function as a reservoir for petroleum, provided there is a mature source rock charging, a trapping structure and a tight cap rock. In reality however, sandstones and carbonates have proven to store most major hydrocarbon accumulations. The quality of a given reservoir is predominantly determined by two essential properties; porosity and permeability. These properties closely relates to the lithology of the reservoir and its texture (Bjørlykke, 2010; Selley & Sonnenberg, 2015).

2.3.3.1 Porosity

Porosity is defined as the ratio between pore volume and bulk rock volume, that can be occupied by fluids (oil/gas/water) (Bjørlykke, 2010). A hydrocarbon reservoir relies on a specific type of porosity, namely effective porosity, meaning there needs to be communication between the pores throughout the rock, thus excluding isolated pores (Selley & Sonnenberg, 2015). Upon deposition, sedimentary rocks develop pore space between the primary grains, often referred to as the primary porosity. A reduction of the primary porosity occurs as the sediment is subsided and the combined effect of cementation and compaction sets in. The primary porosity and subsequent porosity loss highly depends on the lithology and the shape, size, sorting, packing and orientation of grains (Ehrenberg & Nadeau, 2005; Tiab & Donaldson, 2015). Different sediments generally display different initial porosities and rates of porosity loss with burial (Fig. 2.6). As overburden pressure and temperature increases the rock may also develop secondary porosity. Secondary or induced porosity may

develop due to chemical reactions such as dissolution of carbonates and silicate minerals or dolomitization (Bjørlykke, 2010). Structural failure and opening of joints, fissures and fractures in the reservoir rock constitutes another type of secondary porosity, namely fracture porosity (Tiab & Donaldson, 2015).

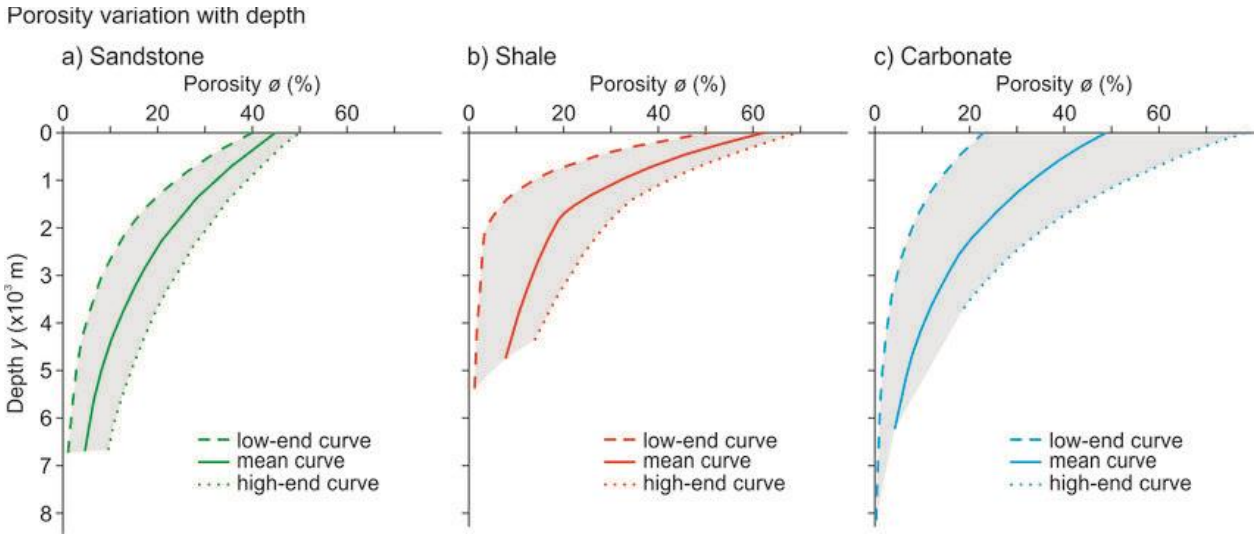

Figure 2.6: Plots of porosity variation with depth; a) sandstone, b) Shale, c) carbonate. Figure from Yeseul (2018).

2.3.3.2 Permeability

In addition to being porous, the reservoir rock also needs to be sufficiently permeable. It must have the ability to conduct fluids through the interconnected network of pores. The permeability of a rock depends on its effective porosity, meaning many of the properties discussed above also applies when discussing permeability. Other factors affecting the permeability include type of clay and cementing material between sand grains. Permeability is measured in Darcy (D) and often given in millidarcy (mD) in the petroleum industry. Most petroleum reservoirs globally are characterized by a permeability of <1 Darcy (Tiab & Donaldson, 2015).

2.3.4 Trap and seal

Trap and seal constitute two of the essential elements needed for an accumulation of petroleum to occur. A trap can be defined as a place where oil and gas are barred from further movement in the subsurface. This simplistic definition does however deserve some supplementation. A trap includes and highly depends on other elements in the petroleum system, which is underlying porous reservoir rock and an overlying impermeable sealing rock. These elements must form a structure that is closed at the top, so that petroleum may be

collected (Bjørlykke, 2010). Generally, the most common hydrocarbon traps can be classified as either structural, stratigraphic or combination traps, depending on their origin (Selley & Sonnenberg, 2015). Selley and Sonnenberg (2015) suggests a crude classification of hydrocarbon traps containing of five different types distinguished by their origin. (1) Structural traps caused by tectonic processes forming either anticlinal or fault traps. (2) Diapiric traps created by flow of ancient mud or salt deposits due to density differences, ultimately resulting in salt or mud diapirs. (3) Stratigraphic traps ultimately formed at the time of deposition or during diagenesis (e.g. pinch-out traps). The geometry of stratigraphic traps is a product of lithological changes in the subsurface. (4) Hydrodynamic traps rely on the movement of formation water to prevent the movement of oil or gas. (5) Combination traps are traps that contain elements from the previously discussed trap types.

2.4 Impact craters and petroleum systems

A collision between Earth and extraterrestrial objects may drastically alter the subsurface and the properties of the subsurface rocks in the target area. These alterations may include the creation or demise of essential elements in a petroleum system such as source rocks, reservoirs and traps (Barton et al., 2009). An impact structure in a marine environment, for instance, might generate a basin with anoxic conditions that are favorable for source rock development. This implies that an impact event could lay the foundation for a hydrocarbon system in a geological setting not considered petroliferous (Grieve, 1997). The effects of brecciation and fracturing may significantly enhance reservoir properties in the target rock (Barton et al., 2009). According to Tsikalas et al. (2010b) these effects may be more important in crystalline rocks, compared to impacts in sedimentary targets. Additionally, impacts may lead to listric-type faults in a geological setting previously dominated by homogeneous, horizontal sedimentary strata. Thus, establishing a trapping structure for oil and gas accumulations (Tsikalas et al., 2010b).

Hydrocarbon accumulations in an impact crater are categorized as epigenetic deposits, meaning they are a result of post-impact processes, more specifically fluid flow into the structural trap formed by the impact structure (Grieve, 1997; Barton et al., 2009). Currently, several impact craters around the globe has proven to be petroliferous. Several of these well-studied structures are located within the basins of North America - Red Wing Creek, Chicxulub, Ames and Avak structure to name a few (Donofrio, 1998, Table 2.1). Within the impact craters that have proven to be productive, the oil and gas has typically accumulated above and within the encircling rim anticlines and on the central uplift (Buthman, 1997). This makes Impact craters unique hydrocarbon structures, as there is a natural exploration and exploitation strategy derived from the typical location of hydrocarbon accumulations (Grieve, 1997). Impact craters in subsiding and uplifted environments, as for the Mjølnir Impact Crater, one also needs to consider the influence tilting and reorientation of the structure hold on the migration within the structure (Buthman, 1997).

Table 2.1: The table summarize information of 4 different petroliferous impact structures. Created from Donofrio (1998) and Tsikalas et al. (2010b).

Structure	Diameter	Geological Age	Reservoir rock	Reserves
Ames Oklahoma, USA	13 km	Early Ordovician	Granite, Carbonates	$3.97*10^6$ Sm^3 oil and $0.42*10^9$ Sm^3 gas
Avak Alaska, USA	12 km	Early/Late Cretaceous	Sandstone	$1.1*10^9$ Sm^3 Gas
Red Wing Creek North Dakota, USA	9 km	Triassic/Jurassic	Carbonates	$3.18*10^6$ Sm^3 oil and $0.71*10^9$ Sm^3
Chicxulub Yucatan Peninsula, Mexico	300 km	Cretaceous	Carbonates	$4.32*10^{12}$ Sm^3 oil and $3.2*10^{11}$ Sm^3

2.5 Seismic reflection theory

The key geophysical method for this study is the seismic reflection method. Seismic surveying is the most important group of geophysical methods for investigating and understanding the subsurface (Kearey et al., 2002). The method enables the identification of horizontal and vertical changes in the subsurface concerning lithology, tectonics and fluid contents within the pores of porous rocks. The collected and processes seismic data can be used to interpret different depositional environment tracts and specific paleo-events, such as the Mjølnir impact event.

An artificial, controlled source creates seismic waves that propagate through the subsurface strata. Some of these waves will be reflected and return to the surface and is recorded by geophones (on land) or hydrophones (offshore) commonly referred to as receivers. Reflected signals originate from geological boundaries, commonly between two stratigraphic layers, that show sufficient contrast in acoustic properties, referred to as reflectors. Every seismic layer in the subsurface has its own acoustic impedance (Z) which is a product of the internal wave velocity (V) and the density of the layer (ρ) (Equation 2.1) (Veeken, 2013).

Equation 2.1 acoustic impedance

$$Z = \rho V$$

Equation 2.1: The Acoustic impedance (Z) is a product of density (ρ) multiplied by the seismic wave velocity (V)

The contrast in acoustic impedance along a geological boundary determines the relative proportion of energy reflected, meaning a larger contrast will yield stronger reflected signals (i.e. higher amplitude). This is best quantified by the reflection coefficient (R), a numerical measure of how the impedance contrast between two layers effect wave propagation (Equation 2.2). The reflection coefficient is given between -1 to 1, where a negative value represents a reduction in acoustic impedance at a given boundary and vice versa for a positive value. A value of 1 or -1 indicates that all incident energy is reflected and a value of 0 indicates no reflected energy (Kearey et al., 2002).

Equation 2.2 reflection coefficient

$$R = \frac{Z_2 - Z_1}{Z_2 + Z_1}$$

Equation 2.2: The Reflection Coefficient (R) for a normal incident ray is determined by the difference contrast in acoustic impedance (Z). Z_1 and Z_2 are the acoustic impedance values of the layer above and below the boundary, respectively.

2.5.1 Seismic resolution

For any given seismic survey, there is a limit to the smallest feature or sedimentary layer that can be detected in the subsurface by a seismic wave. This is known as the resolution of the survey and represents one of the main restrictions of the reflection seismic method. The resolution of a seismic survey is comprised of both vertical and horizontal aspects and is highly dependent on the acquisition and processing of the data collected (Brown, 2004). The resolving power of seismic, concerning both aspects, is always measured in terms of the dominant seismic wavelength (λ). The seismic wavelength is derived from the velocity (V) of the seismic wave and its frequency (F), as shown in Equation 2.3 (Brown, 2004).

Equation 2.3 seismic wavelength

$$\lambda = \frac{V}{F}$$

Equation X.3: λ = Wavelength (m), V = Velocity (m/s), F = frequency (Hz)

The seismic velocity generally increases with depth due to increased compaction and diagenesis of the rocks. The dominant frequency of the seismic wave will decrease with depth, as the higher frequencies of the signal attenuate in the medium. Both these trends result in an increase seismic wavelength with depth as shown in Figure 2.7, making the resolution poorer (Brown, 2004).

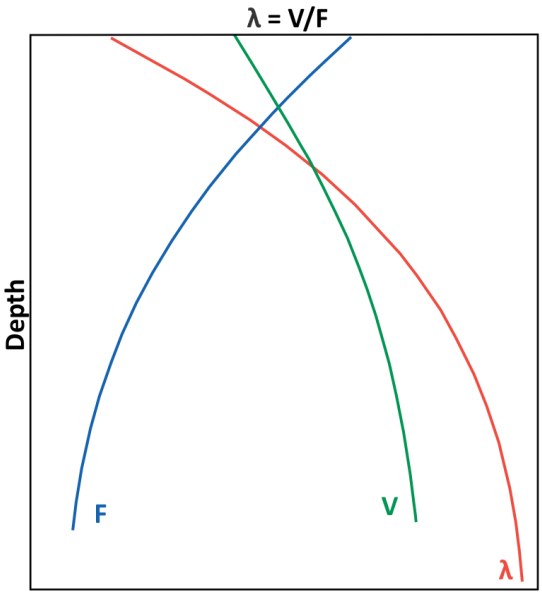

Figure 2.7: Relationship between seismic wavelength, velocity and frequency with depth. Modified from Brown (2004)

2.5.1.1 Vertical resolution

Vertical resolution is a measurement of the seismic surveys ability to distinguish individual, closely spaced reflectors (i.e. the top and the base of a unit) (Kearey et al., 2002). The vertical resolution has two limitations; the limit of separability and the limit of visibility both consequential from wavelet interaction from adjacent reflectors. The limit of separability represents the maximum resolution possible and is given as one-quarter of the dominant wavelength of a single pulse (Fig. 2.8) (Kearey et al., 2002; Brown, 2004). If the reflectors are too closely spaced together, the corresponding seismic reflections will give rise to interference patterns as they overlap in time. The interference may be constructive, giving rise to increased signal amplitudes. If it is destructive, it will decrease the amplitude of the signal (Veeken, 2013). If beds are thinner than this, the amplitudes are gradually attenuated until the limit of visibility is reached, and the reflection is obscured by background noise in the data (Brown, 2004).

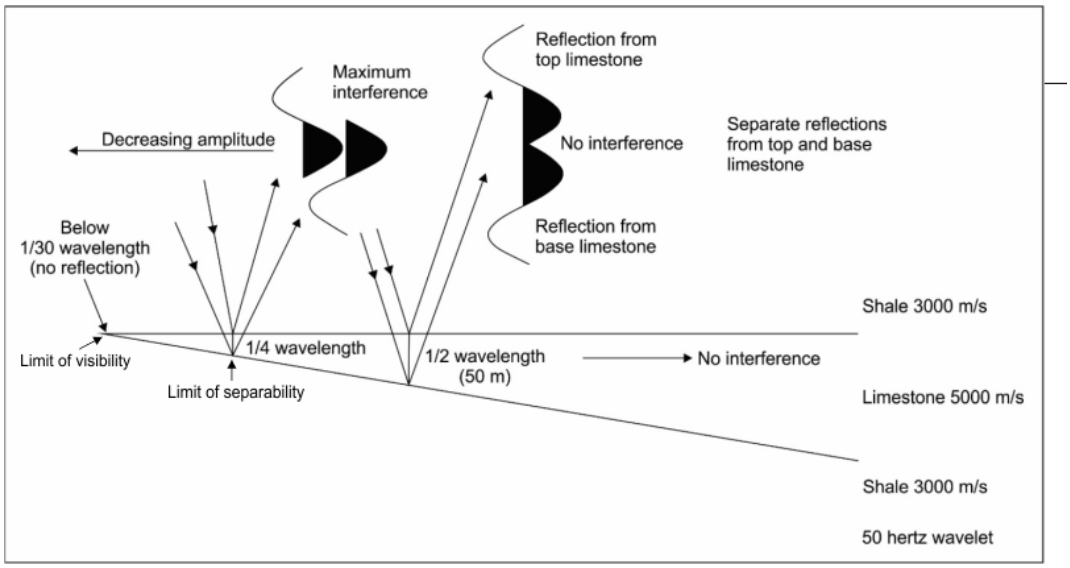

Figure 2.8: Vertical resolution and the effects of a high acoustic impedance wedge surrounded by lower acoustic impedance shale. Modified from Badley (1987)

2.5.1.2 Horizontal resolution

There are also horizontal limitations to any seismic reflection survey. Horizontal resolution is the ability of the seismic to distinguish the lateral extent of features and units (Badley, 1985). There are two primary controls on the horizontal aspect of the resolution, the first of which is determined by the trace spacing and the other being intrinsic to the physical properties of the reflection (Kearey et al., 2002). It is often helpful to visualize seismic reflections as rays originating from a single point in the subsurface. Actual reflections are however a result of interaction between a reflective boundary and the propagating spherical seismic wavefront. The extent of the circular zone that contributes to the reflected signal is termed the Fresnel Zone, representing the latter primary control of horizontal resolution. The size of the Fresnel Zone is dependent on the wavelength (i.e. frequency and velocity) of the signal and the depth of the reflector as the wavefront widens with depth (Veeken, 2013). When discussing horizontal resolution, it is important to consider both the pre- and post-migrated. The pre-migration Fresnel Zone (Equation 2.4) defines the horizontal resolution of pre-migrated data (Badley, 1985).

Equation 2.4 pre-migration Fresnel Zone

$$r_f = \frac{v}{2}\sqrt{\frac{t}{f}}$$

Equation 2.4: r_f = radius of the Fresnel Zone (m), v = average velocity (m/s), t = Two-way time (s), f = dominating frequency (Hz)

Seismic migration is a technique used to improve horizontal resolution through three separate functions; (1) focuses energy within the Fresnel Zone, (2) collapses diffractions from points and edges and (3) corrects for out-of-place reflections due to dip (Brown, 2004). When migrating data from 2-D seismic data, the Fresnel Zone will be reduced to and ellipse perpendicular to the survey direction (Fig. 2.9), thus reducing the lateral extension for a feature to be detected.

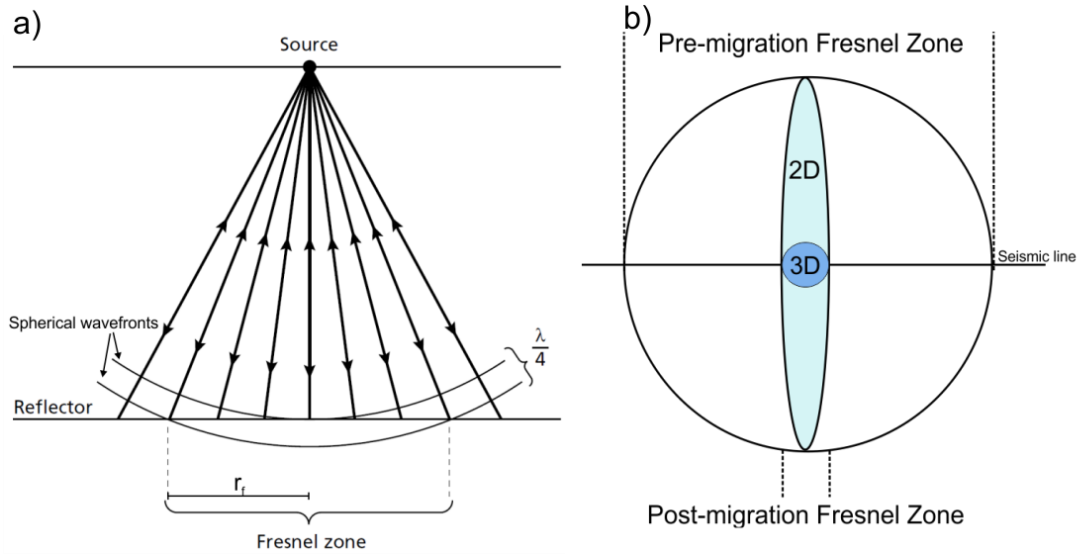

Figure 2.9: A) illustration of the Fresnel Zone. Modified from Kearey et al. (2002). B) illustration of how seismic migration decreases the Fresnel zone for 2D and 3D seismics. Modified from Brown (2004)

2.5.2 Direct hydrocarbon indicators (DHI)

When determining the petroleum potential of a basin, seismic indicators of hydrocarbons accumulations may prove to be very useful. The presence of free gas or oil in pore space of

reservoir rocks may have a drastic effect on seismic velocity, thus altering the acoustic impedance (Andreassen et al., 2007). These changes and subsequent seismic anomalies are termed Direct Hydrocarbon Indicators (DHI's). Seismic anomalies also include amplitude anomalies, which Løseth et al. (2009) define as a local decrease or increase of seismic reflection amplitude. Veeken (2007) suggests that a 5% hydrocarbon saturation is sufficient to generate DHI's. The potential DHI's may also be due to lithological changes in the subsurface, thus implying that one should be cautious when determining their validity (Veeken, 2007; Nanda, 2016).

Bright spots

Bright spots are recognizable by their localized anomalously high amplitudes caused by change in pore fluids. These strong reflections are often associated to the top and bottom of gas saturated sandstone reservoirs and a strong negative reflection coefficient (Kearey & Brooks, 2002). A negative reflection coefficient also implies that the reflected signal will have an opposing polarity to the seabed reflection. There are also examples of recognized light oil-induced bright spots, but these are not as common (Nanda, 2016).

Dim spots

in contrast to a bright spot, a dim spot represents a localized anomalously low amplitude with a positive reflection coefficient. Dim spots are often associated with gas saturated carbonate reservoirs, but may also occur in sandy reservoirs (Nanda, 2016). It is however worth mentioning that amplitude strength of reflections is also caused by lateral thickness changes (tuning effect) and lithological changes (Veeken, 2007).

Flat spots

Flat spots are sub-horizontal events with a positive reflection coefficient that are discordant to the adjacent reflectors (Kearey & Brooks, 2002; Andreassen et al., 2007). Flat spots represent the acoustic impedance changes caused by a fluid contact in a reservoir and they are unique in the sense that the reflection is not related to lithology. Most commonly flat spots represent a gas/water (GWC) or gas/oil contact (GOC), but may also represent an oil/water contact (OWC) under favorable conditions (Veeken, 2007).

Other possible DHI's include pull-down effects, polarity reversal, chimney structures and amplitude shut-off (Veeken, 2007; Nanda, 2016).

3 Geological background

3.1 Regional geology of the Barents Sea Shelf

The Barents Sea Shelf is located in an intracratonic setting in the northwestern parts of the Eurasian plate (Fig. 3.1) (NPD, 2014). It covers an area of approximately 1.3 million km^2, with water depths seldom exceeding 500 m, making it one of the largest areas of continental shelf in the world. It is roughly delimited by the deeper waters of the Norwegian-Greenland Sea to the east, the mainland of both Russia and Norway to the south, the Svalbard archipelagos and Franz Josef Land to the north and Novaya Zemlya to the east (Worsley, 2008; Smelror et al., 2009; Henriksen et al., 2011b). The western and eastern part of the southern Norwegian Barents Sea Shelf show a noticeable difference in time, trend and magnitude of stratigraphic and tectonic development. The boundary between the western margin and the eastern platform is defined by the dominantly north-south to northeast-southwest oriented Ringvassøya-, Loppa- and Bjørnøyrenna fault complexes (NPD, 2014). The western margin is characterized by tectonic activity throughout the Mesozoic and Cenozoic era, and as a result thick sedimentary packages was deposited through the Cretaceous, Paleogene and Neogene in the Tromsø-, Harstad-, and Bjørnøya basins (Faleide et al., 1984). In contrast, the area east of this boundary has been dominated by relatively stable platforms and less profound tectonic activity since the Carboniferous. Stratigraphically it is characterized by thick upper Paleozoic and Mesozoic sequences (Gabrielsen et al., 1990; Smelror et al., 2009; NPD, 2014).

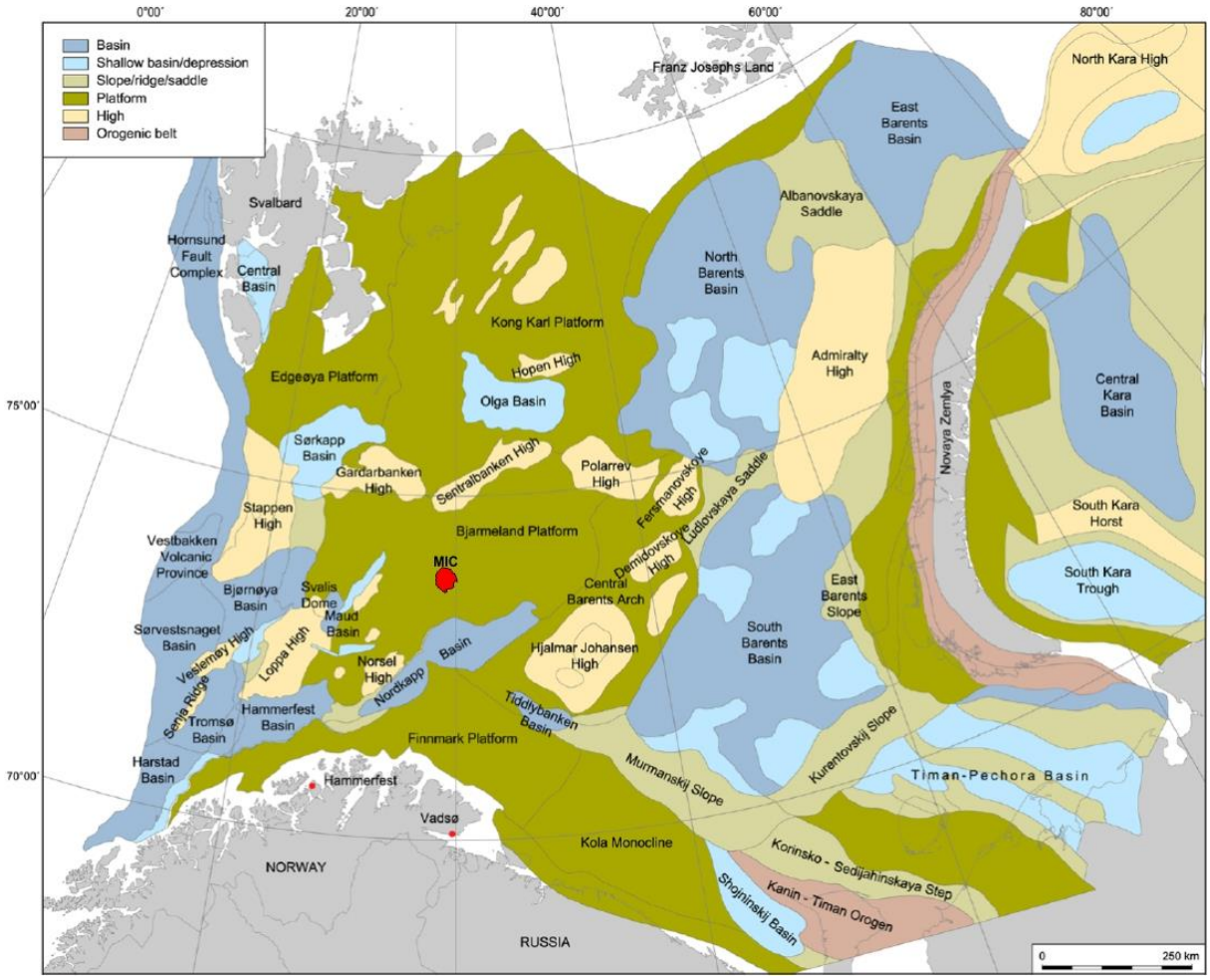

Figure 3.1: The figure shows the structural elements of the greater Barents Sea. The Mjølnir Impact Crater (MIC) is shown in red. Figure modified from Henriksen et al. (2011b)

3.2 Structural and stratigraphic development of the Barents Sea Shelf

The Barents Sea Shelf has been affected by several orogenies, episodes of severe subsidence and young continental break-up (Klitzke et al., 2015). Three orogenies have played a major role for the geological development of the Barents Sea region: the Timanian-, Caledonian- and Uralian Orogeny. Furthermore, the region has been affected by the proto- Atlantic rifting in the west, the opening of the Euramerican Basin in the north and the opening of the Northern Atlantic Ocean in the western margin (Faleide et al., 2008; Smelror et al., 2009). This post-Caledonian geological development is dominated by three rift phases comprised of several tectonic pulses, late Devonian?-Carboniferous, Middle Jurassic-Early Cretaceous and Early Paleogene (Faleide et al., 1993). It has been suggested that most of the major structural trends of the Barents Sea Shelf was established by Devonian times, and this influenced the

subsequent structural development and depositional environments of the region (Gabrielsen et al., 1990; Faleide et al., 1993; Gernigon et al., 2014). Lastly, the region has been subjected to a varying degree of tectonic uplift, glaciation and erosion from the Early Cretaceous to the Holocene (Vorren et al., 1991; Faleide et al., 1996; Smelror et al., 2009; Lasabuda et al., 2018b).

The term "top basement" represents the boundary between the older underlying crystalline rock and the sedimentary load above, thus representing the base of the basins in the Barents Sea (Smelror et al., 2009). The depth of top basement differs greatly when comparing the western and eastern Barents Sea. In the western Barents Sea, the sedimentary package generally tends to be thinner compared to the eastern provinces. On the western platforms the succession is generally about 6 km thick (Smelror et al., 2009). The general trend for the paleoenvironment and resulting stratigraphy reflects a climatic shift from humid, tropic conditions in the Devonian-Carboniferous to a higher latitude climate in Paleogene and Neogene (Worsley, 2008; Henriksen et al., 2011b; Ryseth, 2014). These large scale changes induced by plate movement were also accompanied by several minor tectonic events and regional sea-level variations have further defined the sequences (Worsley, 2008; Smelror et al., 2009). The following sections will present a chronological overview of the structural and stratigraphic development with an emphasis on the eastern parts of the Norwegian sector of the Barents Sea.

3.2.1 Paleozoic (542-251 Ma)

3.2.1.1 Structural development

The history of the crystalline basement rock in the western Barents Sea is closely linked to the Caledonian Orogeny. In the Early Ordovician to the Early Devonian the Caledonian Orogeny took place, where Laurentia and Baltica collided resulting in the closing of the Iapetus Ocean and creation of the Laurasian continent ("The Old Red Continent"). (Smelror et al., 2009). Following the Caledonian Orogeny, the late Paleozoic crustal extension formed a fan-shaped array of half grabens, followed by a widespread tectonic quiet period (sag phase). The sag phase was most likely related to the closure of the Uralian Ocean (Uralian Orogeny) in Baltica to the east.

3.2.1.2 Depositional development and stratigraphy

Ordovician to Devonian strata are yet to be discovered in the Norwegian sector of the Barents Sea. Such successions have however been proven subaerial on adjacent landmasses (Finnmark County and Svalbard) (Henriksen et al., 2011b). During this period, the Caledonian Orogen covered most of the western Barents Sea. As erosion continued to affect the Caledonides, a delta system developed and prograded towards the east (Henriksen et al., 2011b). Entering early Moscovian time, the continental landscape of the western Barents Sea was transgressed, and warm water carbonate shelf conditions dominated along with deposition of evaporites, particularly in the western basins (Henriksen et al., 2011b). Entering the early Permian, platform carbonates of the Gipsdalen Group (Fig 3.2) dominated the Bjarmeland and Finnmark platforms (Larssen et al., 2002). During the Early Permian, the Barents Sea saw drastic changes in the marine circulation system due to the opening of a new seaway. This oceanographic change lead to cool sea water flowing across the shelf and a transition to cool water carbonates represented by the Bjarmeland- and Tempelfjorden groups (Fig 3.2) dominating the Bjarmeland Platform (Stemmerik & Worsley, 2005). The end of carbonate platform dominance in the Barents area is marked by the deposition of marine black spiculitic shales of Late Permian age (Larssen et al., 2002; Henriksen et al., 2011b).

3.2.2 Mesozoic (541-251 Ma)

3.2.2.1 Structural development

The Early Mesozoic is considered to be a tectonically quiet period in the western Barents Sea, characterized by a passive regional subsidence (Riis et al., 2008; Glørstad-Clark et al., 2010; Lundschien et al., 2014). There are observations of minor movements on the Bjarmeland and Finnmark platforms and active faulting on the Loppa High (Smelror et al., 2009; Henriksen et al., 2011b), causing the Loppa High and possibly parts of the Bjarmeland Platform to be uplifted and eroded in the Early Triassic (Smelror et al., 2009). The stratigraphic transition between Perm and Triassic forms a regional unconformity in the Barents region, where the uppermost Permian succession is partly eroded (Worsley, 2008; Henriksen et al., 2011b). The general regional subsidence during the Triassic resulted in a succession exceeding 2500m in thickness across the Norwegian sector, where the Uralian highlands and the Baltic shield acted as an important source of sediment (Riis et al., 2008; Henriksen et al., 2011b).

Halokinetic movement of Late Paleozoic salt was initiated in the Nordkapp- and Maud basins during the Triassic. Subsequently, a series of growth phases occurred, with the main diapiric phase occurring in the Late Cretaceous in the Maud Basin (Gabrielsen et al., 1990; Henriksen et al., 2011b).

The Barents region experienced increased tectonic activity starting in the Middle Jurassic, terminating in the Early Cretaceous. This rifting phase produced the final and present day structural configuration of well-known basins and highs in the Barents Sea (Gabrielsen et al., 1990; Henriksen et al., 2011b). In the transition from the Jurassic to the Cretaceous (142 ± 2.6 Ma) (Smelror et al., 2001), the stable Bjarmeland Platform saw the cataclysmic impact that formed the Mjølnir Impact Crater. This event may have caused short-term catastrophic consequences over a large area and a long-term effect on the regional depositional environment (Smelror et al., 2002; Worsley, 2008).

3.2.2.2 Depositional development and stratigraphy

The stratigraphic units of Triassic age were deposited in a tectonically quiet period in the Barents Sea. The regionally subsiding Barents region received sediments from the uplifted areas towards the east (Urals) and south (Fennoscandian Shield). The region saw a north/northwestward prograding shoreline, and deposition in the Finnmark Platform, Hammerfest- and Nordkapp basins (Klausen et al., 2018b). Large parts of the Norwegian Barents Sea was dominated by delta and shallow-marine shelf conditions(Klausen et al., 2015), and locally subaerially exposed highs (Worsley, 2008). The Sassendalen Group and Storfjorden Subgroup (Fig 3.2) deposited in the Triassic era include formations that all correspond to Arctic regional regressive-transgressive cycles (Mørk et al., 1989; Lundschien et al., 2014). This is indicative of large regional sea-level changes throughout the stages. It has been suggested that the progradation of the coastline reached its maximum in the Carnian. At this point in time, the Barents shelf represented the largest delta plain in earth's history, prograding from the SW to the NW. The delta covered the whole present day Barents Sea, from the Russian and Norwegian mainland to the north-eastern parts of the Svalbard Archipelago (Worsley, 2008; Sømme et al., 2018; Klausen et al., 2019). The presence of reservoir rock and petroleum source rocks are also tied to this cycle, where we find reservoir rocks approximately at levels of maximum regression and source rocks at maximum flooding and/or condensation (Mørk & Elvebakk, 1999; Henriksen et al., 2011b; Sømme et al., 2018).

In the latest Triassic, a supra-regional relative sea level rise in combination with a major shift in structural regime changed the depositional environment of the Barents shelf. Previously dominated by the mentioned progradational system, the Barents Sea transitioned into a shallow marine and coastal environment entering the Jurassic (Worsley, 2008).

Lower Jurassic deposits are represented by the Tubåen Formation in the western Barents Shelf, which reflects this change in environment with sandstones most likely originating from tidal inlets, estuaries and lagoons (Olaussen et al., 1984). Eastern and northern areas of the Barents shelf did however represent wide continental lowlands (peneplains) during Hettangian (Smelror et al., 2009). During the Middle Jurassic, the Barents region saw a renewed regional transgression, creating a deep marine environment with anoxic bottom-water conditions towards the end of the Jurassic. These conditions were favorable for the deposition of the organically rich black shales in the Hekkingen Formation (Fig. 3.2) (Worsley, 2008).

In the Cretaceous a major change in depositional environment took place: the relative sea-level rose, creating open-marine conditions (Midtkandal et al., 2019). The sea-level change was accompanied by improved bottom circulation, ceasing the former regional anoxic conditions. Locally on the Bjarmeland Platform the Jurassic-Cretaceous boundary is highlighted by a thin, organic rich unit (Sindre Bed) possibly stemming from an algal boom induced by the Mjølnir impact event (Smelror et al., 2002; Smelror et al., 2009). The Mjølnir impact event altered the Jurassic and Triassic stratigraphy, creating an array of local, structural features, and created the Ragnarok Formation (breccia deposits) and the Sindre Bed (ejecta deposits) (Fig. 3.2) (Dypvik et al., 2004). Following this event, the northern Barents Sea was uplifted and slightly tilted as a consequence of the opening of the Amerasian Basin. This led to a reduction in areas of marine sedimentation and progradation of fluvial and deltaic systems from the north (Smelror et al., 2009; Henriksen et al., 2011b). During this time the basinal areas of the westernmost Barents Sea was dominated by deposition of fine clastic material, creating a package of up to 700 m thick shales, with intervals of high organic contents (Ryseth et al., 2003). The platform areas are characterized by thinner, carbonate-dominated deposits (Worsley, 2008). Upper Cretaceous deposits are primarily restricted to the southwestern-most part of the Barents Sea, as it continued to subside (for example in the Tromsø- and Sørvestnaget basins) (Faleide et al., 2015).

3.2.3 Cenozoic (66 Ma - present)

3.2.3.1 Structural development

The structural evolution of the western Barents Sea and particularly the western margin is closely tied to the seafloor spreading between Eurasia and Greenland and opening of the Norwegian-Greenland Sea in Eocene/Oligocene. Oligocene (Talwani & Eldholm, 1977; Faleide et al., 2008; Worsley, 2008; Henriksen et al., 2011b). The Mesozoic and Paleozoic sequences on the Bjarmeland Platform were tilted towards the south due to early Cenozoic tectonism (NPD, 2014). It has also been suggested that the Barents Sea was subjected to a varying degree of uplift and erosion associated with the opening of the Norwegian-Greenland Sea. The uplift may be as much as 1-2 km in the platform areas, including the Bjarmeland platform (Worsley, 2008). In the period Miocene-Pleistocene, the entire shelf was characterized by glacially induced subsidence and uplift. The total late Cretaceous and Cenozoic erosion and removal of sediments may have been as much as 2300 m on the Bjarmeland Platform (Cavanagh et al., 2006; Henriksen et al., 2011b; Lasabuda et al., 2018a; Lasabuda et al., 2018b). The variable tectonic movements in the Barents Sea region have led to significant effects on pre-existing hydrocarbon accumulations and play a noteworthy role when it comes to risk-factors in current exploration activity (Worsley, 2008).

3.2.3.2 Depositional development and stratigraphy

The depositional environment in the Barents Sea in the Cenozoic had a general trend of stable, uplifted hinterlands in the central and eastern parts, and major sediment deposition was restricted to the westernmost basins (e.g. Lasabuda et al., 2018a; Lasabuda et al., 2018b). The limited net deposition on adjacent platforms, most likely deposited thin successions, which were subsequently removed as the area was uplifted and glacially eroded (Smelror et al., 2009). On the Finnmark and Bjarmeland platforms and parts of the Loppa High, Cenozoic strata are absent below the base of the Quaternary (Henriksen et al., 2011b). The base of the Quaternary glacial sediments is represented by a well-defined regional unconformity, termed The Upper Regional Unconformity (URU). This boundary separates the glacially derived sediments, corresponding to the Naust Formation, from the pre Paleogene sediments (Richardsen et al., 1993).

3.3 Mesozoic groups and formations

This study focuses on the stratigraphy affected by the Mjølnir impact event. The impact event occurred in the earliest Cretaceous, and the base of the altered stratigraphy is represented by the uppermost Permian deposits (Fig 3.2)**.** This chapter will thus focus on descriptions of the Mesozoic stratigraphic groups in the Norwegian Barents Sea; Sassendalen-, Kapp Toscana- and Adventdalen groups (Fig 3.2). The following stratigraphic descriptions will follow nomenclature according to Mørk et al. (1999).

3.3.1 Sassendalen Group

The Sassendalen Group includes the Havert-, Klappmyss-, Steinkobbe/Kobbe formations representing the Early and Middle Triassic lithostratigraphic units in the Barents Sea. The group varies in thickness from 60 meters on structural highs to over 2500 m on the southwestern shelf (Riis et al., 2008; Worsley, 2008)

3.3.1.1 Havert Formation

The Havert Formation was deposited in the Induan and consists of marine mudstones and siltstones, a coarsening upwards trend to sandstones (NPDfactpages, n.d.-b). Cores from the Svalis Dome has shown that the Havert Formation contains organic content, more specifically total organic carbon (TOC) of about 1% (Mørk & Elvebakk, 1999). The formation was deposited in an open- to marginal marine environment (Dalland et al., 1988).

3.3.1.2 Klappmyss Formation

The Klappmyss Formation was deposited in the Olenekian and consists of dark-grey to green siltstones, interbedded by very fine-grained sandstones (Riis et al., 2008). Cores of the formation has shown TOC-values up to 5 % (Mørk & Elvebakk, 1999). The depositional environment is interpreted to be marginal- to open marine (Riis et al., 2008).

3.3.1.3 Kobbe Formation

The Kobbe Formation is of Anisian age. The base of the formation consists of a thick shale unit that transition into interbedded shale, stiltstone and carbonate cemented sandstone when moving upwards (Dalland et al., 1988; Lundschien et al., 2014). On the Finnmark Platform,

the topmost Kobbe Formation include high-quality reservoirs (Henriksen et al., 2011b; Lundschien et al., 2014; Rossi et al., 2020).

3.3.1.4 Steinkobbe Formation

The Steinkobbe Formation is time equivalent to the upper parts of the Klappmyss Formation and most of the Kobbe Formation in the Hammerfest Basin (Olenekian to Anisian). It consists of dark, phosphatic shale with minor siltstone. The formation is approximately 250 m thick and show TOC-values between 1.5 and 9% in the Svalis Dome area, representing a rich hydrocarbon source rock. The depositional environment is interpreted to be deep shelf environment with restricted water circulation (Mørk & Elvebakk, 1999).

3.3.2 Kapp Toscana Group

The Kapp Toscana Group can be divided into the Storfjorden- and Realgrunnen subgroups (Mørk et al., 1999). The Storfjorden subgroup (Middle to Late Triassic) is comprised of the Snadd Formation, which is over 1400 m thick in certain areas (Worsley, 2008; Klausen et al., 2015). The Realgrunnen Subgroup (Late Triassic to Middle Jurassic) includes the Fruholmen-, Tubåen-, Nordmela- and Stø formations. The Realgrunnen Subgroup embrace the primary reservoir intervals in the Norwegian sector of the Barents Sea (Henriksen et al., 2011b).

3.3.2.1 Snadd Formation

The Snadd Formation is of Ladinian to early Norian age. It consists of grey shales interbedded by siltstones and sandstones. Limestones and calcareous rocks are found in the lower parts of the formation (Dallmann et al., 1999). The lowermost part of the Snadd Formation also show some source potential in some wells (Henriksen et al., 2011b). The depositional environment of the lower Snadd Formation is interpreted as a distal marine environment transitioning into a deltaic system during the Carnian (Klausen et al., 2015; NPDfactpages, n.d.-a).

3.3.2.2 Fruholmen Formation

The Fruholmen Formation represents early Norian to late Rhaetian age. It consists of grey to dark grey shales transitioning upwards into interbedded sandstones, shales and minor coal beds. The lithologies were deposited in an open marine environment gradually shifting into a coastal and fluvial setting (Dalland et al., 1988).

3.3.2.3 Tubåen Formation

The Tubåen Formation is of late Rhaetian to early Hettangian age. It is dominated by sandstones, but also include minor shales and coals. The deposition generally reflects a high energy marine environment, with some indications of coastal and more distal environments (Dalland et al., 1988).

3.3.2.4 Nordmela Formation

The Nordmela Formation represents Sinemurian to late Pleinsbachian age. It consists of interbedded siltstones, sandstones, shale and claystones with minor coals. The sandstones become more prominent in the upper parts of the formation. The formation was deposited in a tidal flat to flood plain environment (Dalland et al., 1988).

3.3.2.5 Stø Formation

The Stø Formation represents late Pliensbachian to Bajocian age. It is dominated by well-sorted, mature sandstones dominate it, but thin units of siltstone and shale occur. The formation was deposited in a prograding coastal regime (Dallmann et al., 1999; Klausen et al., 2018a).

3.3.3 Adventdalen Group

The Adventdalen group (Late Jurassic to Early Cretaceous) is comprised of the Fuglen-, Hekkingen-, Klippfisk/Knurr-, Kolje- and Kolmule formations. This study focuses on the formations affected by the Mjølnir impact event, thus only the Fuglen and Hekkingen formations will be described.

3.3.3.1 Fuglen Formation

The Fuglen Formation is of late Callovian to Oxfordian age. It consists of dark brown shales with interbedded white to brownish limestones. The formation was deposited in a marine environment (Dalland et al., 1988).

3.3.3.2 Hekkingen Formation

The Hekkingen Formation represents late Oxfordian to Berriasian age. It consists of darkly colored shale and claystone with some occurrences of limestone, dolomite, siltstone and sandstone. The formation was deposited in a marine, deep water environment with dominating anoxic conditions (Dalland et al., 1988). The formation represent an excellent

source rock in the western Barents Sea with Total Organic Carbon (TOC) values up to 20% (Leith et al., 1993; Henriksen et al., 2011b).

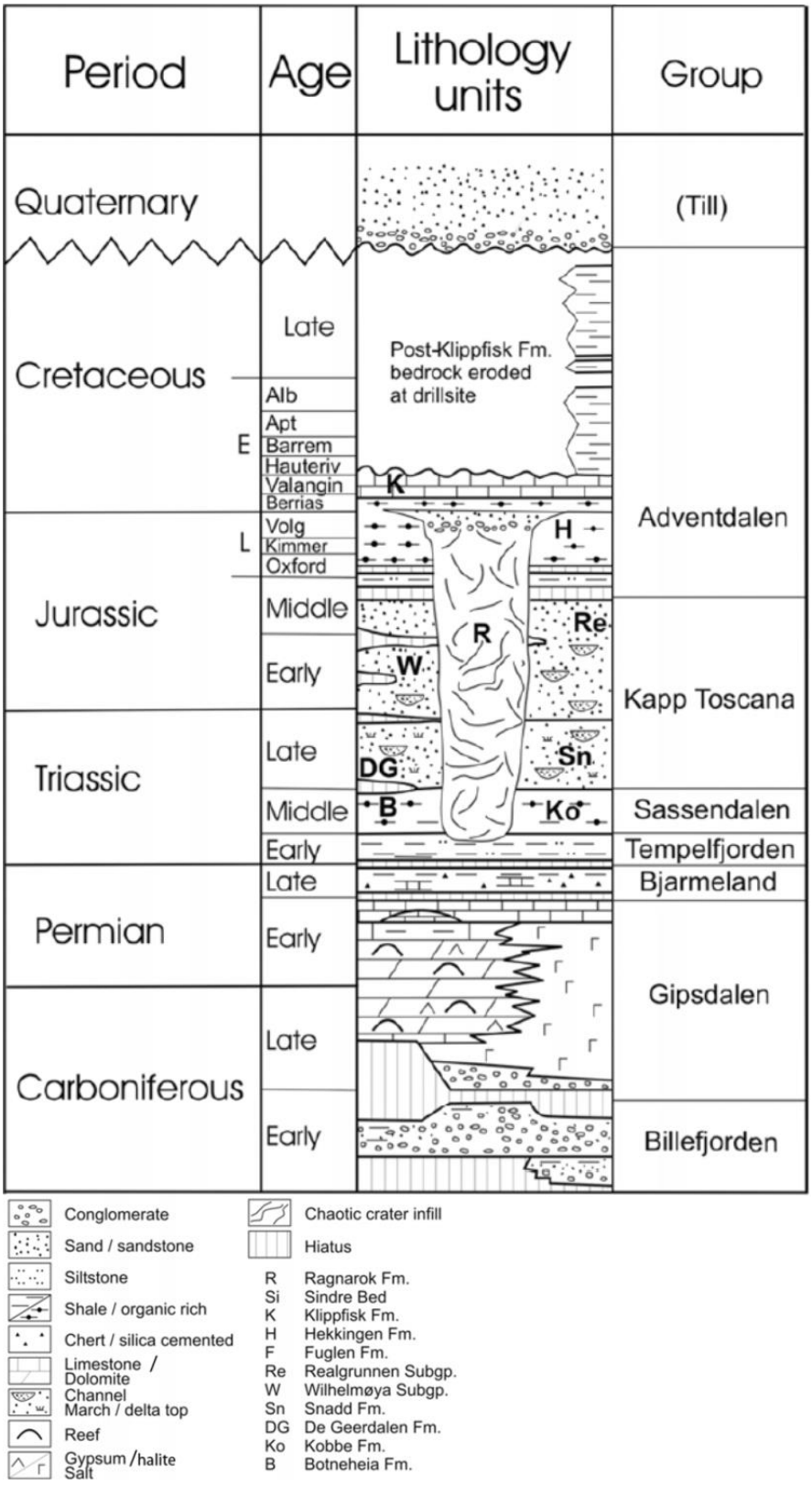

Figure 3.2: Lithostratigraphic chart of the Barents Sea, with the Mjølnir Impact Crater represented by the Ragnarok Fm. (R). The chaotic crater infill also indicates the sedimentary successions affected by the impact event. Lithostratigraphical units of Svalbard are indicated on the left side, and units occurring on the Bjarmeland Platform are indicated on the right side. Figure modified from Dypvik et al. (2004).

4 Data and methodology

4.1 Wells

No exploration wells have been drilled in the study area. Two shallow boreholes are drilled in the study area: 7430/10-U-01 in 1988 prior to the interpretation of Mjølnir as an impact crater and 7329/03-U-01 in 1998 to recover impact related strata (Fig. 2.1) (Tsikalas et al., 2010a). These shallow boreholes do not give significant tie to the stratigraphy. For the purpose of seismic tie, exploration well 7435/12-1 (Korpfjell) located 170 km to the northeast at the Haapet Dome has been used in this study. The well was drilled in 2017 by Statoil Petroleum AS (now Equinor) at the coordinates 74° 4' 18.21" N, 35° 48' 31.06" E (NPDfactpages, n.d.-c, Fig. 4.1). The well is used to correlate the seismic stratigraphy to well tops provided by the NPD (chapter 5.1) and velocity calculations (chapter 4.2.2).

4.2 Seismic data

This study has utilized high-resolution seismic 2D vintages and ultrahigh resolution P-cable data covering the Mjølnir Impact Crater, large parts of the Bjarmeland Platform and adjacent structural elements (Fig. 4.1, Table 4.1). The seismic data used in this study was acquired in the period 2008 to 2015 and was distributed by the Norwegian Petroleum Directorate. The 2D seismic database is comprised of survey NBR08, SS1302 and NBR14. The P-cable survey, HR15, provides ultrahigh resolution 2D images, allowing detailed interpretation of the shallow subsurface (<1000 ms TWT). The datasets cover large areas and many structural elements in the Barents Sea. This decreases the relevance of many seismic 2D lines; thus, the full seismic datasets were not utilized in this study. Figure 4.1 displays the seismic 2D lines regarded as relevant, and partly defines the determined study area (further elaborated in chapter 5.1). Table 4.1 summarizes information regarding the different surveys.

The seismic database used is generally of high quality. The seismic surveys are comprised of seismic 2D lines of primarily four different orientations and the spacing between the 2D lines varies (<11km) (Fig. 4.1). This results in a variable data coverage (grid size) within the study area. The limited data coverage introduces challenges and uncertainties in the structural and stratigraphic interpretations.

Table 4.1: The table shows information regarding the seismic 2d surveys utilized in this study.

Survey Name	Sub type	Year	Company responsible	Number of lines	Total length (km)	Vertical depth (TWT)
NBR08	2D	2008	Fugro-Geoteam AS	63	10178	10 000 ms
SS1302	2D	2013	Searcher Seismic CT Pty Ltd	41	6169	4500 ms
NBR14	2D	2014	TGS	58	9396	5900 ms
HR15	2D – P-cable	2015	P-Cable 3D Seismic AS	8	1108	1000 ms

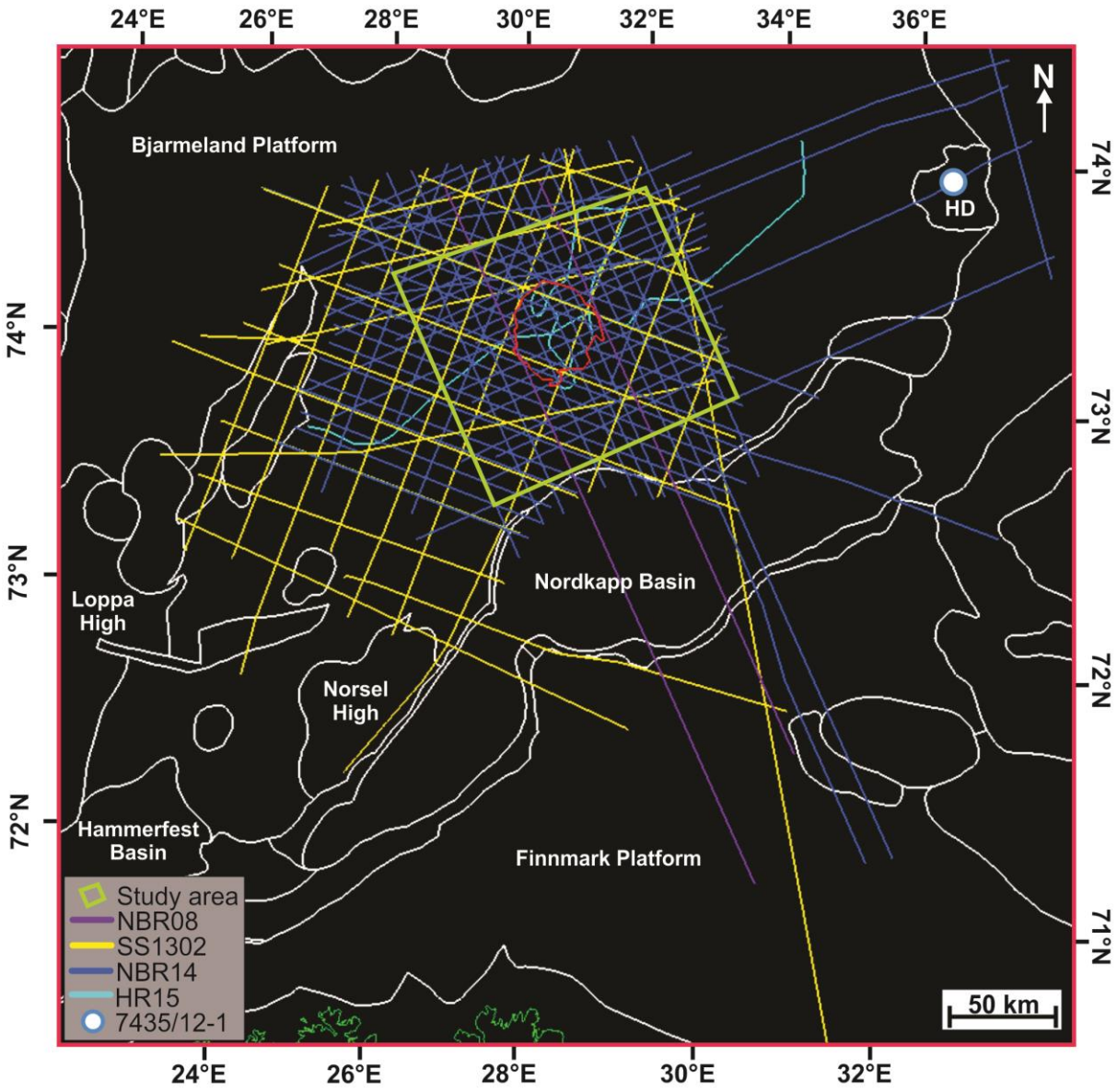

Figure 4.1: The figure displays the seismic database and the outline of the defined study area (green square) and well 7435/12-1 (Korpfjell). The white polygons represent structural elements in the Barents Sea. The Mjølnir Impact Crater is outlined in red. HD = Haapet Dome. Structural elements are from the NPD.

4.2.1 Phase and polarity

A seismic wave represents a periodic waveform, which may be described according to its amplitude, polarity and phase. There are two main conventions of seismic phase: minimum-phase and zero-phase (Fig. 4.2). Polarity is a term used to describe if the reflection is positive or negative, as described by the reflection coefficient. There are two polarity conventions, the polarity convention of Badley (1985) and the Society of Exploration Geophysicists (SEG) convention of Sheriff (1999). This study will use the SEG standard polarity convention**.**

As shown in Figure 4.2, minimum-phase, normal polarity is displayed as a trough directly under the reflected boundary, followed by a peak. Zero-phase, normal polarity is characterized by a trough just above the interface, a main peak in the center of the interface followed by a trough below the boundary. The seismic data applied all have zero phase wavelets, and an example of the wavelet from the seabed in dataset SS1302 is illustrated in Figure 4.2.

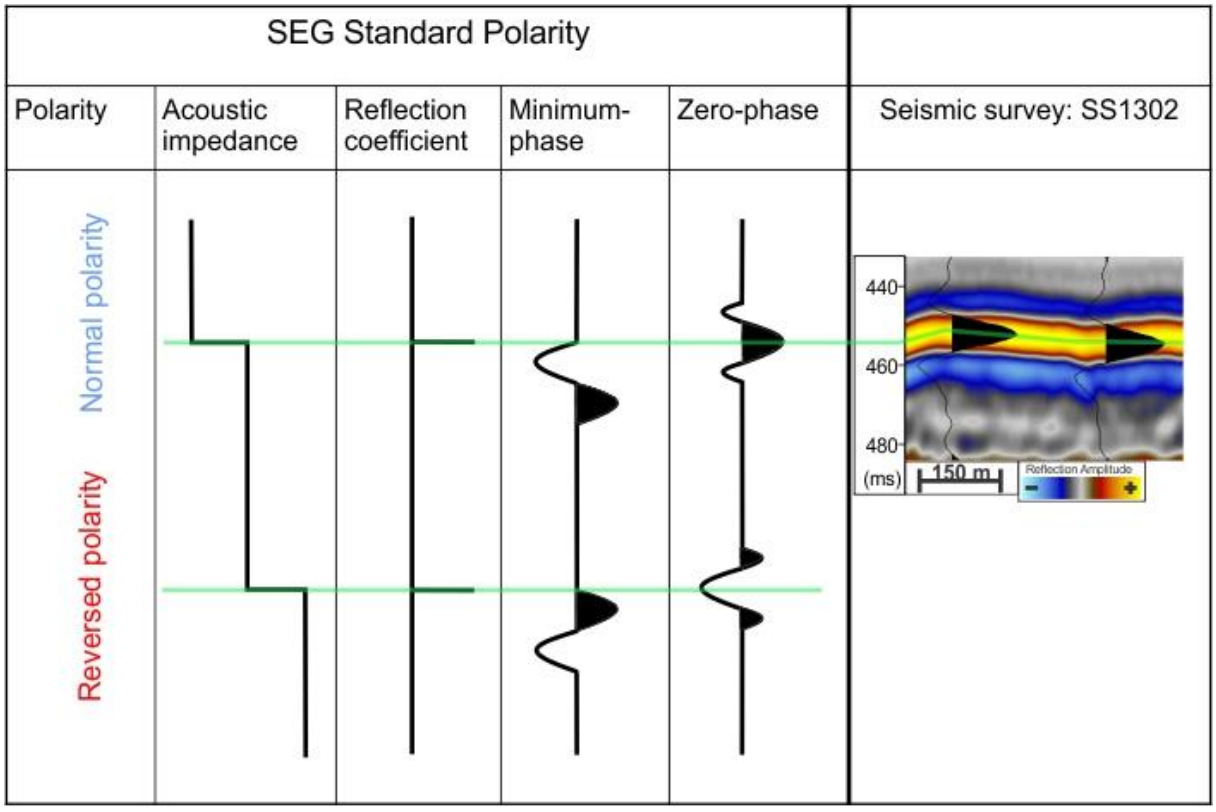

Figure 4.2: The polarity and phase conventions for plotting seismic signals at given acoustic boundaries marked in green following SEG standard. A seabed reflection of a seismic 2D line from survey SS1302 is shown and interpreted as zero-phase normal polarity.

4.2.2 Seismic velocity, frequency and resolution

In order to calculate the resolution of the seismic surveys used, seismic velocities need to be obtained. The well data provided from well 7435/12-1 (Korpfjell) did not include a complete sonic log. The Korpfjell well was instead used to obtain formation depths in two-way-travel-time and in meters. This enables the calculation for each unit (Table 4.2). In order to calculate the velocities, the following equation was used:

Equation 4.1 internal seismic velocity

$$v_{unit} = \frac{d_{unit}}{t_{unit}}$$

Equation 4.1: v_{unit} = Internal velocity of unit x (m/s), d_{unit} = Thickness of unit x (m), t_{unit} = One way travel time of unit (s).

Table 4.2: The table lists values acquired from well 7435/12-1 (Korpfjell) for each formation/unit using Petrel. This includes the depth of formation tops both in meters and time. The unit thickness in time was calculated by subtracting the formation top from the formation base, dividing by two to get the one-way-time and subsequently converting it to seconds. The unit thickness in meters was calculated by subtracting the true vertical depth of the top from the base. Lastly, the unit thickness (m) was divided by the unit thickness (s) to obtain the internal velocity (m/s).

Formation/unit	Depth TWT (ms)	Unit thickness (s)	True Vertical Depth (TVD) (m)	Unit thickness (m)	Velocity (m/s)
Seabed	351.14		291.05		
Cretaceous unit		0.086465		206.47	2388
Top Hekkingen	524.07		497.52		
Hekkingen Fm.		0.01628		40.99	2518
Top Fuglen	556.63		538.51		
Fuglen Fm.		0.0147		37.99	2584
Top Stø	586.03		576.5		
Realgrunnen Subgroup		0.069955		203	2902
Top Snadd	725.94		779.5		
Snadd Fm.		0.116855		388.45	3324
Top Kobbe	959.65		1167.95		

The median frequency of each data set is obtained by using the spectral analysis tool in petrel. Figure 4.3 shows the frequency spectra as a graph for representative 2D lines of each seismic survey. The peak-values (frequency value at which the Power (dB) is 0) of each survey is collected (Table 4.3) and is indicated by color-coded arrows in Figure 4.3. Wavelengths for the cretaceous unit and the Snadd Formation were calculated using Equation 2.3 (Table 4.3).

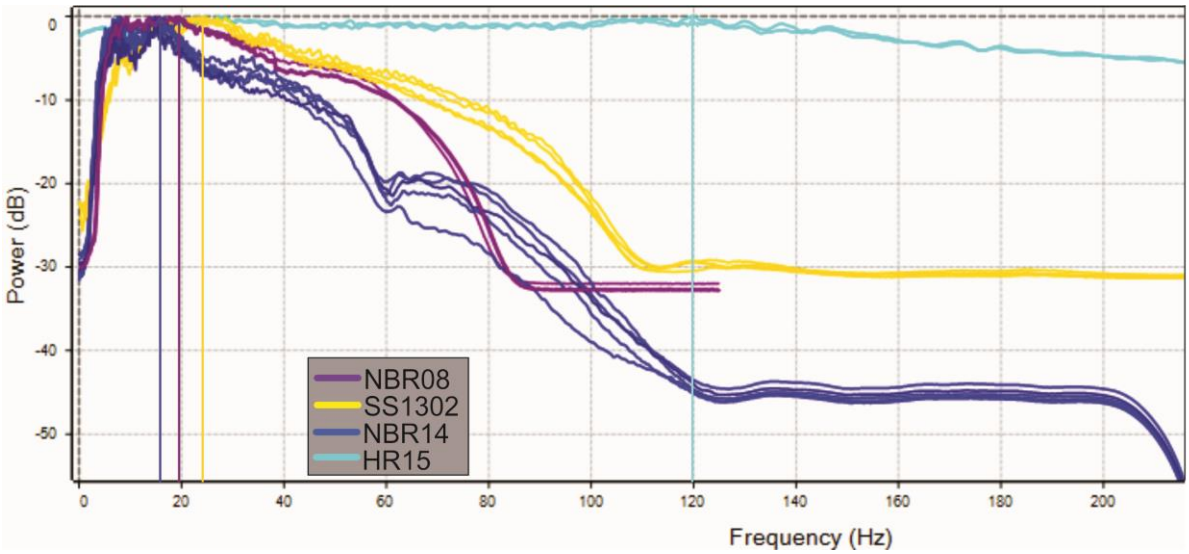

Figure 4.3: The figure shows the frequency spectra of selected seismic lines in the different seismic surveys used in this study. The peak values (median frequency) are indicated by color-coded lines.

Table 4.3: Peak frequency (Hz) and calculated velocity (m/s) is used to calculate the wavelength (m). Subsequently, these values are used to calculate the vertical resolution for chosen units, to illustrate how frequency and seismic velocity affects the resolution.

Dataset	**Interval**	**Velocity (m/s)**	**Peak frequency (f)**	**Wavelength (m)** $\boldsymbol{\lambda = \frac{V}{f}}$	**Vertical resolution (m)** $\boldsymbol{v_r = \frac{\lambda}{4}}$
NBR08	Cretaceous unit	2388 m/s	20 Hz	119 m	29,75 m
NBR08	Snadd Fm.	3324 m/s	20 Hz	166.2 m	41.6 m
SS1302	Cretaceous unit	2388 m/s	24 Hz	99.5 m	24,9 m
SS1302	Snadd Fm.	3324 m/s	24 Hz	138.5 m	34.6 m
NBR14	Cretaceous unit	2388 m/s	16 Hz	149,3 m	37,3 m
NBR14	Snadd Fm.	3324 m/s	16 Hz	207,8 m	86.6 m
HR15	Cretaceous unit	2388 m/s	120 Hz	19,9 m	5 m
HR15	Snadd Fm.	3324 m/s	120 Hz	27.7 m	6.9 m

The horizontal resolution of the different surveys used in this study is calculated based on the formation depths at well 7435/12-1 (Korpfjell). The calculated values are summarized in Table 4.4, using Equation 2.4.

Table 4.4: Peak frequency (Hz), depth TWT (s) and velocity (m/s) were used to calculate the horizontal resolution. The horizontal resolution is presented as the radius of the pre-migration Fresnel Zone, thus the horizontal resolution of the seismic data is higher than calculated.

Dataset	Horizon	Velocity (m/s)	Peak frequency (f)	Depth TWT (s)	Horizontal resolution unmigrated (m)
NBR08	Top Hekkingen	2388 m/s	20 Hz	0.524 s	193.3 m
NBR08	Top Snadd	3324 m/s	20 Hz	0.726 s	316.7 m
SS1302	Top Hekkingen	2388 m/s	24 Hz	0.524 s	176.4 m
SS1302	Top Snadd.	3324 m/s	24 Hz	0.726 s	289.1 m
NBR14	Top Hekkingen	2388 m/s	16 Hz	0.524 s	216.1 m
NBR14	Top Snadd	3324 m/s	16 Hz	0.726 s	354 m
HR15	Top Hekkingen	2388 m/s	120 Hz	0.524 s	78.9 m
HR15	Top Snadd	3324 m/s	120 Hz	0.726 s	129.3 m

4.2.3 Seismic artifacts and noise

Sheriff (2002) defines artifact as an incidental unintended effect produced by acquisition or processing, also known as footprint. When interpreting seismic data, such footprints must be disregarded as it is not related to the true geology of the subsurface. Artifacts are observed on two separate lines in seismic survey SS1302 in the northwestern study area (Fig. 4.4). These artifacts are seemingly long-path multiples of the seabed reflection. These occur when reflections undergo more than once bounce (Badley, 1985). The multiples crosscut the reflections that represent the true geology of the subsurface and must be disregarded.

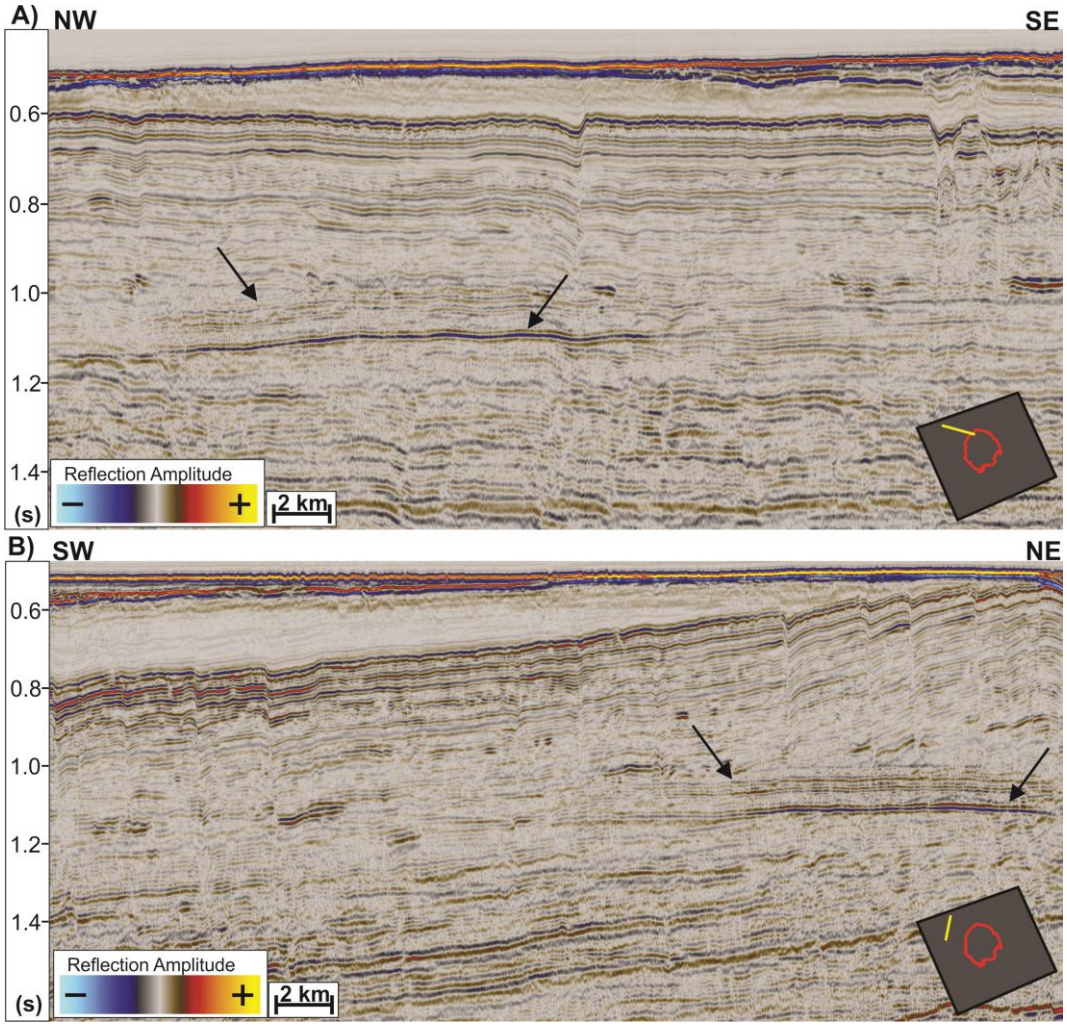

Figure 4.4: A) The figure shows seismic 2D line SS1302-126 in the northwestern study area. B) Shows seismic 2D line SS1302-035 in the northwestern study area. Both seismic lines show seabed multiples occurring at about two times the seabed TWT (black arrows). These are not geological features, but seismic artifacts that cross-cut geological reflections.

The Mjølnir Impact Crater is generally characterized by systematic loss of reflection coherency from distal and deeper parts to the central and upper parts, seen as chaotic and transparent zones (Fig. 4.5). This seismic disturbance is caused by diffractions and disrupted layering, creating a disturbance zone (DZ) (Tsikalas et al., 2010a). Tsikalas et al. (1998a) formally identified the disturbance zone (DZ) in vintage seismic data, and it is characterized by a "inverted-sombrero" shape, commonly seen in complex marine impact craters (Melosh, 2013). The DZ makes structural and stratigraphic interpretation within the central Mjølnir Impact Crater challenging.

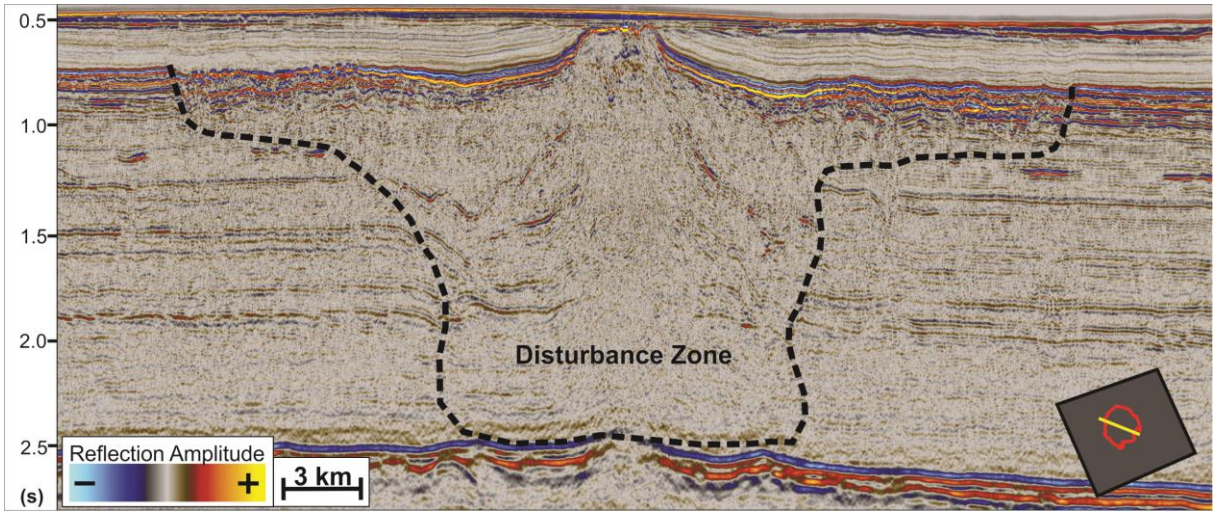

Figure 4.5: The figure shows seismic 2D line NBR14-362688 through the Mjølnir Impact Crater. The seismic sections show the seismic disturbance (reflection free zones and chaotic seismic) within the disturbance zone (DZ) (black stippled line).

4.3 Methodology

4.3.1 Software

The interpretation and analysis of seismic 2D data and well data has been carried out by using Petrel E&P software version 2019.2, produced by Schlumberger. The software was primarily used to interpret horizons, correlate the well data to seismic data, generate surfaces and time-thickness maps. All figures and illustrations have been made in CorelDRAW 2017.

5 Results

This chapter presents all observations made in the study area covering the Mjølnir Impact Crater. The results consist of seismic well tie, stratigraphic interpretation, structural interpretation and seismic anomalies found in and adjacent to the Mjølnir Impact Crater. The seismic interpretations are limited to the outlined study area (Fig. 5.1) surrounding the Mjølnir Impact Crater, approximately covering 110 km x 120 km. The area is defined based on seismic data coverage, structural elements and termination of key strata: there is limited seismic data towards the east and west (Fig 4.1), the Nordkapp Basin bounds the study area to the south and parts of the stratigraphy is eroded towards the north. Tsikalas et al. (1998c) established the key features and subdivision of the Mjølnir Impact Crater, also included in this study. These features include an outer zone, annular depression and central high (Fig. 5.1).

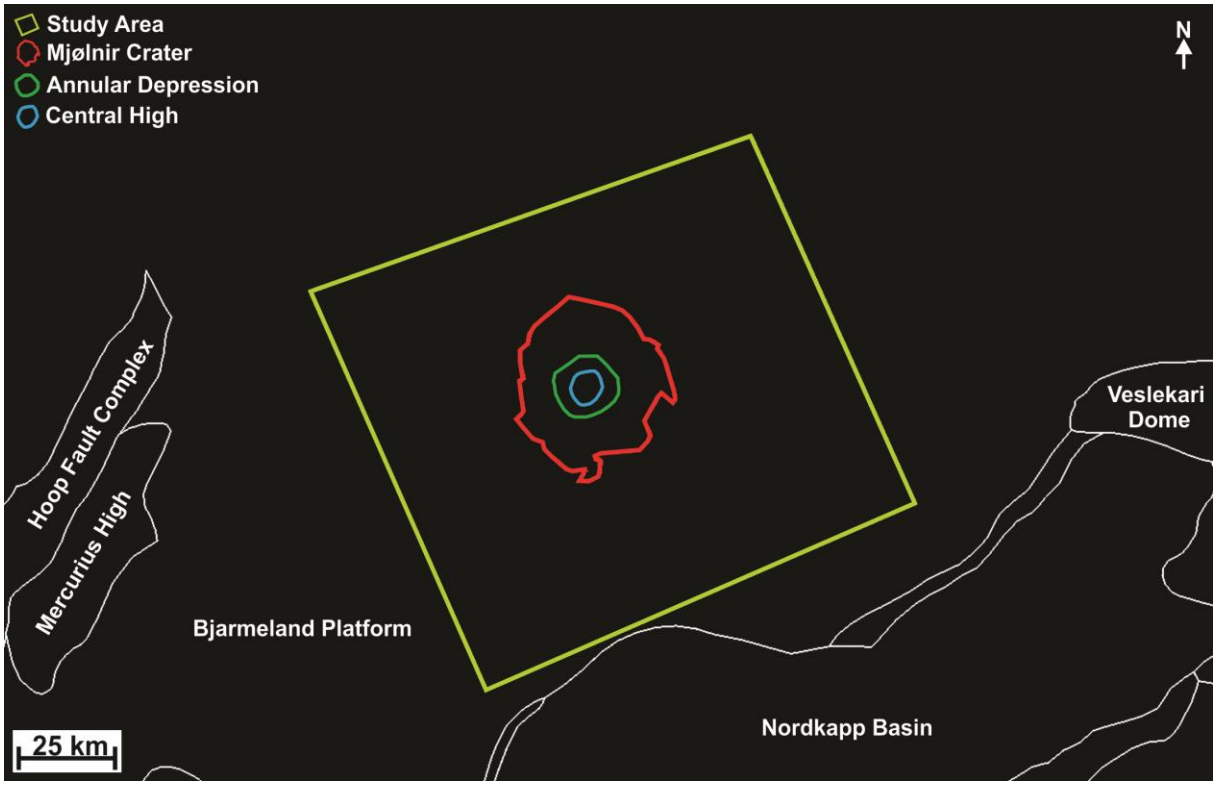

Figure 5.1: Overview of the defined study area around the Mjølnir Impact Crater. Also shows the internal division of the Mjølnir Impact Crater: outer boundary of the annular depression (green) and central high (blue). The structural elements, outline of the Mjølnir Impact Crater and the internal division are imported shapefiles obtained from the NPD.

5.1 Seismic well tie

The seismic stratigraphy is correlated to well 7435/12-1 (Korpfjell) (Figs. 5.2-5.3), on the Haapet Dome, located 170 km northeast of the Mjølnir Impact Crater. The interpretations are based on the stratigraphic boundaries of well tops for the Korpfjell well provided by the NPD. The well drilled through stratigraphy of the Lower Cretaceous Knurr Formation just below seabed and terminated in the Middle Triassic Kobbe Formation (Fig 5.3). Deeper stratigraphic boundaries are following Corseri et al. (2020)

5.2 Seismic stratigraphic subdivision and horizons

This sub-chapter presents the interpreted horizons (Figs. 5.4-5.9) and the stratigraphy in and around the Mjølnir Impact Crater. This study emphasizes on the strata disturbed and deposited following the Mjølnir impact event, which primarily includes Lower Cretaceous, Jurassic and Triassic formations. Tsikalas et al. (1998a) established a seismic stratigraphic nomenclature constraining the stratigraphic position of the impact event based on markers from shallow borehole 7430/10-U-01, namely the Top Disturbance (TD), Upper Boundary (UB) and Lower Boundary (LB). Top disturbance (TD) is defined as the top of the seismic disturbance. The Upper- (UB) and Lower boundary (LB) constrain the time of the impact. This nomenclature will be included in this study.

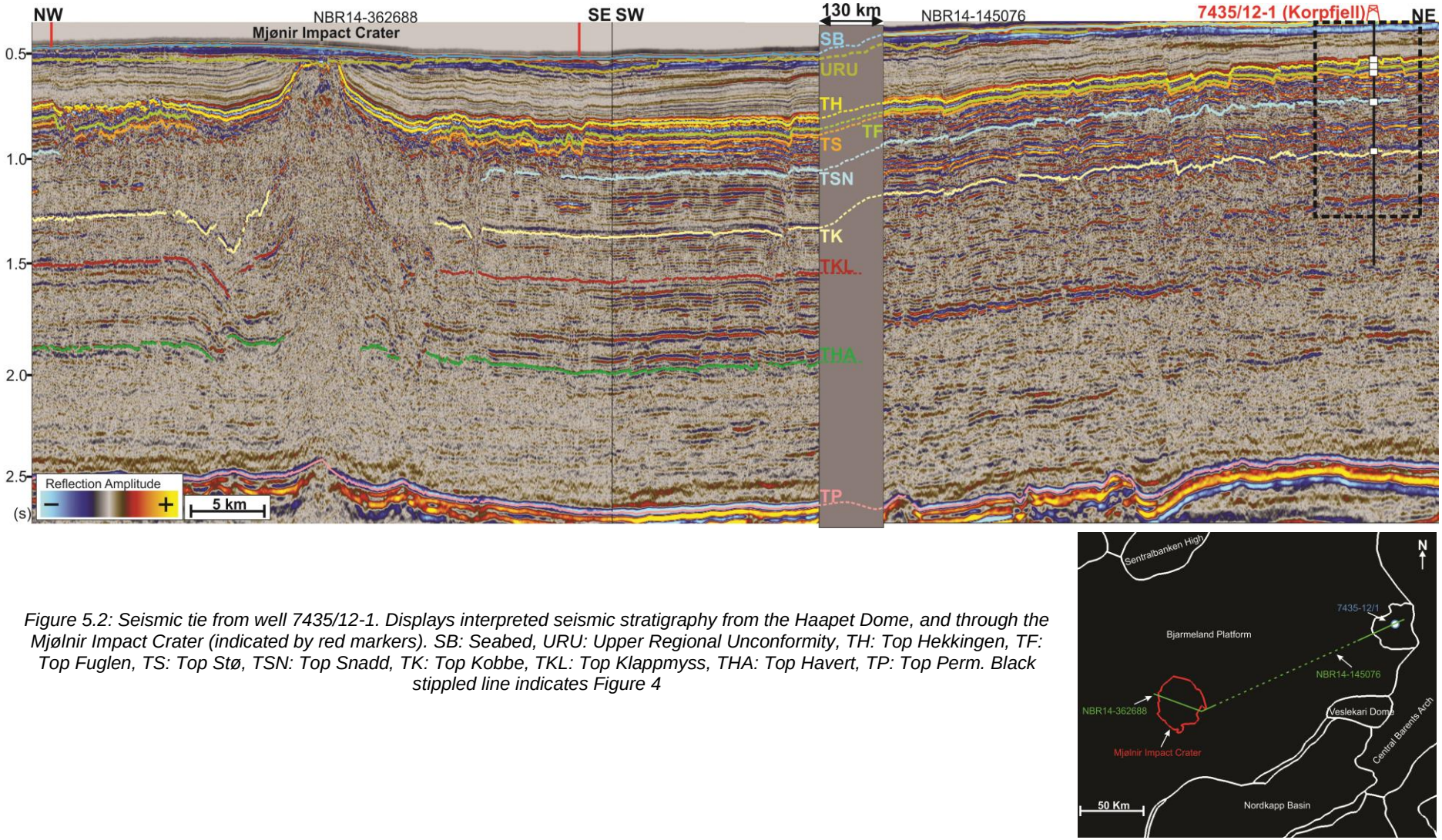

Figure 5.2: Seismic tie from well 7435/12-1. Displays interpreted seismic stratigraphy from the Haapet Dome, and through the Mjølnir Impact Crater (indicated by red markers). SB: Seabed, URU: Upper Regional Unconformity, TH: Top Hekkingen, TF: Top Fuglen, TS: Top Stø, TSN: Top Snadd, TK: Top Kobbe, TKL: Top Klappmyss, THA: Top Havert, TP: Top Perm. Black stippled line indicates Figure 4

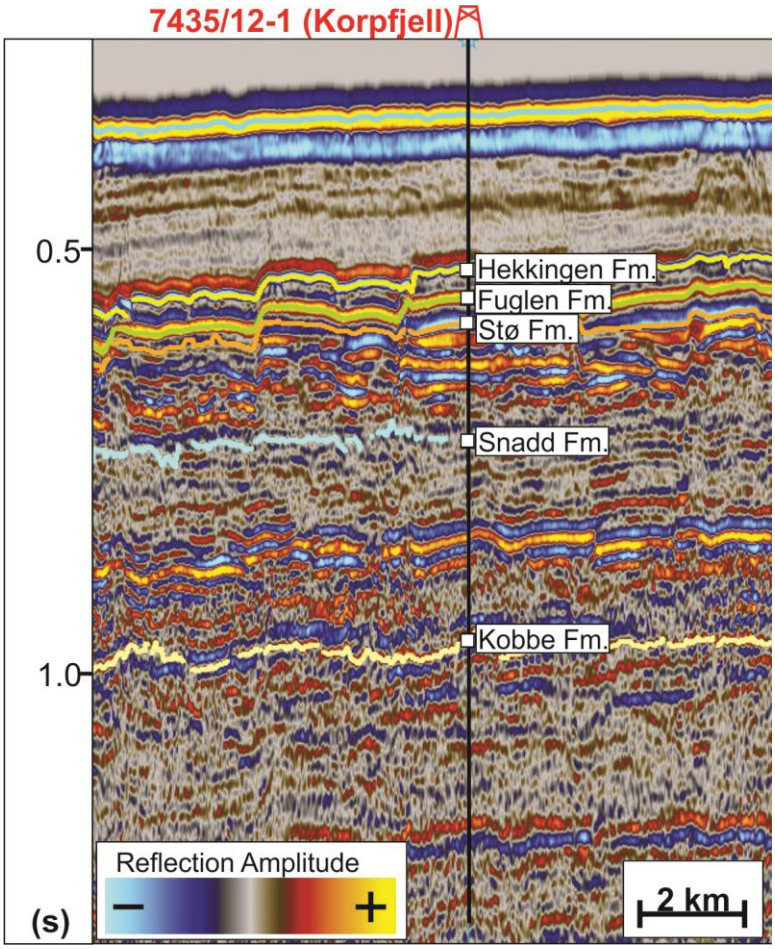

Figure 5.3: Zoomed in view from Figure 5.2 of the well tops of well 7435/12-1 with the provided well tops (white boxes) and interpreted horizons.

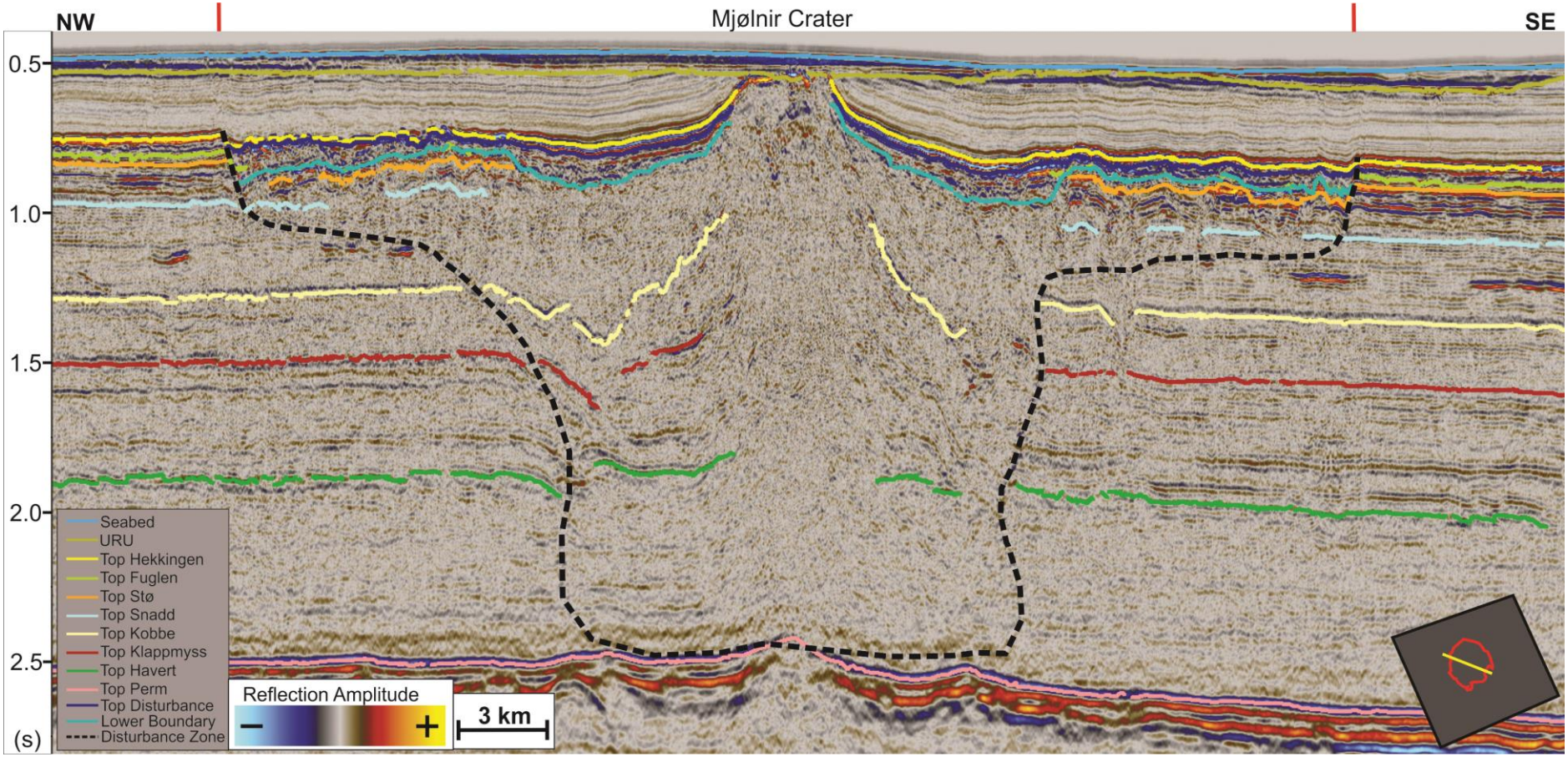

Figure 5.4: Seismic 2D line NBR14-362688 through the Mjølnir Impact Crater (indicated by red markers) and its central high. Displaying interpreted horizons and outline of the disturbance zone (DZ)

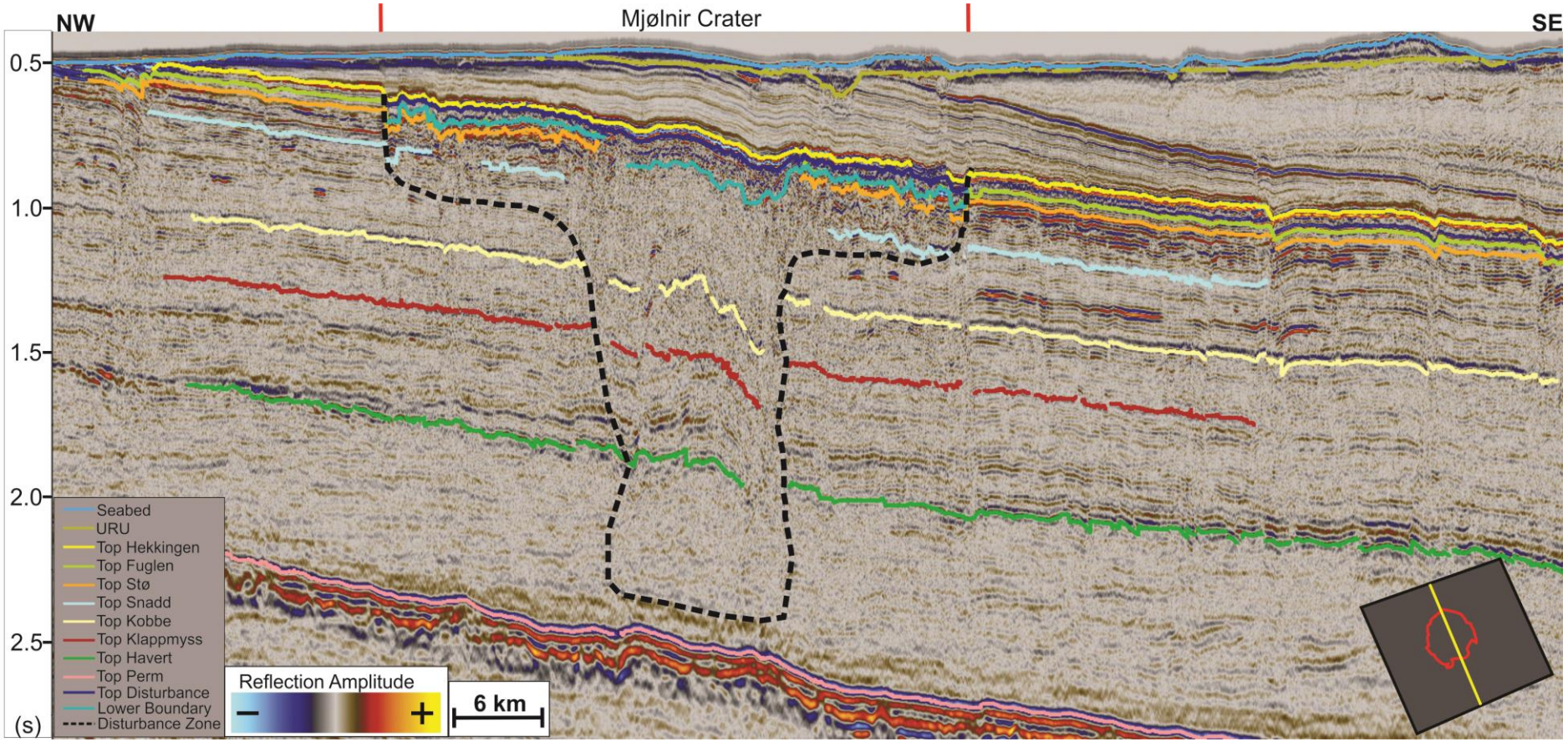

Figure 5.5: Seismic 2D line NBR14-266837 through the Mjølnir Impact Crater (indicated by red markers), displaying the southward dipping regional trend, faulting of the adjacent Bjarmeland Platform and wedge-shaped reflections in the URU – Top Hekkingen interval. It is also showing interpreted horizons and outline of the disturbance zone (DZ) (black stippled line).

5.2.1 Horizons

A total of 11 separate horizons are interpreted (Fig. 4.2 & 4.4), described in this sub-chapter and presented as generated TWT maps (ms) (Figs. 5.5-5.10).

5.2.1.1 Top Permian

The Top Permian horizon represents the boundary between the overlying Triassic formations and the underlying Permian formations. The horizon is interpreted on a seismic reflection characterized by a strong seismic amplitude with a negative reflection coefficient (Fig. 5.2). The horizon depth varies between 2100 ms and 3100 ms TWT (Fig. 5.6A). The Top Permian horizon represents the deepest horizon that is affected by the Mjølnir impact event, seen in the seismic section as a minor "peak" underneath the central high (Fig 5.2). The horizon has good continuity and can be tracked with high confidence throughout the study area. The generated TWT map (Fig. 5.6A) displays a deepening trend towards the south.

5.2.1.2 Top Klappmyss

The Top Klappmyss horizon represents the boundary between the Kobbe/Steinkobbe- and Klappmyss formations. The horizon is represented by a reflection characterized by a low-to-medium seismic amplitude with a positive reflection coefficient (Fig 5.2). The amplitude of the reflection is generally stronger in the western parts of the study area, gradually weakening towards the east. The horizon depth varies between 1150 ms and 1950 ms within the study area, deepening to the south (Fig. 5.7A). The horizon has good continuity and is present in most of the study area. Within the disturbance zone (DZ) the horizon becomes discontinuous and uplifted (Fig 5.4), which also becomes evident on the TWT map, where the horizon shows irregularities within the DZ (Fig. 5.7A).

5.2.1.3 Top Kobbe

The Top Kobbe horizon represents the upper boundary of the Kobbe Formation, coinciding with the boundary between the Kapp Toscana- and Sassendalen groups. The horizon is represented by a reflection characterized by a medium seismic amplitude with a positive reflection coefficient, represented by a peak and two associated troughs in the seismic section (Fig. 5.2). The depth of the horizon varies between 950 ms and 1850 ms (TWT) (Fig. 5.7B) and displays a general dip towards the south. The horizon is continuous in the platform-area

surrounding the Mjølnir Impact Crater and within the outer zone. Within the disturbance zone, the horizon is discontinuous and is showing high dip (close to subvertical) towards the central high (Fig. 5.4). The TWT map (Fig 5.7B) is smooth in the platform-area and the outer zone of the crater but displays a deepening in the annular depression and anomalously low values (ms) when approaching the central high.

5.2.1.4 Top Snadd

The Top Snadd horizon represents the boundary between the Upper Triassic Fruholmen Formation above, and the Snadd Formation below. The horizon is represented by a reflection characterized by as positive reflection coefficient, and a low seismic amplitude (Fig 5.2). The reflection is semi-continuous in the platform-area surrounding the crater and is only traceable within parts of the crater due to chaotic seismic reflections. The horizon gradually loses continuity and is increasingly more difficult to recognize moving from the periphery of the Mjølnir Impact Crater towards the annular depression (Fig 5.4). Within the annular depression and the central high the horizon is no longer visible in the chaotic seismic reflections, as also illustrated in the TWT map in Figure 5.8A. The depth of the horizon varies between 600 ms and 1500 ms, deepening from north to south (Fig. 5.8A). The horizon is truncated by the URU/seabed north of the study area and deepens towards the south.

5.2.1.5 Top Stø

The Top Stø horizon represents the upper boundary of the Stø Formation and corresponds to the boundary between the Adventdalen Group and the Realgrunnen Subgroup. The horizon is represented by a reflection characterized by a medium- to strong seismic amplitude with a negative reflection coefficient (Fig. 5.2). The depth of the horizon varies between 500 ms and 1300 ms (TWT), with a deepening trend from the north towards the south. The reflection is continuous in the platform-area surrounding the Mjølnir Impact Crater. For the Top Stø horizon the disturbance zone coincides with the outer boundary of the Mjølnir Impact Crater (Fig. 5.8B). This may be seen by the slight irregularities within the Mjølnir Impact Crater, especially in the periphery (outer zone), on the generated TWT map (Fig. 5.8B). The horizon is lost in the chaotic seismic concentrically at the outer boarders of the annular depression of the Mjølnir Impact Crater (Fig. 5.8B).

5.2.1.6 Top Fuglen

The Top Fuglen horizon represents the upper boundary of the Jurassic Fuglen Formation. The horizon is represented by a reflection characterized by a high seismic amplitude with a positive reflection coefficient, represented by a peak in the vertical seismic sections (Fig. 5.2). The horizon varies in depth between 450 ms and 1250 ms (TWT) (Fig 5.9A). The deepest areas are towards the Nordkapp Basin in the south, and it is truncated by the seabed/URU north of the Mjølnir Impact Crater (Fig 5.5). The reflection is only visible in the outer zone of the Mjølnir Impact Crater, as it is lost within the chaotic seismic reflections at the outer boundary of the annular depression, establishing a circular pattern (Fig 5.9A). Within the outer zone of the Mjølnir Impact Crater, the interpreted Top Fuglen horizon corresponds to the Lower Boundary (LB) (Tsikalas et al., 1998a).

5.2.1.7 Top Hekkingen

The Top Hekkingen horizon represents the boundary between the Lower Cretaceous Knurr Formation above and the Upper Jurassic to Lower Cretaceous Hekkingen Formation below. The horizon is represented by a reflection characterized by a high seismic amplitude with a negative reflection coefficient, represented by a trough in the seismic data (Fig. 5.2). The reflector is continuous, allowing for highly confident interpretation throughout the study area. The depth of the horizon varies between 450 ms and 1200 ms (TWT), with a general trend of deepening from the north towards the south (Fig. 5.9B). The horizon is truncated by the seabed/URU in the northern parts of the study area and intersected by the central high (Fig. 5.4). The TWT map is characterized by a smooth surface, with anomalously low values (ms) at the central high (Fig. 4.9B). The Top Hekkingen horizon corresponds to the upper boundary (UB) (Tsikalas et al., 1998a).

5.2.1.8 Upper Regional Unconformity (URU)

Upper Regional Unconformity horizon represents the uppermost-interpreted stratigraphic horizon in this study. URU represents the boundary between overlying glaci-genic deposits (Naust Formation) and underlying Cretaceous strata in the study area. The horizon is represented by a reflection characterized by a medium-to-low seismic amplitude with a positive reflection coefficient (Fig. 5.2). The horizon is map-able in the southern parts of the study area, but in the northern parts, it is not distinguishable from the Seabed most likely due to limited vertical resolution of the data. The depth of the horizon varies between 400 ms and

600 ms (TWT), with a general trend of deepening to the west (Fig 5.10A). Above the southeastern part of the Mjølnir Impact Crater, the URU surface displays three distinct depressions (Fig. 5.10A) (discussed in chapter 5.2.2.9)**.**

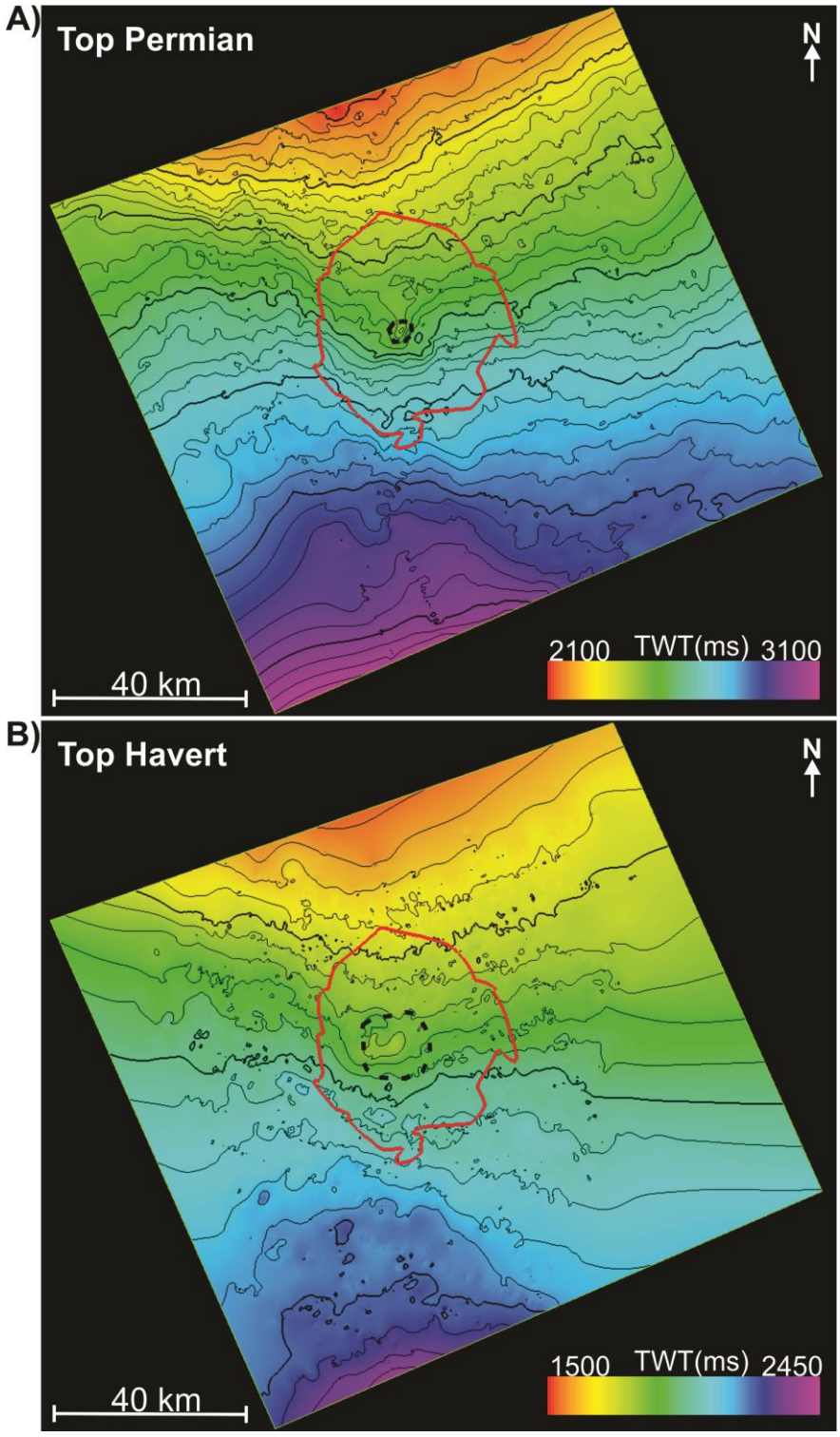

Figure 5.6: A) Two-Way-Time (ms) map of the Top Permian horizon with a contour line increment of 30 ms. B) Two-Way-Time (ms) map of the Top Havert horizon with a contour line increment of 50 ms. Black stippled line indicated the disturbance zone, Mjølnir Impact Crater outlined in red.

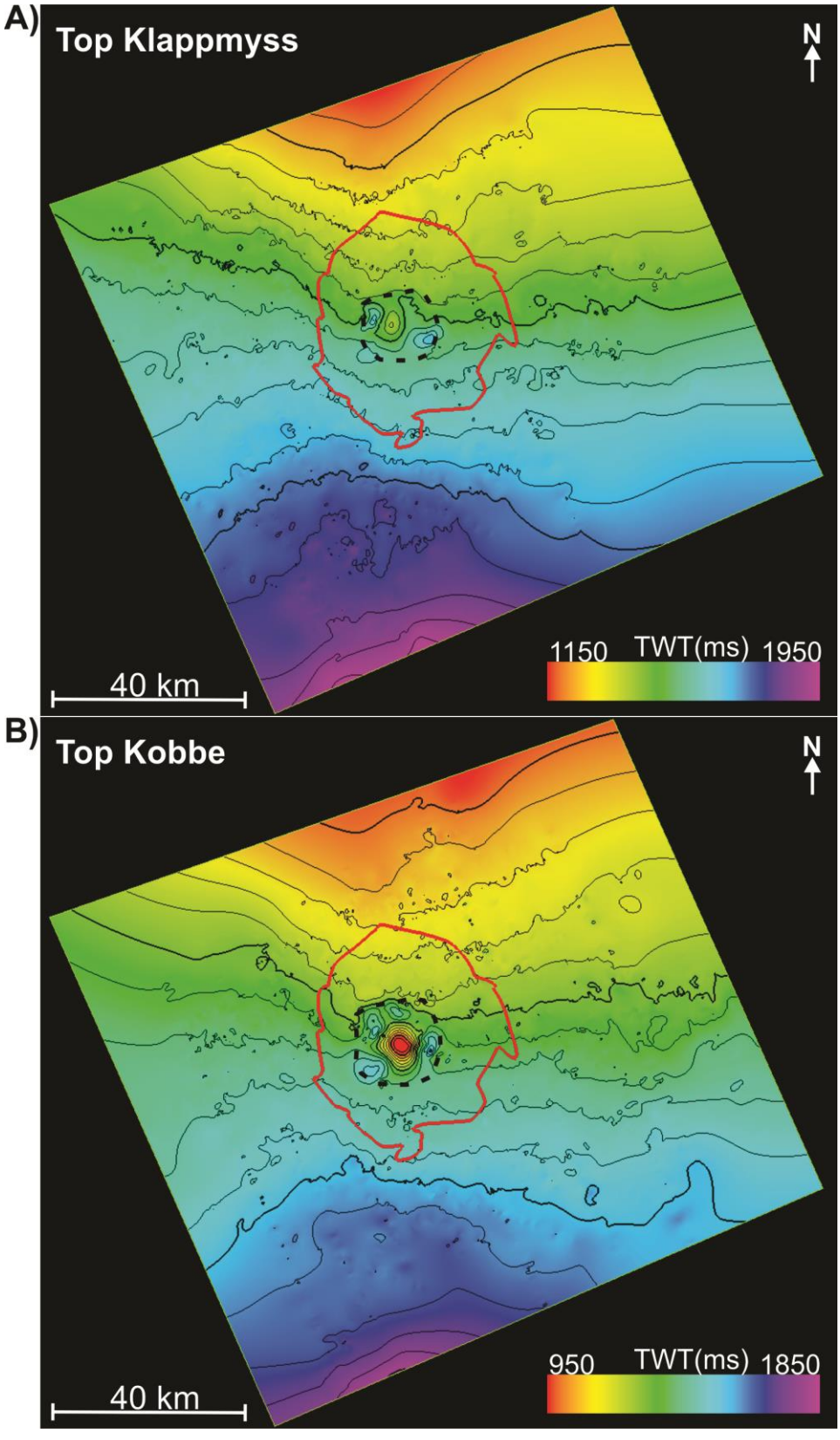

Figure 5.7: A) Two-Way-Time (ms) map of the Klappmyss horizon with a contour line increment of 50 ms. B) Two-Way-Time (ms) map of the Top Kobbe horizon with a contour line increment of 50 ms. Black stippled line indicated the disturbance zone, Mjølnir Impact Crater outlined in red.

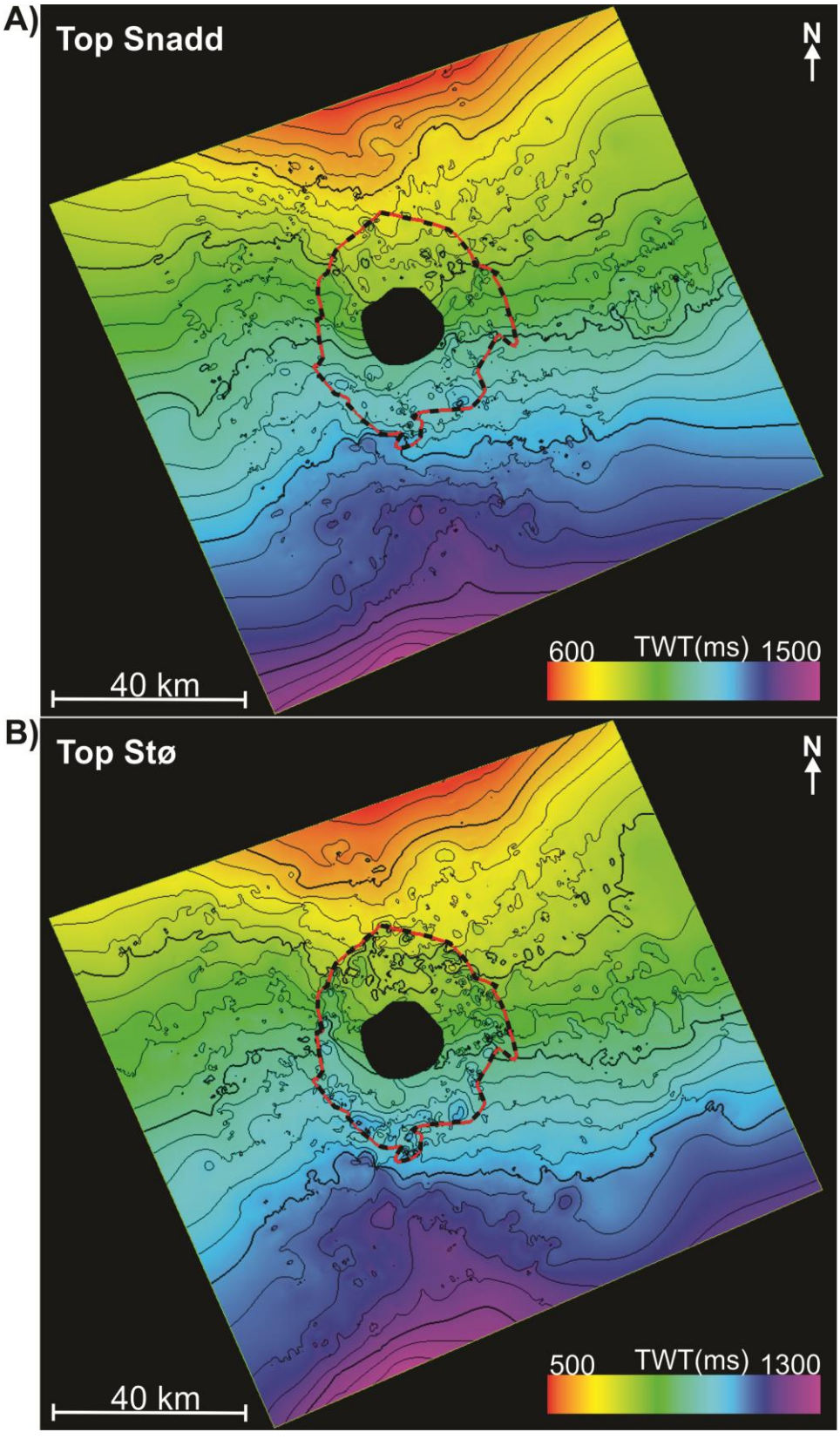

Figure 5.8: A) Two-Way-Time (ms) map of the Top Snadd horizon with a contour line increment of 30 ms. B) Two-Way-Time (ms) map of the Top Stø horizon with a contour line increment of 30 ms. Black stippled line indicated the disturbance zone, Mjølnir Impact Crater outlined in red.

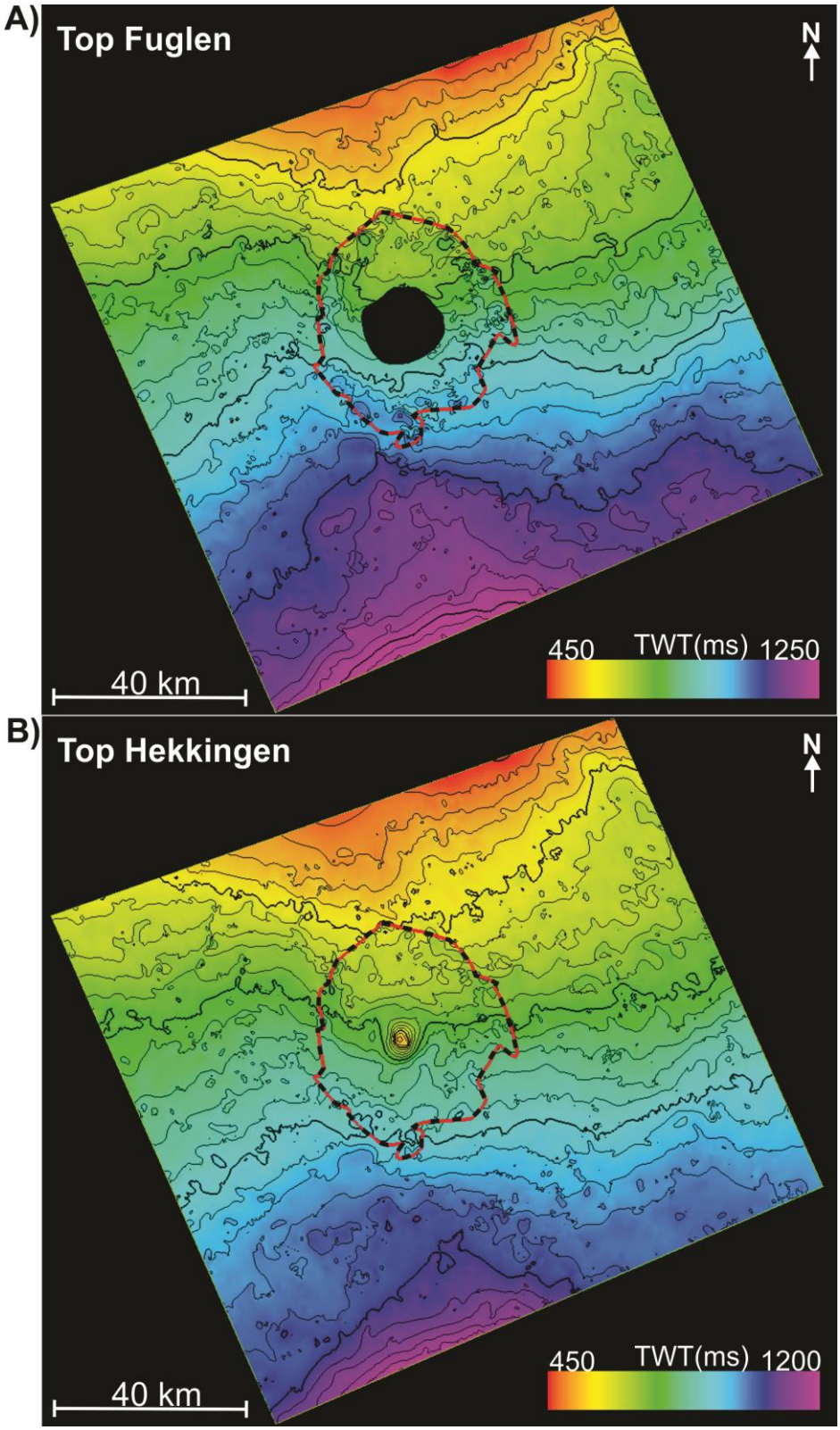

Figure 5.9: A) Two-Way-Time (ms) map of the Top Fuglen horizon with a contour line increment of 30 ms. B) Two-Way-Time (ms) map of the Top Hekkingen horizon with a contour line increment of 30 ms. Black stippled line indicated the disturbance zone, Mjølnir Impact Crater outlined in red.

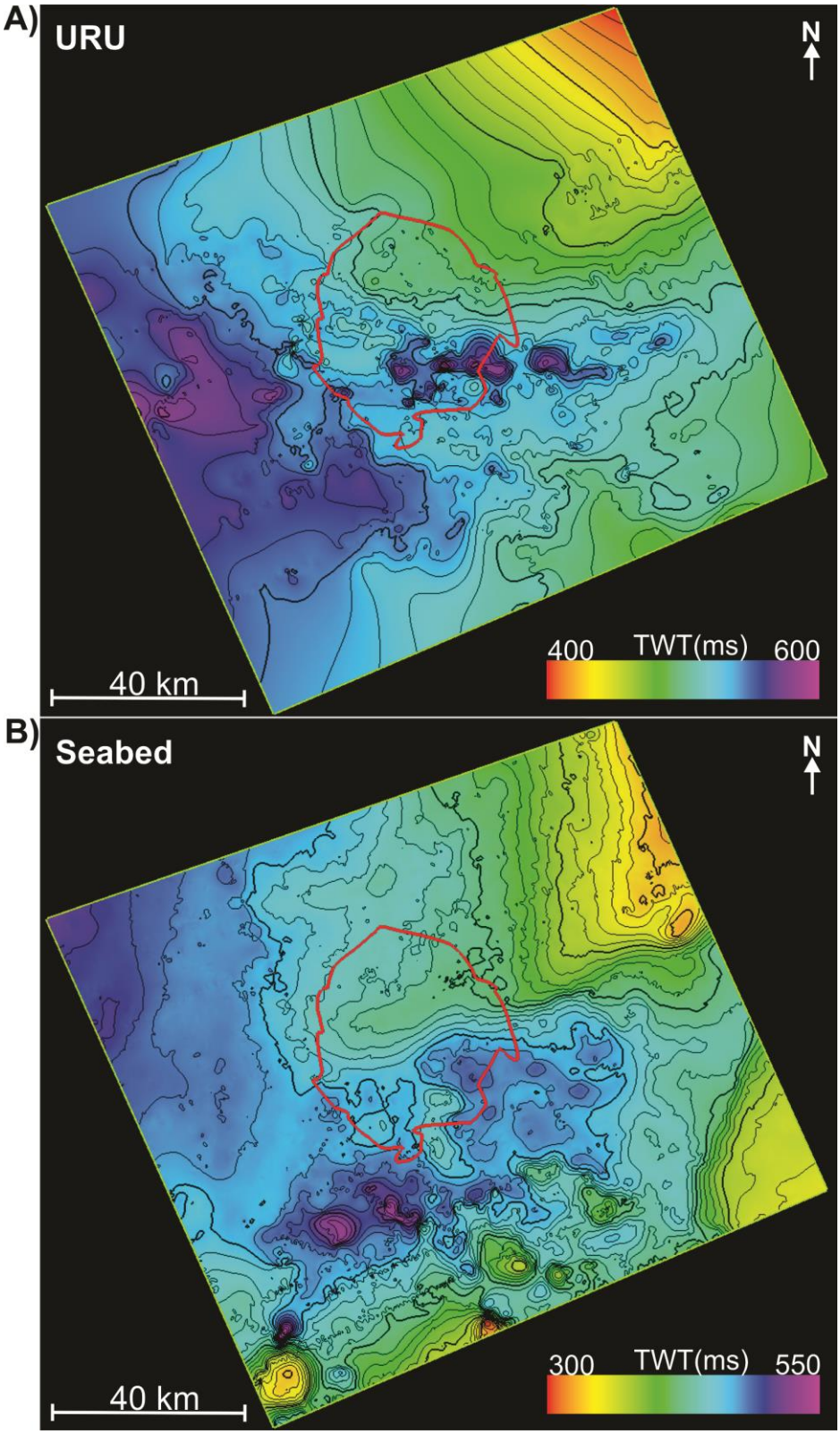

Figure 5.10: A) Two-Way-Time (ms) map of the URU horizon with a contour line increment of 10 ms. B) Two-Way-Time (ms) map of the Seabed horizon with a contour line increment of 10 ms. Mjølnir Impact Crater outlined in red.

5.2.2 Stratigraphic units

A total of 10 stratigraphic units have been identified (Fig 5.11-5.16). The units are described in the following sub-chapters and the thickness conversion for the Top Kobbe horizon – seabed horizon interval is done using the seismic velocities presented in Table 4.2. Velocities for the Top Kobbe horizon – Top Permian horizon interval is following Ktenas et al. (2018) (Appendix 9.1)

5.2.2.1 Havert Formation

The Havert Formation is confined at the base by the Top Permian horizon (Fig 5.6A) and at the top by the Top Havert horizon (Fig. 5.6B). The internal seismic signature of the formation is characterized by discontinuous, subparallel reflections of very low to transparent seismic amplitude (Fig. 5.4). Within the disturbance zone (DZ) the internal reflections lose continuity and turn chaotic. The formation ranges in time-thickness from 520 ms (1248 m) in the northwestern study area, gradually thickening towards the depocenter (associated with the Nordkapp Basin) located in southeast with a maximum thickness of 760 ms (1824 m) (Fig. 5.11A). The time-thickness map in Figure 5.11A also show small, localized anomalously high and low values in the annular depression of the Mjølnir Impact Crater.

5.2.2.2 Klappmyss Formation

The Klappmyss Formation is confined at the base by the Top Havert horizon (Fig. 5.6B) and at the top by the Top Klappmyss horizon (Fig. 5.7A). The internal seismic signature of the Klappmyss Formation is characterized by parallel to subparallel, disrupted seismic reflections of medium to low amplitude. Moving from the periphery, towards the center of the Mjølnir Impact Crater, the seismic signature becomes gradually more chaotic (Fig 5.4). The time-thickness ranges between 340 ms (816 m) and 460 ms (1104 m) and shows thinning towards the northwest (Fig. 5.11B). The time-thickness map in figure 5.11B also show local thinning of the formation within the annular depression and central high of the Mjølnir Impact Crater (i.e. within the disturbance zone).

5.2.2.3 Kobbe Formation

The Kobbe Formation is confined at the base by the Top Klappmyss horizon (Fig. 5.7A) and at the top by the Top Kobbe horizon (Fig 5.7B). The internal seismic reflection configuration is characterized by sub-parallel, discontinuous seismic reflections of low amplitude, transitioning into chaotic seismic signals within the disturbance zone (Fig 5.4). The formation

time-thickness range between 150 ms (285 m) and 275 ms (522 m) in the study area (Fig. 5.12A). The time-thickness map in Figure 5.12A displays a depocenter to the east and it thins out towards the north and the east. In the central high of the Mjølnir Impact Crater the thickness of the Kobbe Formation is characterized by anomalously high values (ms) (Fig. 5.12A). This is probably due to the absence of the Top Kobbe horizon in the central high. In the annular depression the time-thickness of the Kobbe Formation is characterized by anomalously low values (ms).

5.2.2.4 Snadd Formation

The Snadd Formation is confined at the base by the Top Kobbe horizon (Fig 5.7B) and at the top by the Top Snadd horizon (Fig. 4.8A). The internal seismic signature of the Snadd Formation is characterized by parallel to subparallel seismic reflections of medium to low amplitude in the surrounding Bjarmeland Platform. In the outer zone of the Mjølnir Impact Crater the upper part of the formation is incorporated in the disturbance zone (Fig. 5.4). The internal seismic signature gradually becomes more chaotic, and deeper levels of the formation is included in the DZ moving from the outer parts of the crater towards the annular depression (Fig. 5.4). The Snadd Formation is also characterized by ellipse-shaped high amplitudes throughout the study area (Fig. 5.4-5.5). The lobes occur throughout the formation vertically, but more frequently in central parts. Their measured size in the vertical section vary from a few hundred meters to several kilometers in length. The time-thickness of the formation varies between 220 ms (366 m) in the east and 400 ms (665 m) in the west (Fig. 5.12B). Thus, the thickness-map shows a trend of gradual thinning from east to west.

5.2.2.5 Realgrunnen Subgroup

The Realgrunnen Subgroup is confined at the base by the Top Snadd horizon (Fig. 5.8A) and at the top by the Top Stø horizon (Fig. 5.8B). The subgroup comprises the Stø-, Nordmela-, Tubåen- and Fruholmen formations, which are challenging to separate due to limitations in data quality and resolution. The internal seismic reflection configuration is characterized by parallel to subparallel seismic reflections of high to low amplitude in the platform areas. Within the Mjølnir Impact Crater where the Realgrunnen Subgroup is mapped, the seismic signature is characterized by highly deformed and chaotic seismic reflections (Fig. 5.4). The time-thickness map displays that the Realgrunnen Subgroup has higher values (ms) in the southern study area, becoming thinner towards the north (Fig. 5.13A). In the periphery of the

Mjølnir Impact Crater the subgroup is considerably thinner compared to on the adjacent Bjarmeland Platform (Fig. 5.13A). The faulting and disturbance of the interpreted Top Stø horizon compared to the underlying Top Snadd horizon is the reason for the variation in time thickness in the periphery of the crater (Fig. 4.13A). The time-thickness map shows the thickness variations as localized and circular, but this is assumed to be related to the sparse data-coverage and subsequent interpolation of horizons.

5.2.2.6 Fuglen Formation

The Fuglen Formation is confined at the base by the Top Stø horizon (Fig. 5.8B) and at the top by the Top Fuglen horizon (Fig. 5.9A). The internal seismic signature is characterized by continuous reflections of medium amplitude (Fig 5.4). Within the disturbance zone the Fuglen Formation is highly deformed and cannot be mapped inward of the annular depression (Fig. 5.2). The time-thickness of the Fuglen Formation varies between 10 ms (15 m) and 70 ms (101 m) within the study area, with no apparent trends (Fig. 5.13B). The time-thickness map of the Fuglen Formation (Fig. 5.13B) shows similar thickness variation trends in the periphery of the Mjølnir Impact Crater, as described for the Realgrunnen Subgroup (Fig. 5.13A).

5.2.2.7 Hekkingen Formation

The Hekkingen Formation is confined by the Top Hekkingen horizon (Fig. 5.9B) throughout the study area. The base of the formation is represented by the Top Fuglen horizon (Fig. 4.9A) on the Bjarmeland Platform, and by the previously termed Top Disturbance (TD) within the Mjølnir Impact Crater (Fig 5.4). The internal configuration is characterized by continuous, parallel reflections of high to medium amplitude (Fig. 5.4). The time-thickness map of the Hekkingen Formation shows depocenters in the south-southeast parts of the study area, where the thickness is about 90 ms TWT (113 m), and it becomes thinner towards the north-northeast, where the thickness is about 25 ms TWT (31 m). Within the boundaries of the Mjølnir Impact Crater, the Hekkingen Formation is considerably thinner, ranging only from a few milliseconds to 50 ms TWT (63 m) (Fig. 5.14A)

5.2.2.8 Cretaceous unit

The base of the Cretaceous unit is represented by the Top Hekkingen horizon (Fig. 5.9B), and its top is represented by Upper Regional Unconformity horizon (Fig. 5.10A) and the Seabed horizon (Fig. 5.10B). The Cretaceous unit most likely encompass formations from the upper Adventdalen group (Knurr-, Klippfisk-, Kolje-, and Kolmule formations), indicated from the

well tops of well 7435/12-1 (Korpfjell). The internal seismic signature is characterized by parallel reflections of medium to low amplitude (Fig. 5.4). There are also visible wedge-shaped reflections within the unit, that seemingly gradually become thinner towards the South East (Fig. 5.5). The time-thickness values (ms) are highest in the southern parts of the study area, where the thickness is 600 ms TWT (716 m) (Fig. 5.14B). The unit gradually becomes thinner towards the northern parts of the study area, where it is truncated by the URU/Seabed (Fig. 5.5). The time-thickness map shows anomalously low values (ms) on the central high of the Mjølnir Impact Crater (Fig. 5.14B).

5.2.2.9 Naust Formation

The Naust Formation is confined at the base by the Upper Regional Unconformity horizon (URU) (Fig. 5.10A) and at the top by the Seabed horizon (Fig. 4.10B) and represents the Quaternary deposits in the study area. The formation is not mappable within parts of the study area, as URU cannot be distinguished from the Seabed horizon, since the formation thickness is most likely below the vertical resolution of the 2D seismic data. The internal reflection configuration of the Naust Formation is characterized by subparallel reflections of low amplitude to transparent reflections (Fig. 5.4). The time-thickness of the Naust Formation range between 0 ms and 120 ms within the study area. The time-thickness map shows four prominent depocenters with an approximate thickness of 120 ms (108 m) located along the edges of the study area – two located in the south, one in the northeast and one to the east (Fig. 5.15). The Naust Formation is also characterized by a ridge located directly above the central uplift of the Mjølnir Impact Crater, shown as an elongated lobe with a west-east orientation (Fig. 5.15.). There are also four small, localized depocenters within the boundaries of the Mjølnir Impact Crater. Three of these coincide with the previously mentioned depressions in the interpreted URU horizon (Fig. 5.15), where the internal Cretaceous reflectors below are truncated by the depression (Fig. 5.17). Figure 5.17A-C displays Depressions 1-3 in a vertical seismic section. Depression 1 is shown on an ultra-high resolution P-cable line, which shows internal semi-continuous reflections within the depression (Fig 5.17A).

5.2.2.10 Ragnarok Formation Unit II

The top Ragnarok Formation Unit II is represented by the Top Disturbance horizon and its base is represented by the Lower Boundary horizon (Fig. 5.4). The interpreted unit is only

mapped within the boundaries of the Mjølnir Impact Crater. The internal seismic configuration of the unit is characterized by discontinuous chaotic to transparent reflections in the outer zone. In the annular depression, the interpreted unit display some discontinuous, subparallel reflections (Figs. 5.4-5.5). The time-thickness map of the unit fluctuates between 20 ms and 120 ms within the Mjølnir Impact Crater (Fig. 5.16). The unit displays a general concentric trend of thickness variations (Fig. 5.16). Along the outer boundary of the Mjølnir Impact Crater, the unit has a thickness exceeding 100 ms (TWT) in many places. Inwards in the outer zone, the unit gradually becomes thinner until reaching the annular depression. Within the annular depression, the unit becomes thicker (>100ms), forming a concentric depocenter surrounding the central high of the Mjølnir Impact Crater. From the annular depression towards the central high, the Ragnarok Formation Unit II gradually thins out (Fig. 5.4), displayed as low values (~20 ms) in Figure 5.16.

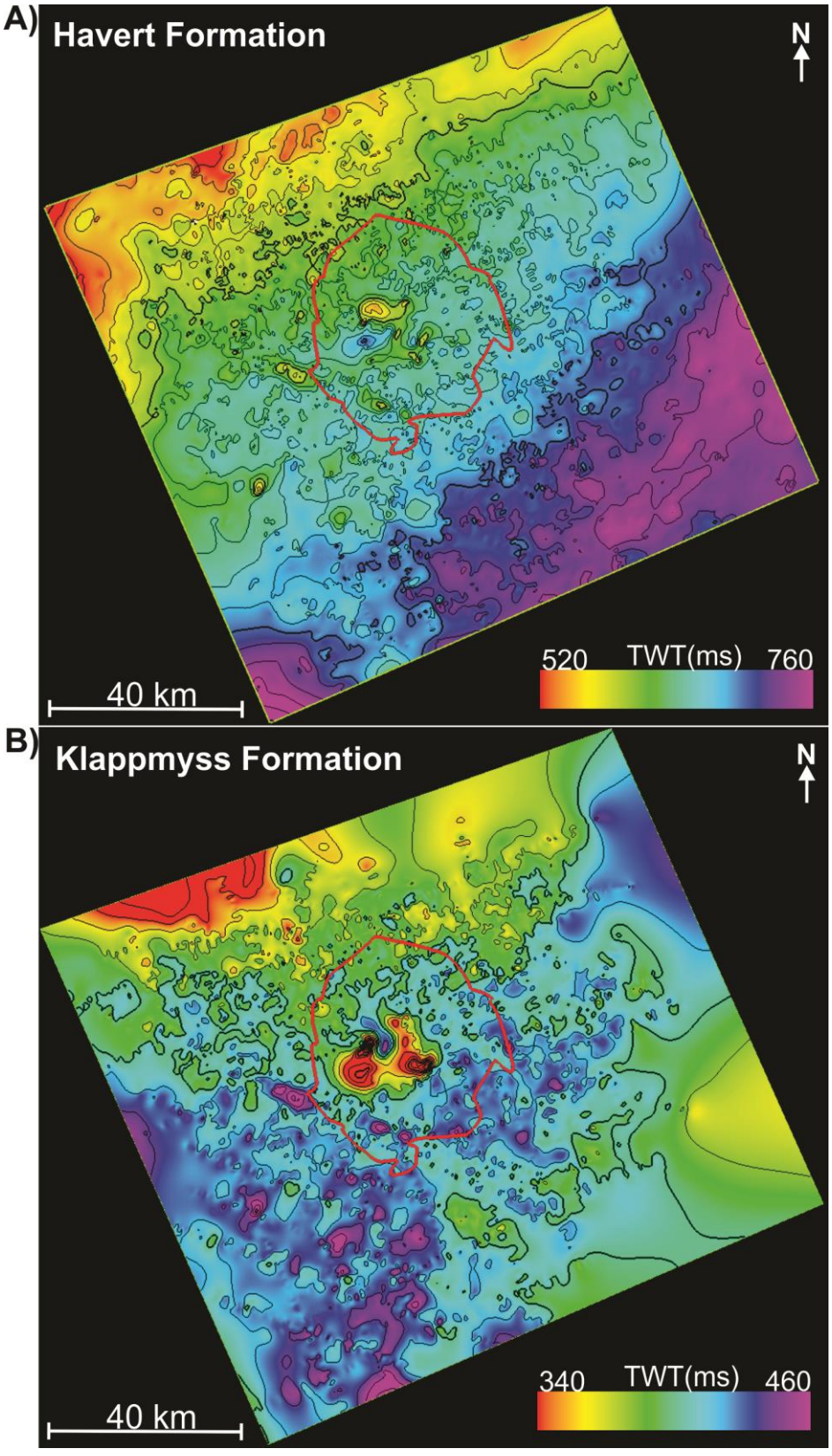

Figure 5.11: A) Time-thickness map TWT (ms) of the Havert Formation with a contour line increment of 20 ms. B) Time-thickness map TWT (ms) of the Klappmyss Formation with a contour line increment of 20 ms. Mjølnir Impact Crater outlined in Red.

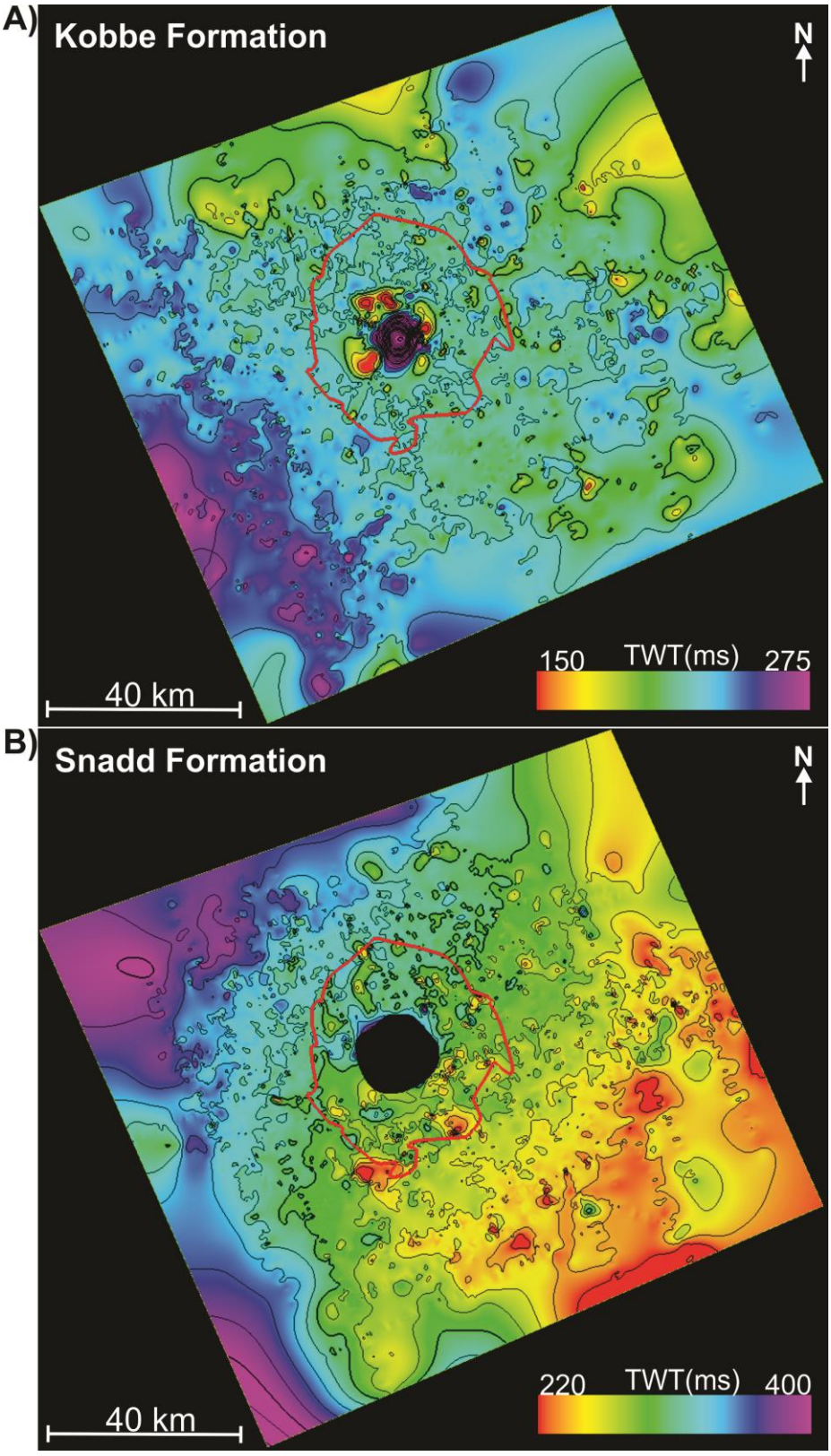

Figure 5.12: A) Time-thickness map TWT (ms) of the Kobbe Formation with a contour line increment of 20 ms. B) Time-thickness map TWT (ms) of the Snadd Formation with a contour line increment of 20 ms. Mjølnir Impact Crater outlined in Red.

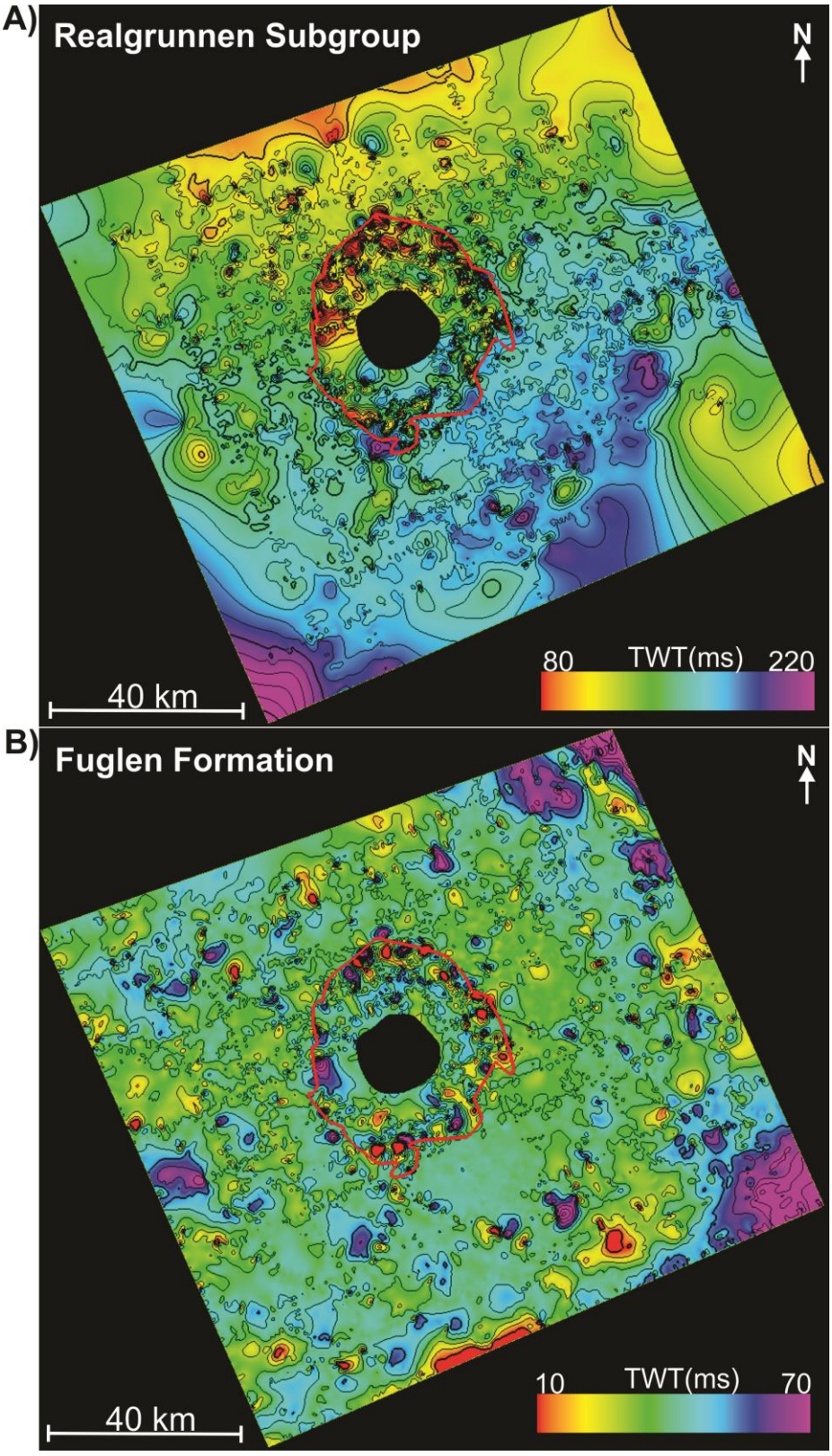

Figure 5.13: A) Time-thickness map TWT (ms) of the Realgrunnen Subgroup with a contour line increment of 10 ms. B) Time-thickness map TWT (ms) of the Fuglen Formation with a contour line increment of 10 ms. Mjølnir Impact Crater outlined in Red.

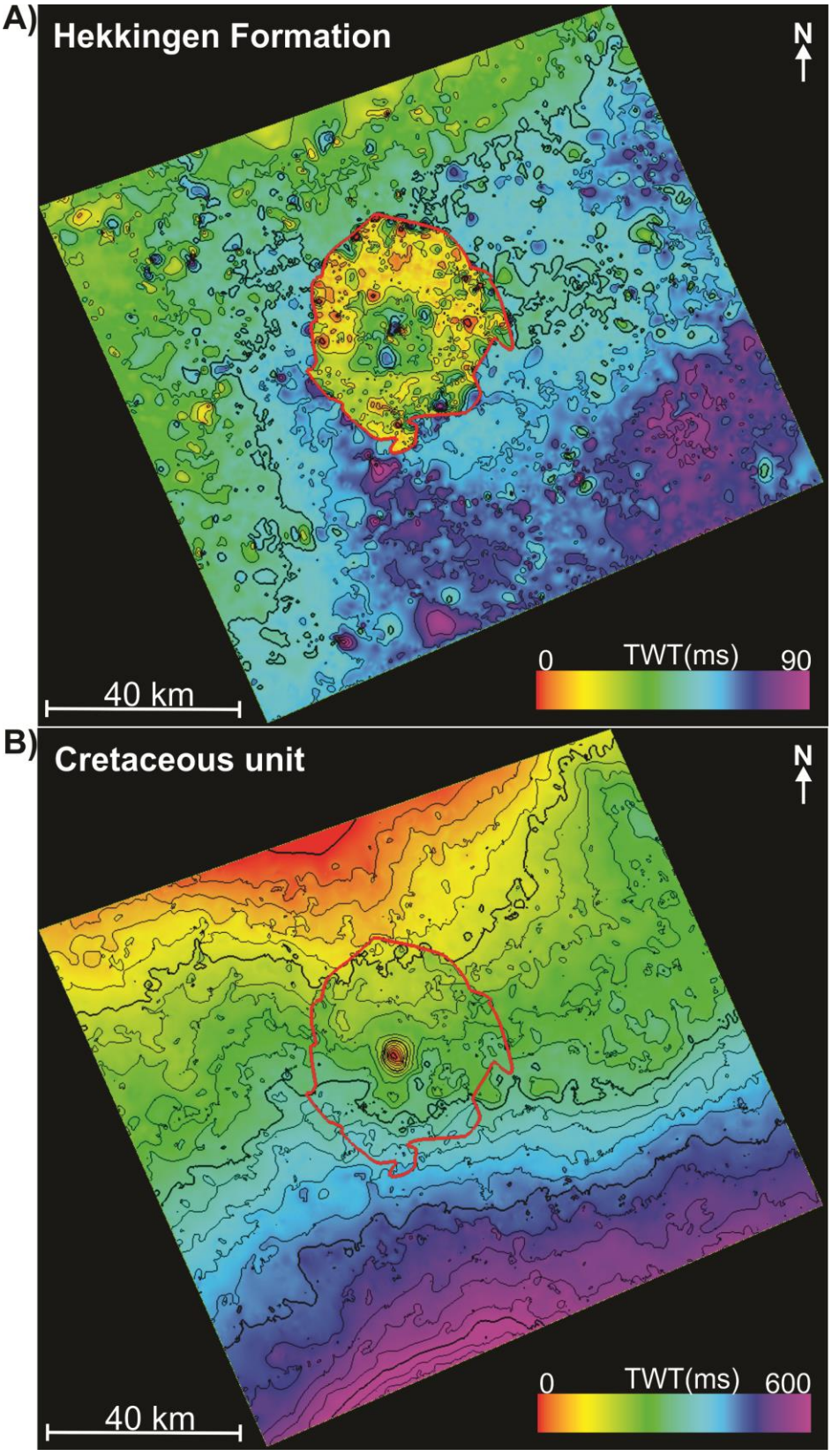

Figure 5.14: A) Time-thickness map TWT (ms) of the Hekkingen Formation with a contour line increment of 10 ms. B) Time-thickness map TWT (ms) of the Cretaceous unit with a contour line increment of 30 ms. Mjølnir Impact Crater outlined in Red.

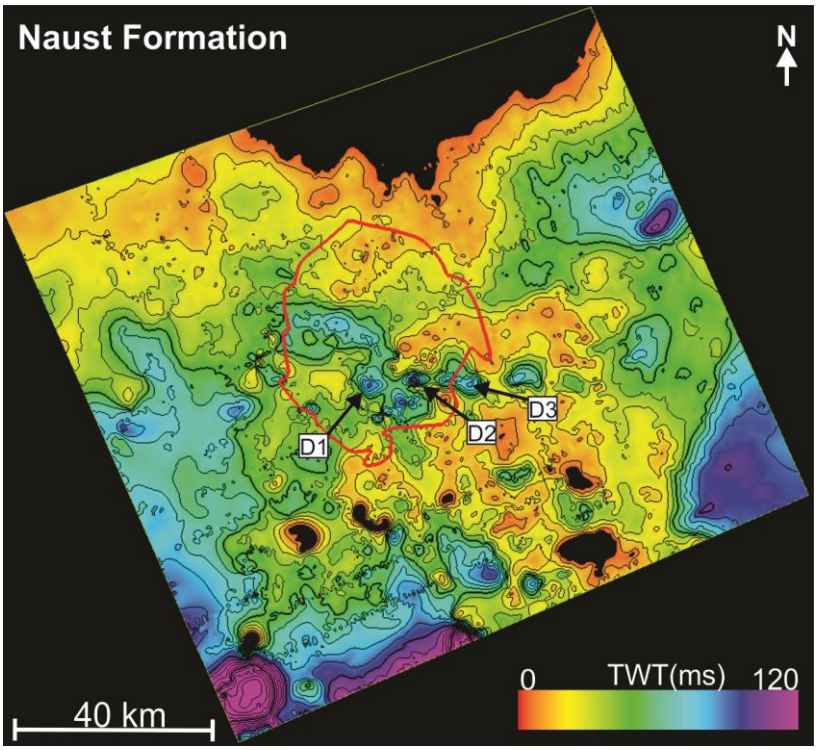

Figure 5.15: Time-thickness map TWT (ms) of the Naust Formation with a contour line increment of 10 ms. Depressions (D1, D2, D3) are indicated by black arrows. Mjølnir Impact Crater outlined in red.

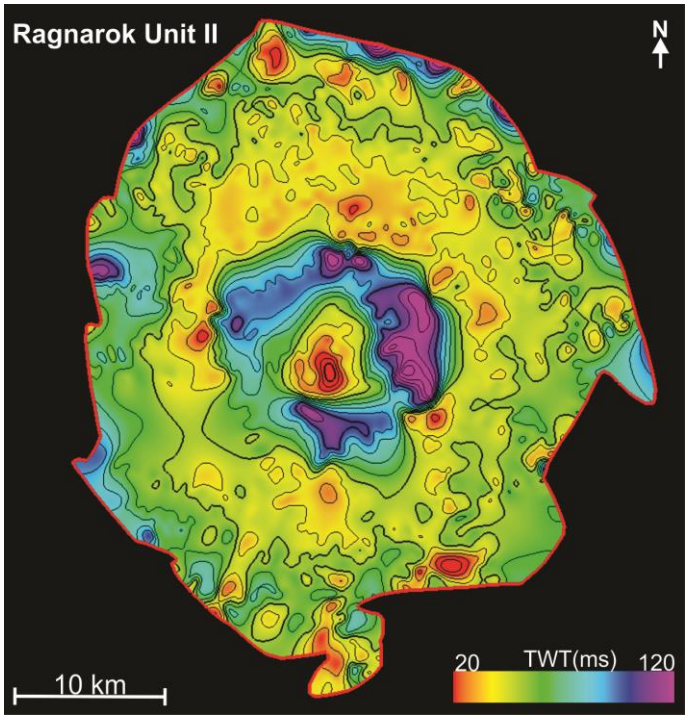

Figure 5.16: Time-thickness map TWT (ms) of the Ragnarok Formation Unit II within the Mjølnir Impact Crater (red outline). Contour line increment is set to 10 ms.

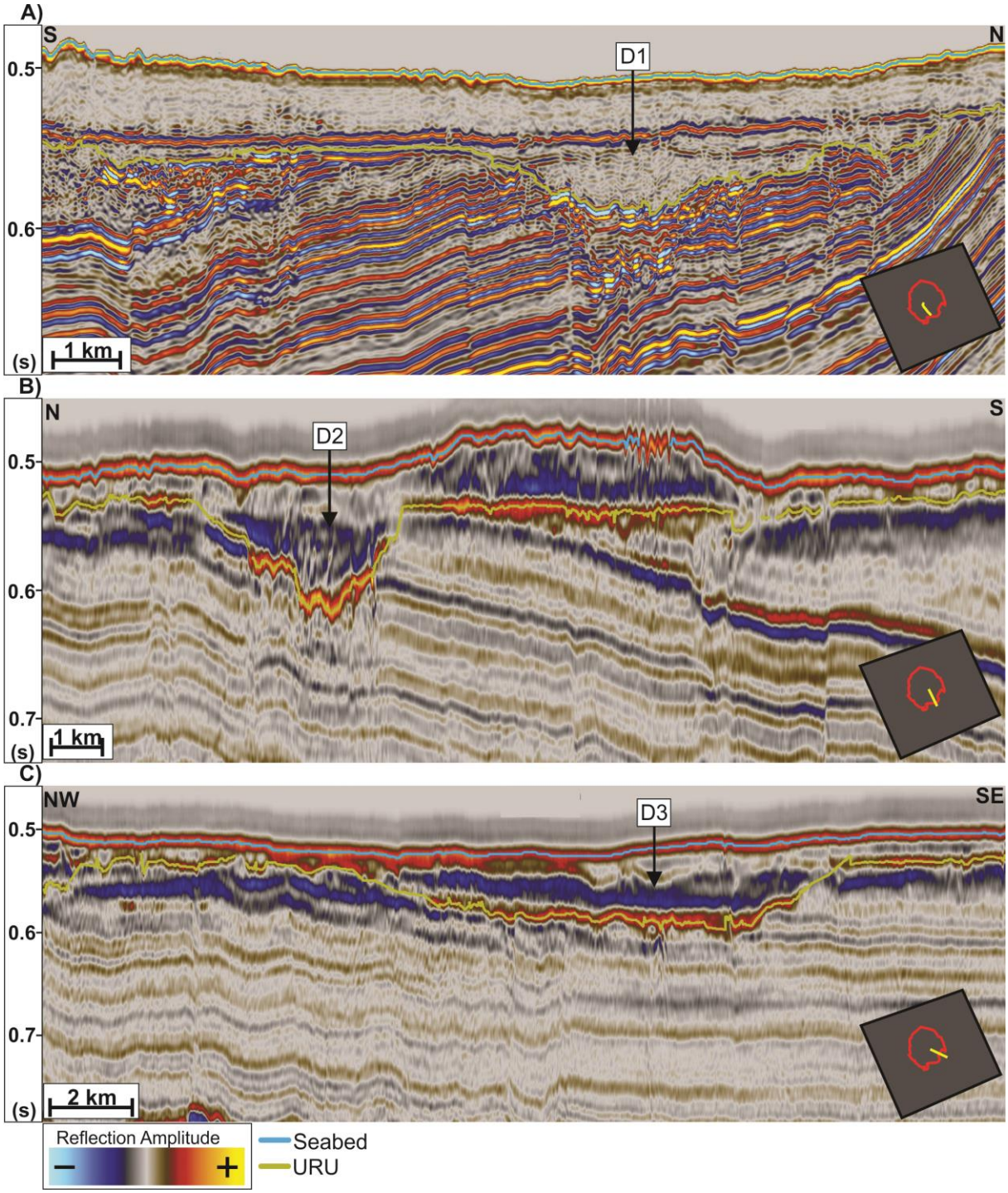

Figure 5.17: A) Displays an ultra-high resolution P-cable line (TGS15002) through depression 1 (D1), showing the semi-continuous reflections within the depression. B) Displays a 2D seismic line (NBR14-266837) through depression 2 (D2). C) Displays a 2D seismic line (NBR14-362688) through depression 3 (D3).

5.3 Faults

The Mjølnir Impact Crater is characterized by deformation and faulting of the stratigraphic units described in chapter 5.2.2. The outer boundary of the structure is represented by major faults crosscutting strata from the Upper Triassic to URU (Figs. 5.18-5.24). These prominent faults correspond to rim faults, representing the horizontal limit of the deformation induced by the Mjølnir impact event (Figs. 5.23-5.25)**.** The rim faults mark a distinct transition from the unaffected Bjarmeland Platform, to highly faulted and deformed strata within the Mjølnir Impact Crater. The nature of the deformation and chaotic seismic signal that characterize the Mjølnir Impact Crater makes it challenging to identify and interpret faults. This, in combination with data coverage also make it difficult to laterally map and distinguish certain faults and determine the exact strike orientation. The following subchapters describe faulting according to the distinct radial zones – the outer zone, annular depression and central high (Tsikalas et al., 1998c).

5.3.1 Rim faults

The outer boundary of the Mjølnir Impact Crater and start of the outer zone is defined by rim faults (Figs. 5.18-5.25). The rim faults correspond to the outermost horizontal limit of the disturbance zone. Rim faults of the Mjølnir Impact Crater have an apparent dip towards the center of the structure, creating a concentric strike pattern. The rim faults have a vertical extent affecting post-impact intervals up to URU and their lower extent is limited to the interpreted Snadd Formation. It is difficult to map exactly where the rim faults terminate within the Snadd Formation due to the disturbed seismic pattern, but the slope angle seemingly decrease with depth (Figs. 5.20-5.22). The vertical displacement of reflectors along the rim faults are largest in the Jurassic intervals. The rim faults generally show a varying vertical throw between 65 ms and 100 ms (TWT) along the Top Stø horizon. The younger Hekkingen Formation and Cretaceous unit are less vertically displaced, compared to the deeper strata, with a vertical throw between 20 ms and 30 ms (TWT). In the northern parts of the Mjølnir Impact Crater, one seismic line shows an anomalously high vertical displacement along a rim fault, where the Top Stø horizon is displaced 130 ms, and 72 ms for reflections of the Cretaceous unit (Fig. 5.18).

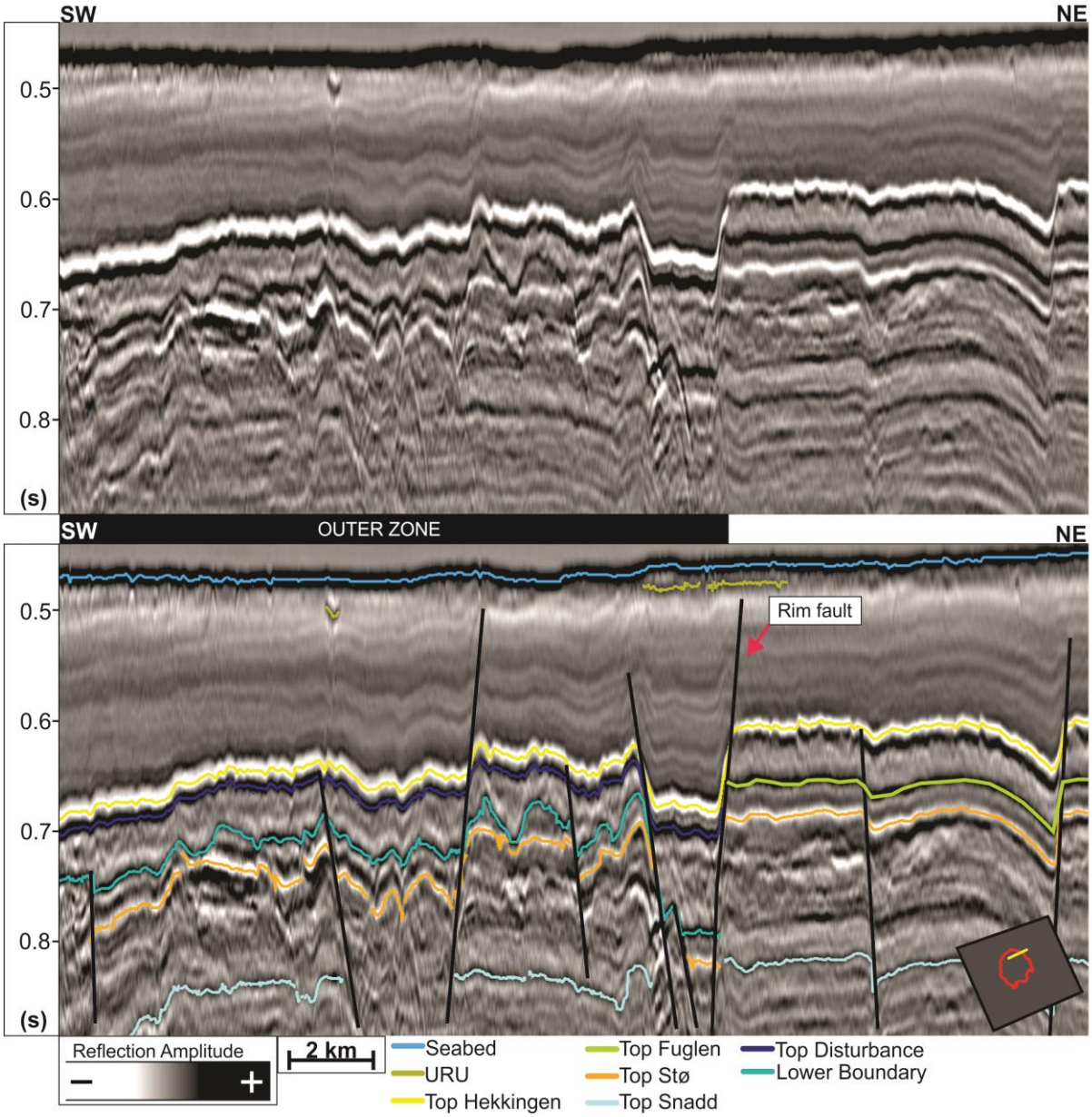

Figure 5.18: The figure displays a uninterpreted (top) and interpreted (bottom) 2D seismic line (NBR14-148000) of the outer zone of the northern Mjølnir Impact Crater and the adjacent platform-area. The highlighted rim fault represents the boundary between the Bjarmeland Platform and the Mjølnir Impact Crater and is characterized by an anomalously high vertical displacement of the seismic reflections.

5.3.2 Outer zone

Inward from the rim faults in the outer zone of the Mjølnir Impact Crater, the structural characterization and deformation vary. The distal outer zone comprises features such as half grabens and horst and graben structures. The formation of horst and graben structures are most prominent in the eastern Mjølnir Impact Crater (Fig. 5.19). Horst and graben structures are also observed in the northern- (Fig. 5.20) and southern outer zone (Fig. 5.21). The distal outer zone of the eastern crater shows well-defined horst and graben structures, comprised by faults that have a variable vertical extent. The most prominent faults extend from URU and terminate within the Snadd Formation (Figs. 5.19 & 5.21). A majority of the faults within the outer zone does however seem to be limited to the Top Disturbance (TD) – Top Kobbe interval (Fig 5.20-5.22). The faults of the outer zone share some of the same characteristics as the adjacent rim faults. They seem to share the same strike orientation, dipping towards the central high or the opposing direction. The faults of the distal outer zone vertically displace the Late Triassic – Jurassic interval more than the overlying Cretaceous unit. Generally, the Top Stø – LB interval is vertically offset by several 10s of milliseconds, while the TD – URU interval is less affected by the faults. The Cretaceous unit above the eastern Mjølnir Impact Crater also display highly deformed and folded reflectors within the grabens (Figs. 5.19 & 5.23). The outer zone of the western Mjølnir Impact Crater contrasts, as the affected reflections are less vertically displaced (excluding the rim faults). The area is however characterized by highly distorted reflections (Fig. 5.22). The westernmost distal outer zone is seemingly dominated by half-grabens with internally tilted reflections, where faults generally dip towards the center of the crater (Fig. 5.22). The faulting of the distal outer zone in the western areas vertically displace the reflections a few milliseconds (Figs. 5.22-5.23).

Towards the annular depression, faults are more frequently observed in the southern and eastern crater. The dense faulting is primarily limited to the Top Hekkingen – LB interval (Figs. 5.21, 5.23, 5.24). The faulting is restricted to a relatively thin interval, thus making it hard to interpret on seismic lines with lower resolution. In the southern and eastern parts of the Mjølnir Impact Crater, there are visible faults offsetting the interval URU – LB in the proximal outer zone (Fig. 5.23&5.24). The proximal outer zone generally displays increasingly deformed reflectors, and the disturbance zone extends vertically, eventually affecting the strata down to the Top Kobbe horizon. Figure 5.25 displays two prominent faults

dipping towards the central high, coinciding with the boundary between the outer zone and the annular depression.

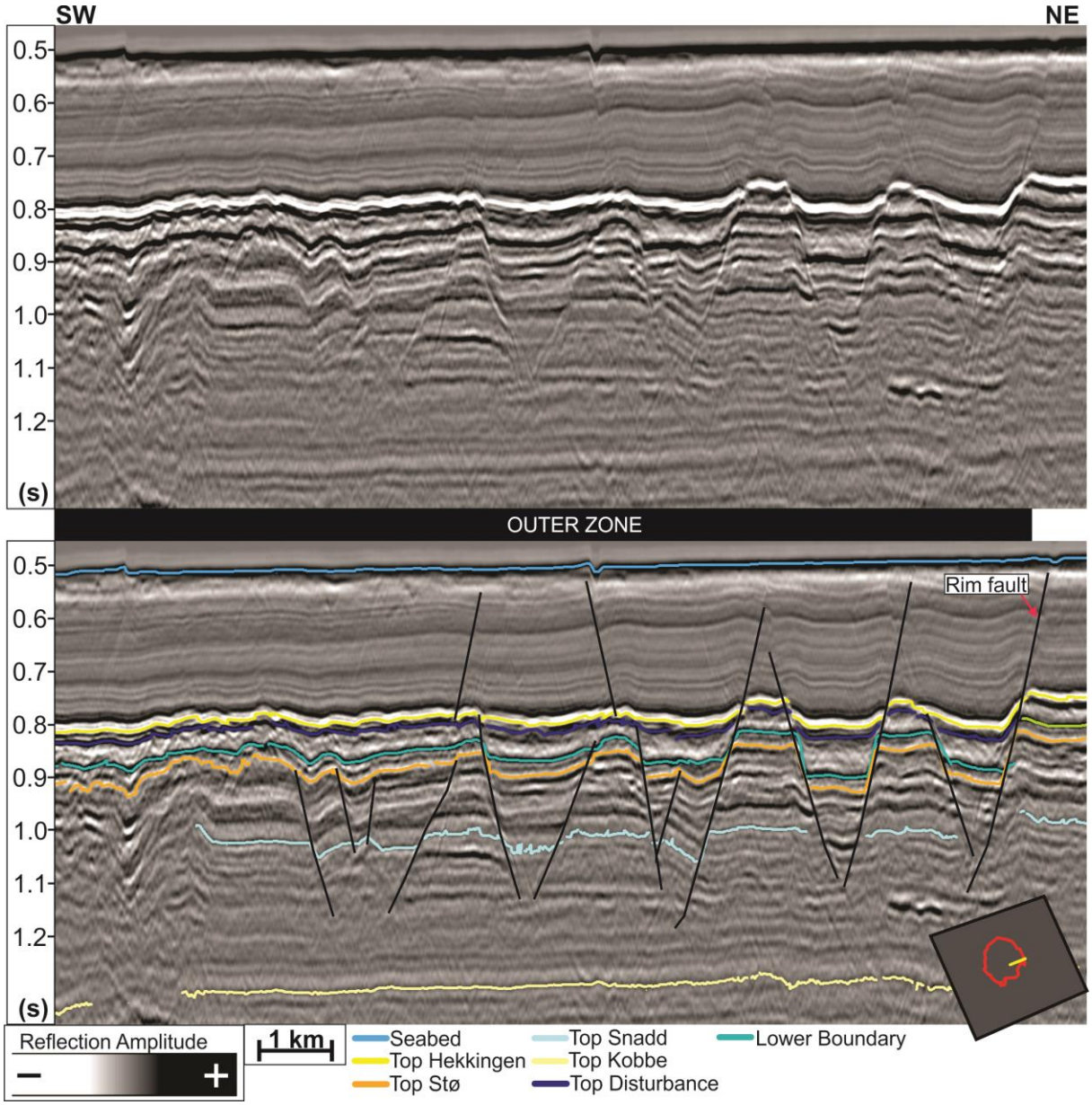

Figure 5.19: The figure displays the uninterpreted (top) and interpreted (bottom) 2D seismic line (NBR14-145787) of the outer zone of the eastern Mjølnir Impact Crater. The interpretation shows repetitive horst and graben structures in the interval URU – Intra Snadd Formation at the distal outer zone, in the grabens the internal reflections of the Cretaceous unit show signs of deformation.

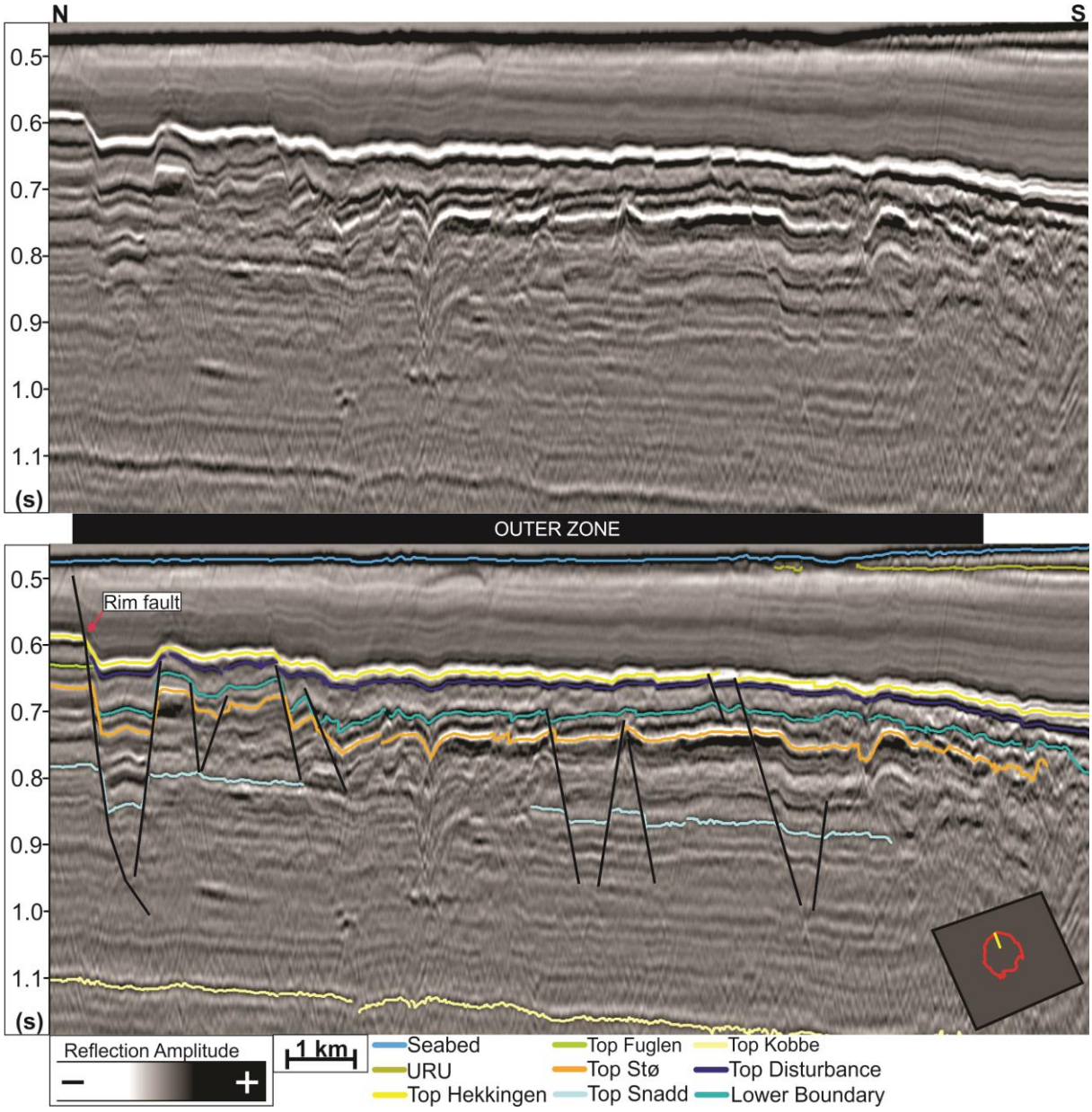

Figure 5.20: The figure displays the uninterpreted (top) and interpreted (bottom) 2D seismic line (NBR14-266837) of the outer zone of the northern Mjølnir Impact Crater. The interpretation shows less developed horst and graben structures at the distal outer zone, compared to the eastern areas (Fig. 5.21).

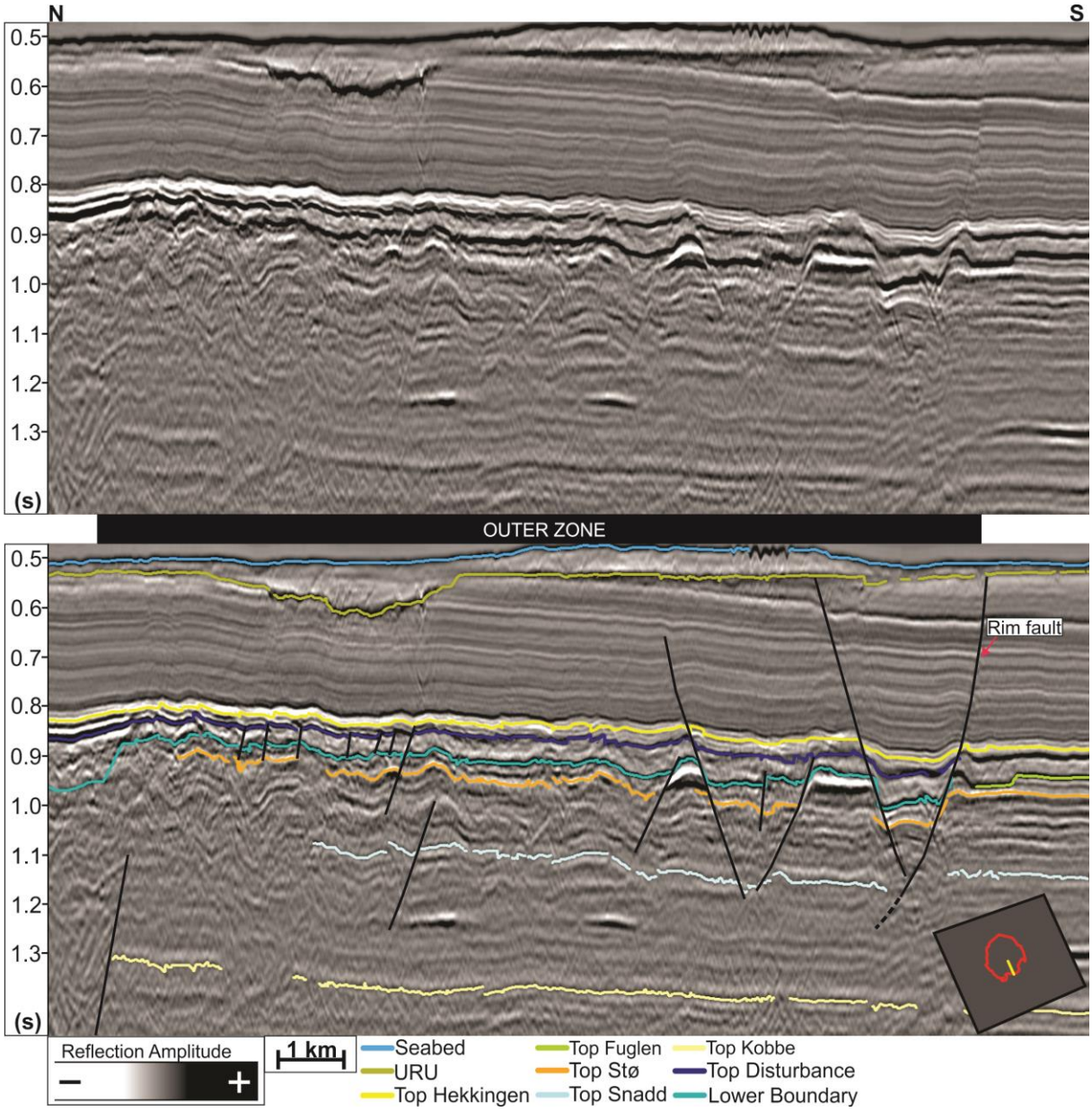

Figure 5.21: The figure displays an uninterpreted (top) and interpreted (bottom) 2D seismic line (NBR14-266837) of the outer zone of the southern Mjølnir Impact Crater.

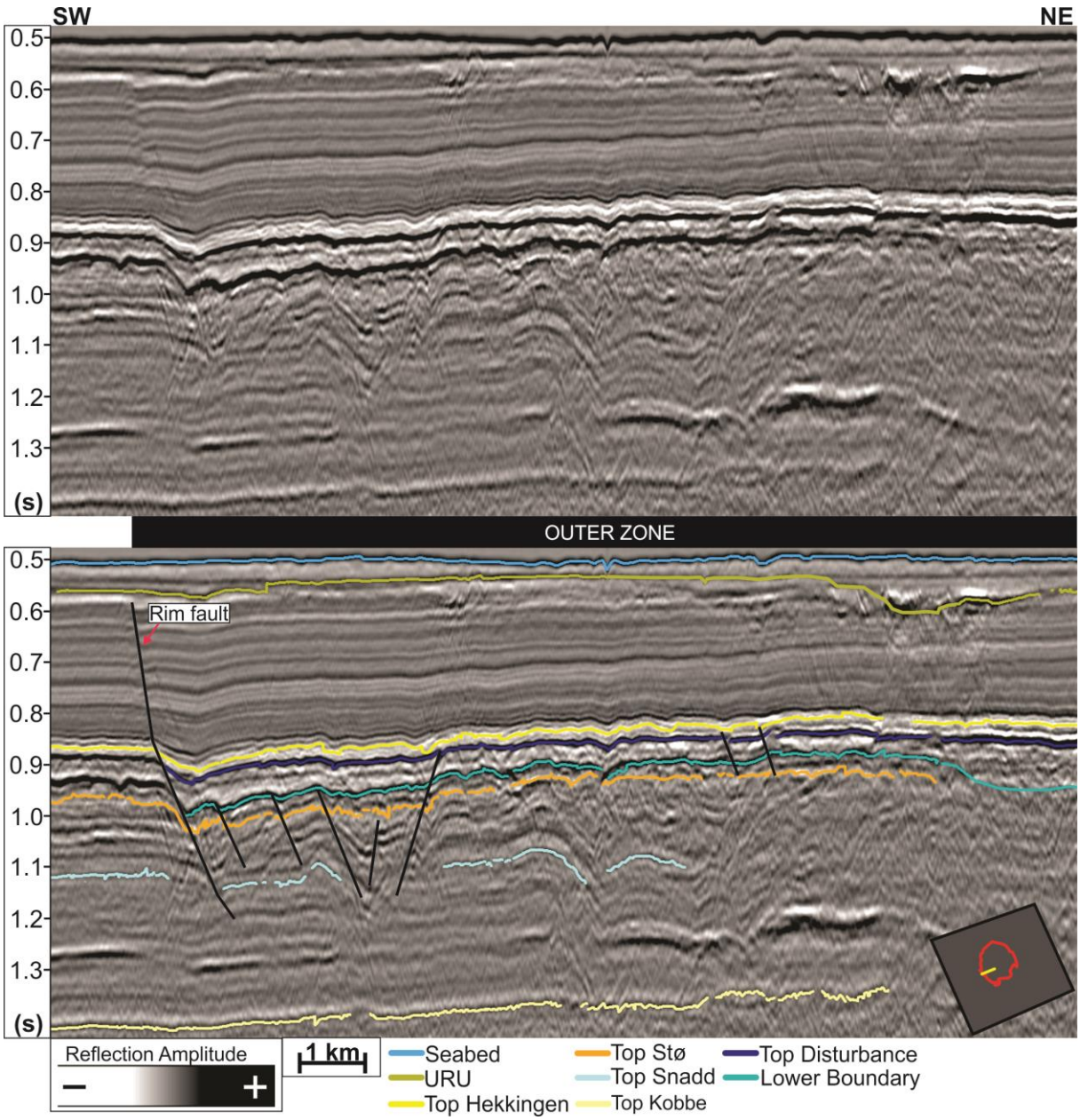

Figure 5.22: The figure displays an uninterpreted (top) and interpreted (bottom) 2D seismic line (NBR14-145787) of the outer zone of the western Mjølnir Impact Crater. The faulting here is characterized by rotated fault blocks with less vertical offset, in contrast to the horst and graben structures elsewhere in the outer zone.

5.3.3 Annular depression and central high

The investigation of the annular depression and central high is limited by data coverage. More specifically, this study is limited to a single conventional seismic line and two P-cable lines displaying the central high. The central parts of the Mjølnir Impact Crater (annular depression and central high) are also characterized by increasing chaotic reflections and transparent seismic reflections, making it challenging to identify faulting, and determine their vertical extent.

The annular depression is generally characterized by little faulting of strata in the shallow subsurface (URU – TD interval) (Figs. 5.23&5.24). The most prominent faulting is located in the southern annular depression, where two faults vertically displace reflectors from URU to intra Ragnarok Formation Unit II (Fig. 5.24). In the upper part of the Cretaceous unit, a few faults are observed (Figs. 5.23&5.24). The located faults all show structural dip away from the central high, displacing internal reflectors rising towards the central high. These shallow faults are not seen westward of the central high (Fig. 5.23). In the conventional 2D seismic line (Fig. 5.25), deeper-seated faults are identified. These faults construct a graben-like structure limited to the annular depression. The deeper seated, outer faults of these graben structures dip towards the central high, seemingly coinciding with the outline of the disturbance zone. The deep-seated faults proximal to the central high of the graben structure dip away from the center of the Mjølnir Impact Crater (Fig. 5.25). The faults vertically displace the Kobbe-, Klappmyss- and upper Havert formations downward. Northwest of the central high, internal faulting within the graben structure is also identified (Fig. 5.25).

On the flanks of the central high outward-dipping faults are interpreted. The upper extent of these faults is limited to the impact associated LB horizon, displacing the Ragnarok Formation Unit II onto terraces on the flanks of the central high (Figs. 5.23-5.24). It is difficult to determine how deep these faults extend, due to the chaotic reflections in the strata of the central high.

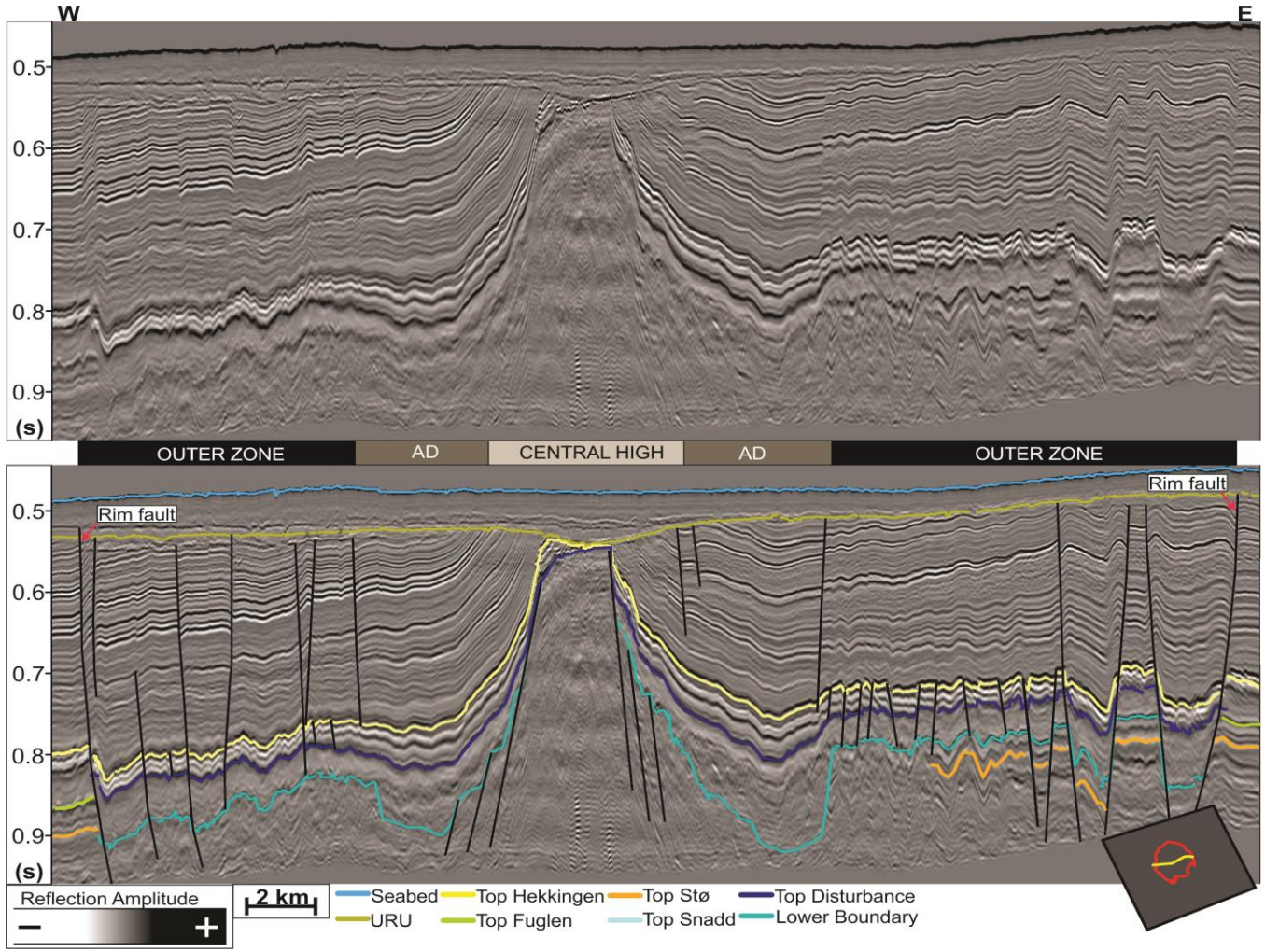

Figure 5.23: The figure displays the uninterpreted (top) and interpreted (bottom) west-east oriented P-cable line (TGS15002-HR15) through the Mjølnir Impact Crater. The figure shows prominent horst and grabens in the eastern outer zone and rotated fault blocks in the western parts. AD: Annular Depression

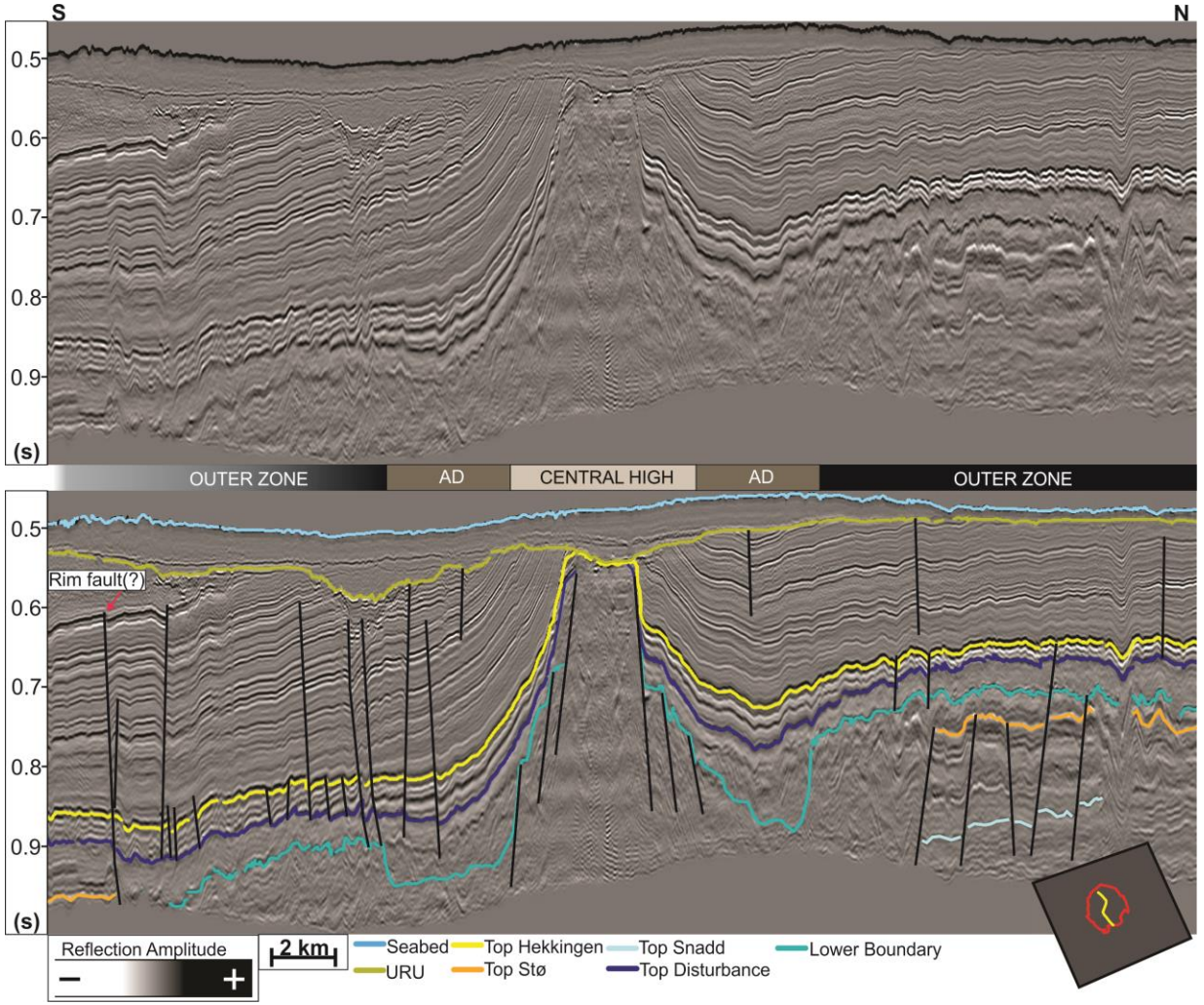

Figure 5.24: The figure displays the uninterpreted (top) and interpreted (bottom) north-south oriented P-cable line (TGS15002-HR15) through the Mjølnir Impact Crater. The line does not cross the rim faults of the northern Crater and does not cover the vertical extent of the rim faults to the south, thus identification is uncertain. AD = Annular Depression

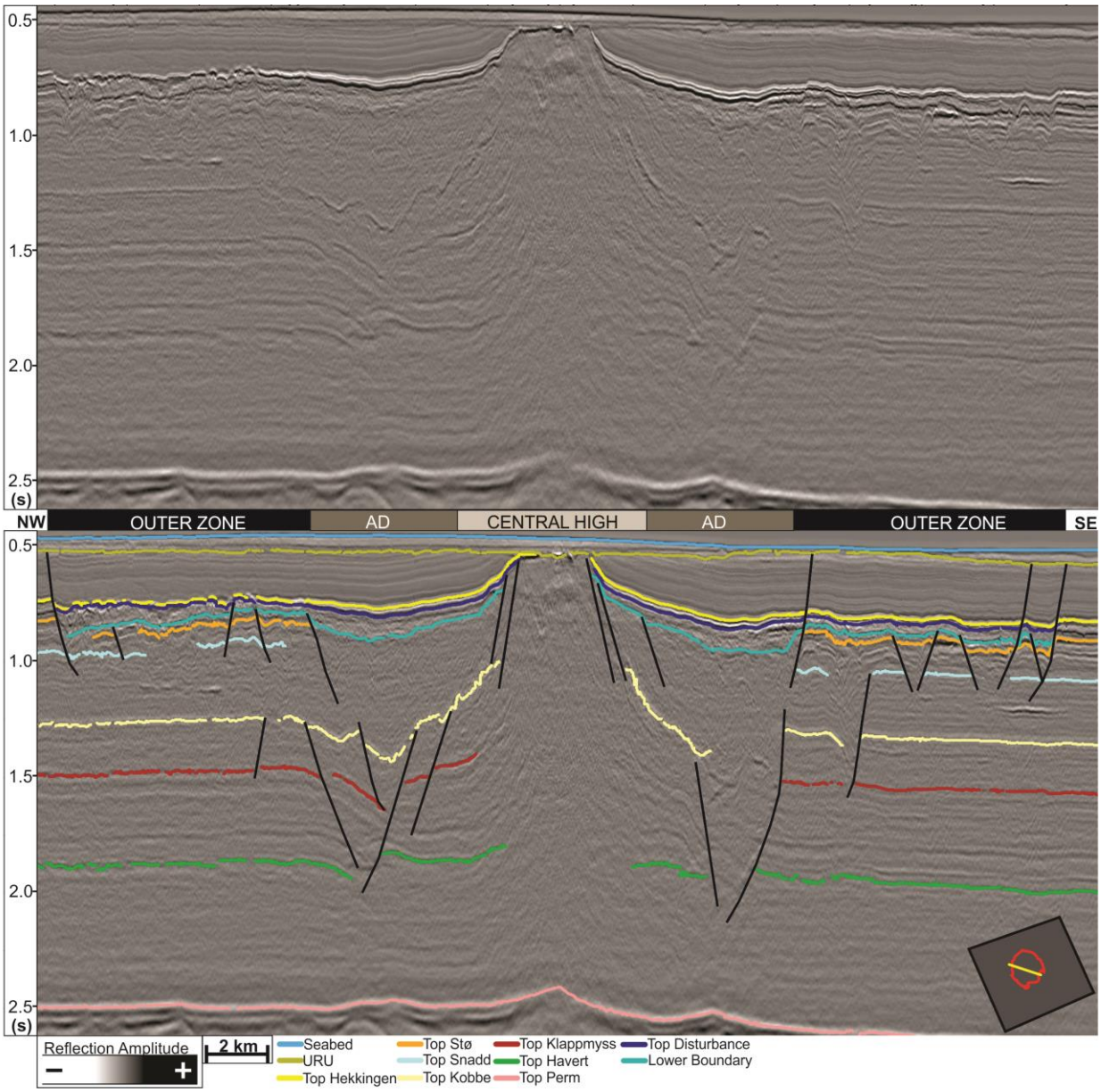

Figure 5.25: The figure displays the uninterpreted (top) and interpreted (bottom) seismic 2D line (NBR14-362688) through the Mjølnir Impact Crater. The outer zone shows contrasts when comparing east and west; the eastern areas show horst and graben structures and the western area shows faulting of less vertical throw, possibly rotated fault blocks. The annular depression shows deep-seated faults affecting the Top Kobbe – intra Havert Formation interval, constructing grabens.

5.4 Seismic amplitude anomalies

Amplitude anomalies are mapped within the Mjølnir Impact Crater and along the interpreted rim faults. The amplitude anomalies are primarily concentrated to the southern parts of the Mjølnir Impact Crater (Fig. 5.26). The presented amplitude anomalies encompass previously described bright spots, chimney structures and possible flat spots (chapter 2.5.2). Due to the data coverage and apparent size of the anomalies, most anomalies are only visible and displayed on one seismic line (Figs. 5.27-5.34), constraining detailed descriptions and size estimates. For simplicity the anomalies are annotated as amplitude anomalies (AA) and given numbers. The distribution and stratigraphic position of amplitude anomalies is displayed in Figure 5.26.

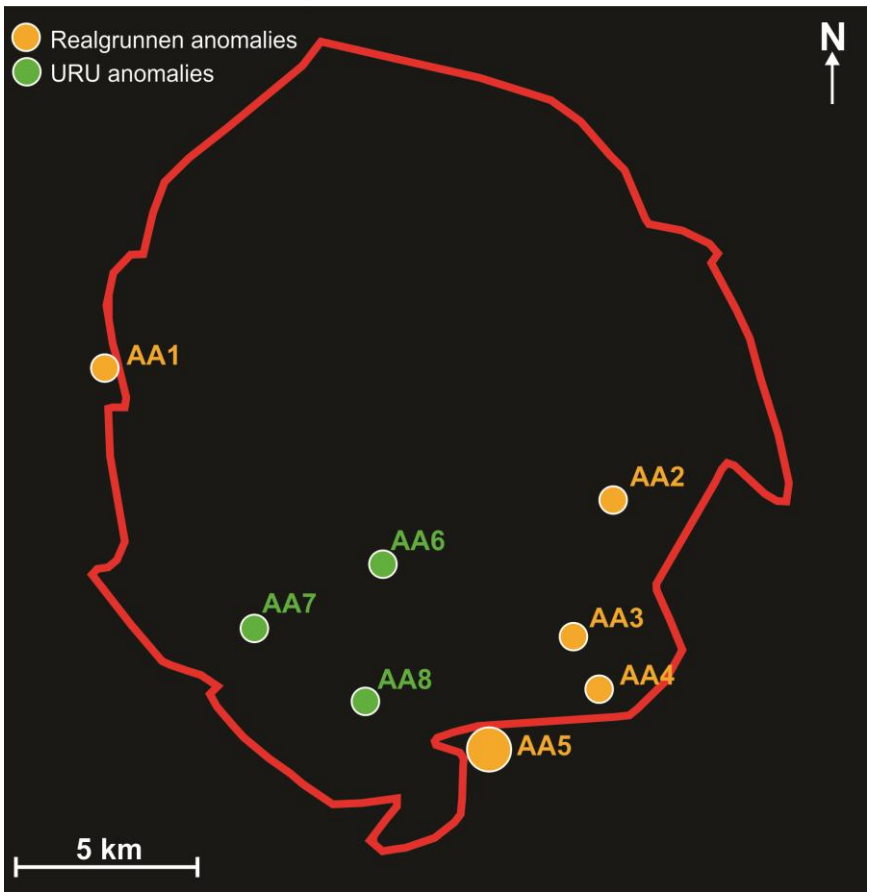

Figure 5.26: The figure shows amplitude anomalies (AA) 1-8 and their position in relation to the outer boundary the Mjølnir Impact Crater (red outline) and stratigraphic position (see legend). This map is just to illustrate the location of the amplitude anomalies, AA5 is shown with a larger circle as it is visible on several seismic lines.

5.4.1 Amplitude anomalies – Realgrunnen Subgroup

A majority of the identified seismic amplitude anomalies have been identified at the interpreted Top Stø horizon (Figs. 5.27-5.32). These anomalies are all characterized by a localized increase in amplitude of the reflection corresponding to the Top Stø horizon. The amplitude anomalies are primarily located within or along the rim faults of the south-southeastern crater (AA2-AA5), apart from a identified amplitude shut-off (AA1) and accompanied anomalies, which are positioned adjacent to a rim fault of the western Mjølnir Impact Crater. Amplitude anomaly 1 (AA1) is not located within the Mjølnir Impact Crater, but on the adjacent platform-area, along a rim fault (on the western margin). The anomaly is seen in the seismic section (Fig. 5.27) as a localized high amplitude – an overlying negative reflection (trough), where the amplitude decreases with depth (TWT) and an underlying positive rflection (peak) characterized by a "flat" amplitude shut-off with depth (TWT). The seismic line also displays two reflections located beneath AA1 that is characterized by a slight increase in amplitude. Lastly, there is a vertical zone of chaotic seismic in the overlying Cretaceous unit, creating a localized, seismic disturbance zone above the amplitude anomaly (Fig. 5.27).

Three of the amplitude anomalies (AA2-AA4) found in the top Realgrunnen Subgroup share many of the same characteristics (Figs. 5.28-5.29). These anomalies are all found within the southeastern Mjølnir Impact Crater. More specifically, the anomalies are observed within horsts in the distal outer zone. The uppermost negative reflection of the located bright spots all coincide with the interpreted Top Stø horizon.

The last amplitude anomaly (AA5) found within the Realgrunnen Subgroup is observed along the rim faul of the southern Mjølnir Impact Crater (Figs. 5.30-5.32). More specifically, AA5 is located outside of the Mjølnir Impact Crater, bounded by rim faults towards the north and faults towards the south. The high amplitude reflections (bright spot) corresponding to AA5 may be seen on three different seismic lines, bounded by faults in both directions on all lines (Figs. 5.30-5.32). The bright spot also seemingly include a flat spot, as shown in Figure 5.30.

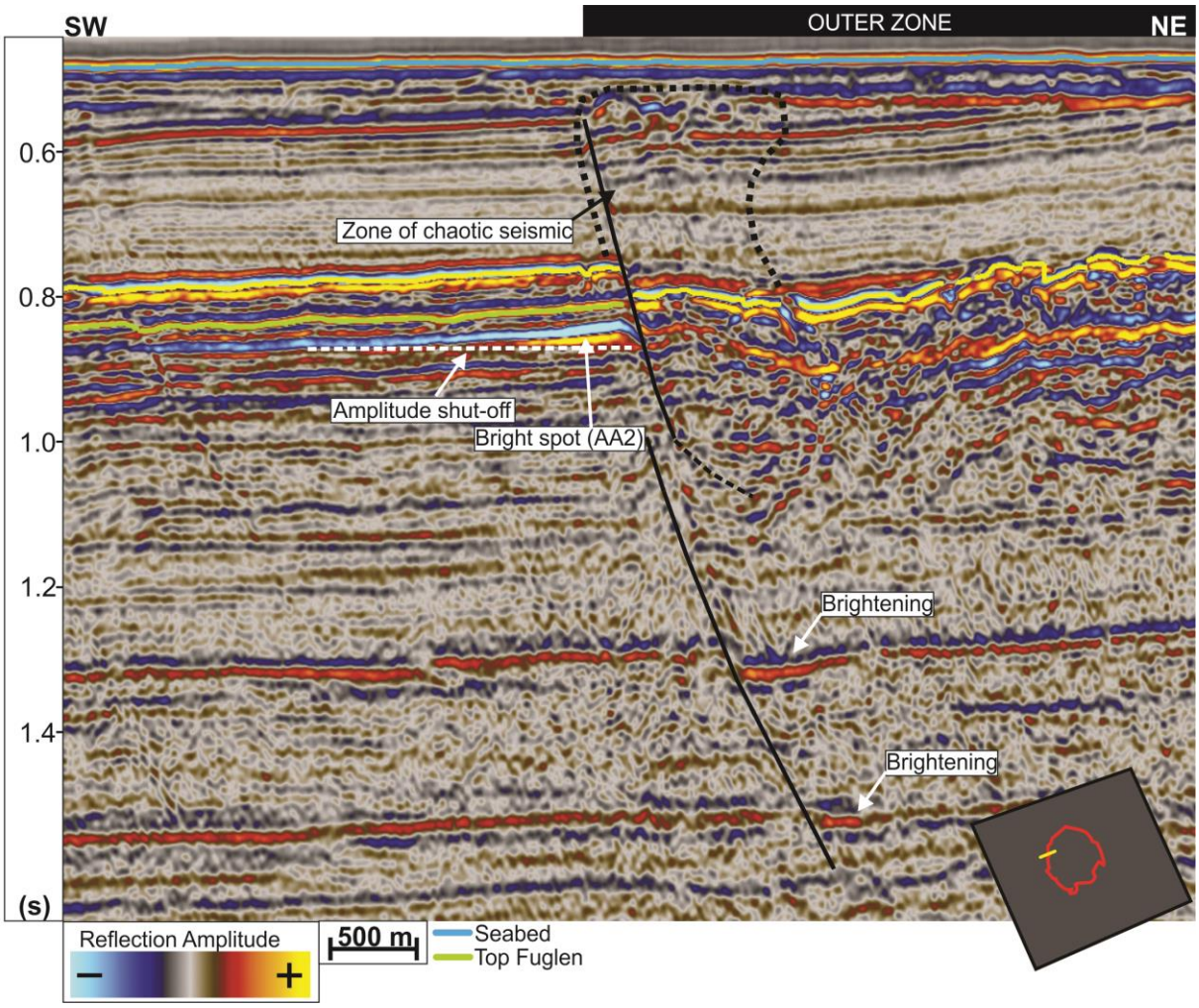

Figure 5.27: The figure displays seismic 2D line NBR14-147482 with AA1 and accompanied anomalies: brightening of deeper laying reflections (Top Klappmyss and Top Kobbe horizons), a horizontal amplitude shut-off/flat spot (white stippled line), and an overlying vertical zone of chaotic seismic (black stippled line).

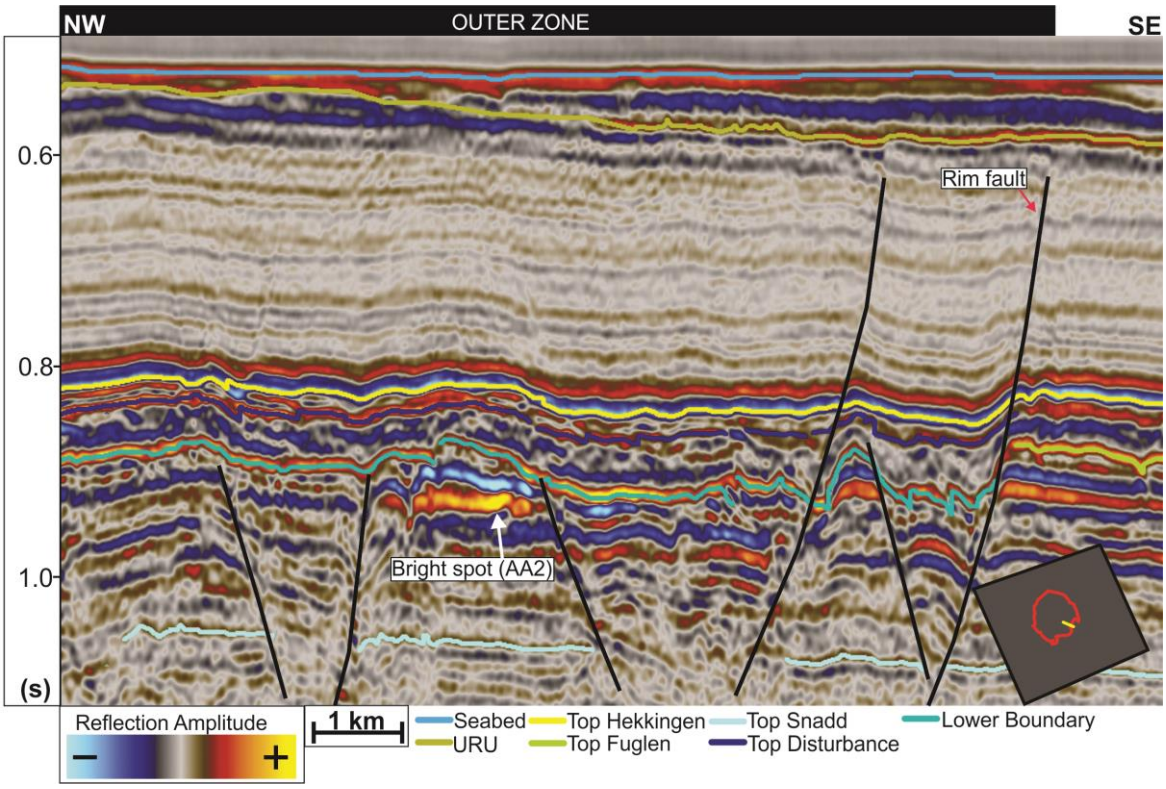

Figure 5.28: The figure shows seismic 2D line NBR14-362688 with amplitude anomaly 2 in the southeastern outer zone of the Mjølnir Impact Crater. The bright spot (AA2) corresponds to the Top Stø horizon and bounded within an interpreted horst.

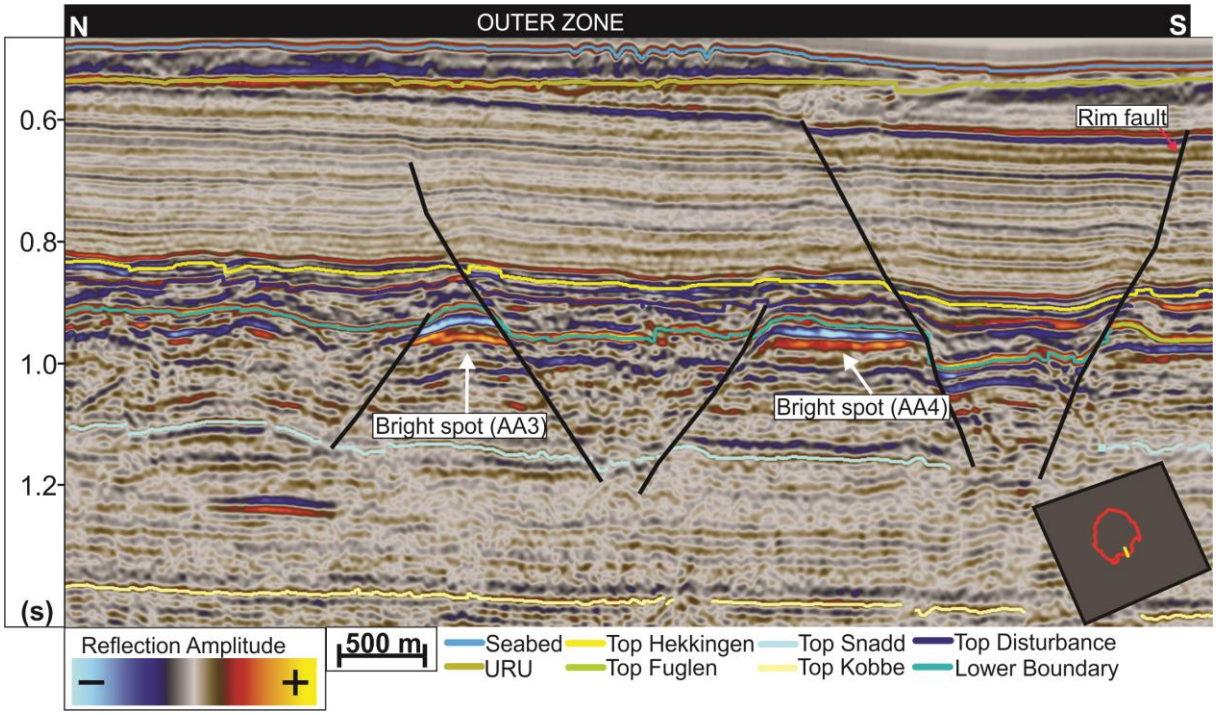

Figure 5.29: The figure shows seismic 2D line NBR14-266837 with AA3 (left) and AA4 (right) in the southern outer zone of the Mjølnir Impact Crater. The bright spots (AA3&AA4) both correspond to the Top Stø horizon, AA4 is located within a horst structure and AA3 is located adjacent to a prominent fault.

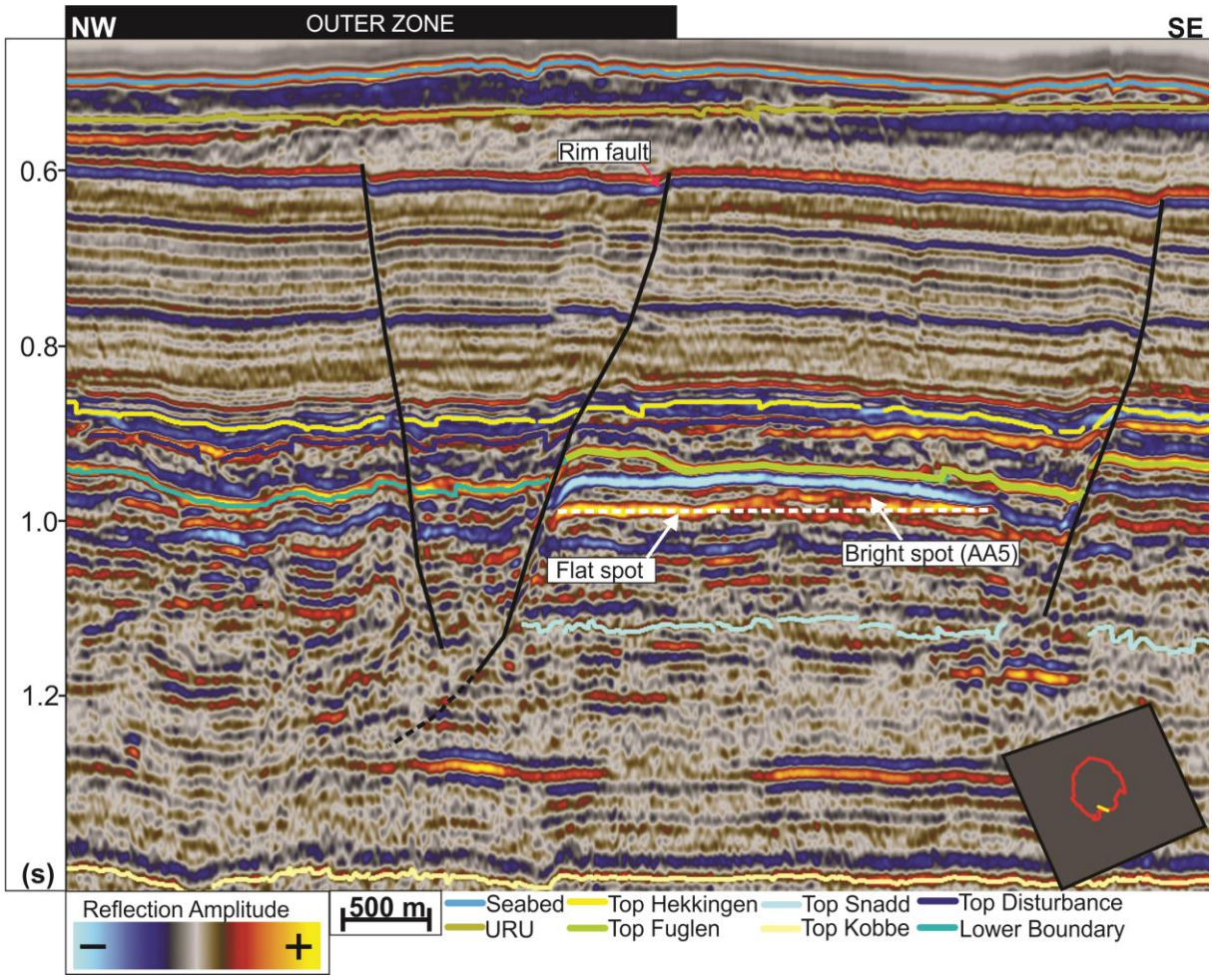

Figure 5.30: The figure shows seismic 2D line NBR14-361497 with amplitude anomaly 5 (AA5) on the platform area just south of the Mjølnir Impact Crater. The bright spot corresponds to the Top Stø horizon. AA5 is bounded by a rim fault towards the north, and a fault of the Bjarmeland Platform to the south. The amplitude also includes a potential flat spot (white stippled line), crosscutting other reflections.

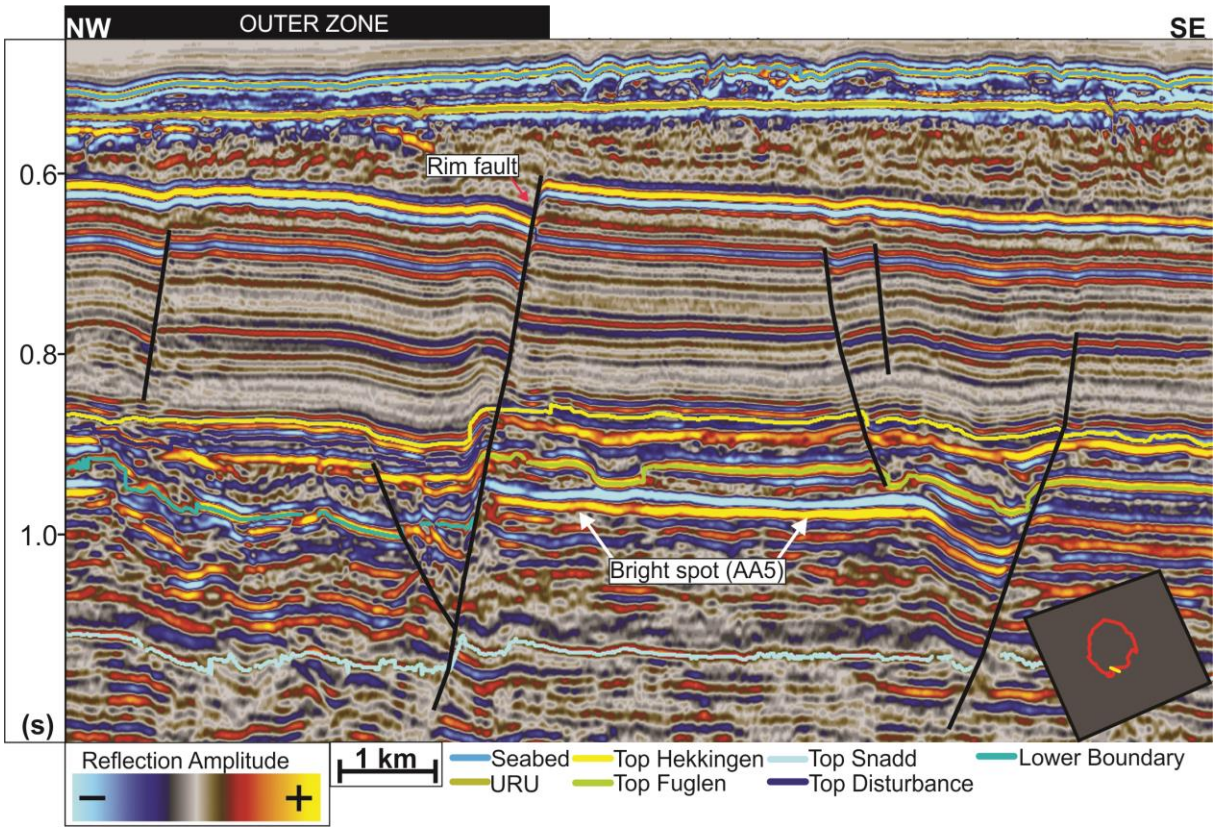

Figure 5.31: The figure shows seismic 2D line SS1301-110-1 with amplitude anomaly 5 (AA5) on the platform area on the platform area south of the Mjølnir Impact Crater. The bright spot corresponds to the Top Stø horizon. AA5 is bounded by a rim faults to the north and seemingly shut off with depth towards the south.

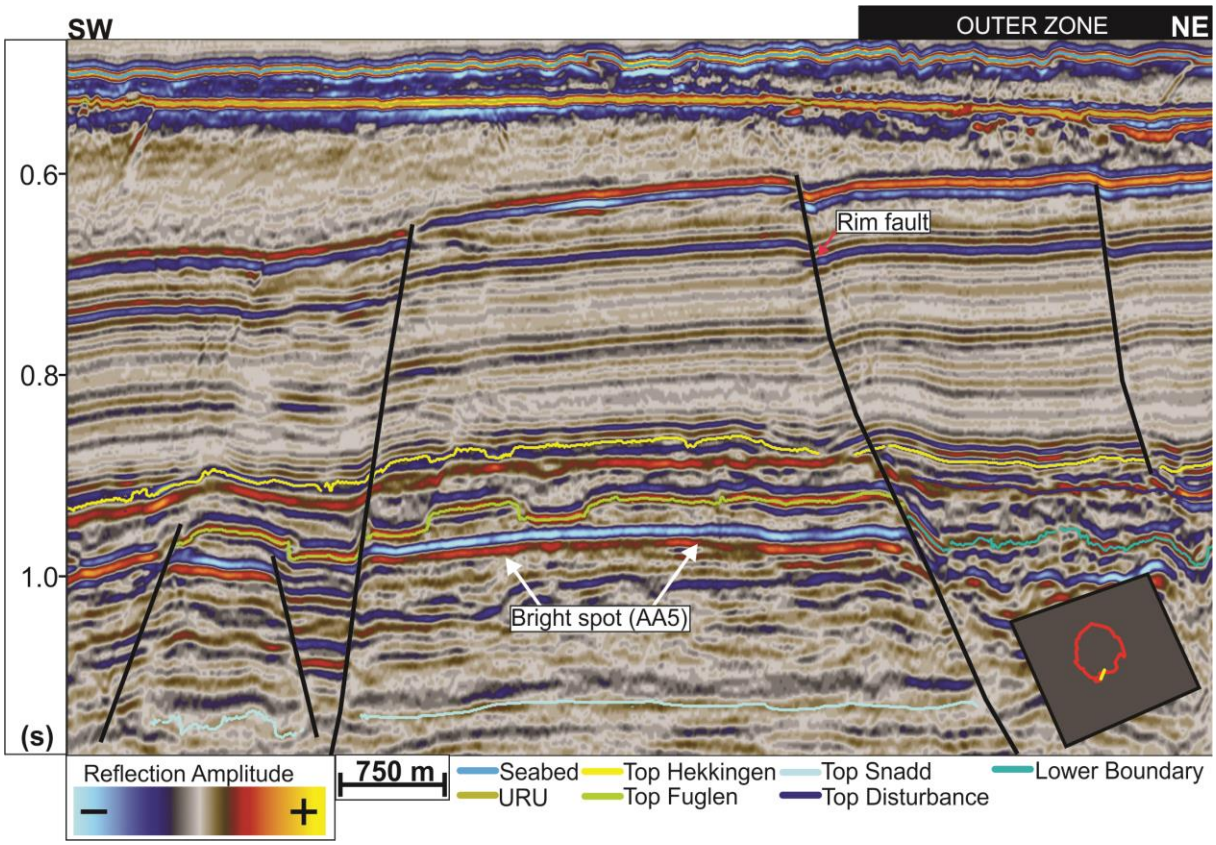

Figure 5.32: The figure shows seismic 2D line SS1301-055 with amplitude anomaly 5 (AA5) on the platform area on the platform area south of the Mjølnir Impact Crater. The bright spot corresponds to the Top Stø horizon. AA5 is found within a horst, bounded by a rim faults to the northeast and a fault towards the southwest.

5.4.2 Amplitude anomalies – Upper Regional Unconformity

Amplitude anomalies are also mapped just below/along the Upper Regional Unconformity (URU). The most prominent of these anomalies is amplitude anomaly 7 (Fig. 5.33) which encompasses strong internal reflections of both positive and negative amplitudes. The reflections are partly deformed and semi-continuous. AA6 has a horizontal extent of about 2 km, located in the western Mjølnir Impact Crater (Fig. 5.26). Below the bright spot there is a vertical section of heavily deteriorated seismic reflections (vertical zone of chaotic seismic). The vertical zone of chaotic seismic is challenging to track below the strong reflection representing Top Hekkingen, into the chaotic seismic reflections. Amplitude anomaly 7 (Fig. 5.33) and 8 (Fig. 5.34) share the same characteristics as AA7, but they are less profound. These are characterized by slightly brighter amplitudes than the surrounding reflections, and they are seemingly underlain by a vertical zone of chaotic seismic.

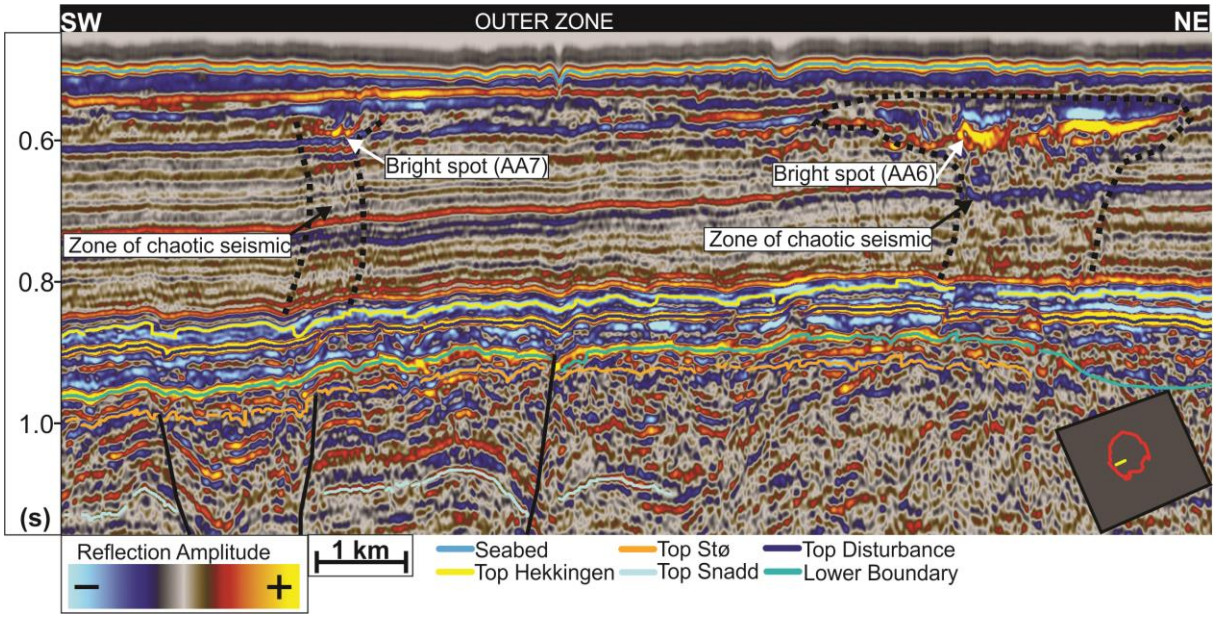

Figure 5.33: The Figure shows seismic 2D line NBR14-145787 with AA6 (right) and AA7 (left) in the outer zone of the western Mjølnir Impact Crater. Both bright spots are underlain by a vertical zone of chaotic seismic (black stippled line).

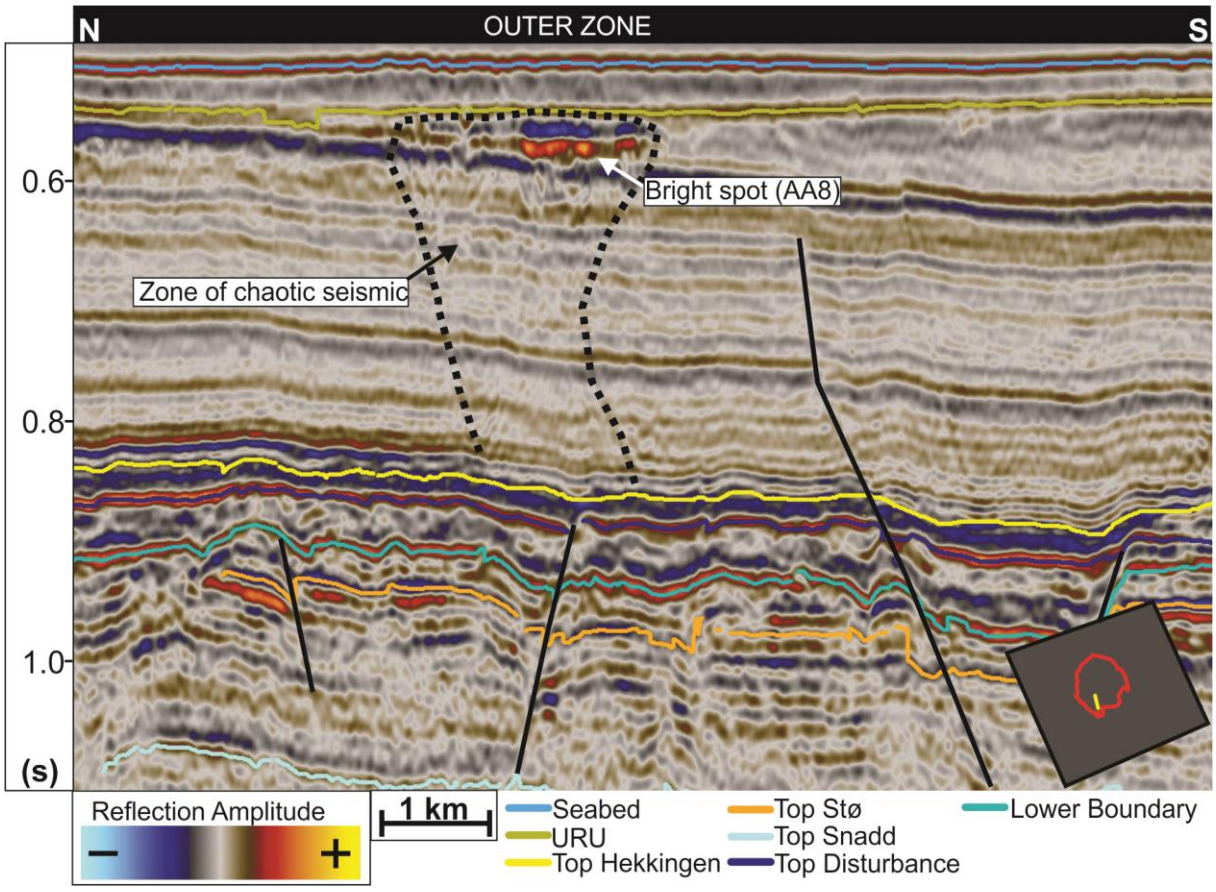

Figure 5.34: The figure shows seismic 2D line NBR14-265769 with amplitude anomaly 8 in the outer zone of the southern Mjølnir Impact Crater. The bright spot is underlain by a zone of very weakly smudged reflections (Black stippled line).

6 Discussion

This chapter is dedicated to discussing the presented results and integrate it with previous studies of the Mjølnir Impact Crater. Firstly, this is done by modeling the evolution and morphology of the Mjølnir Impact Crater is presented. Subsequently, the Mjølnir Impact Crater is assessed as a petroleum system.

6.1 Evolution and morphology of the Mjølnir Impact Crater

The circular-shaped Mjølnir Impact Crater constitutes a structural anomaly with respect to the surrounding, stable Bjarmeland Platform. The Mjølnir Impact Crater may be described as a pristine terrestrial crater, belonging to the class of marine-target impacts (Kenkmann et al., 2013). This implies that the structure has been highly preserved, due to the post-impact sedimentation that commenced shortly after impact. Seismic data has shown that the Mjølnir Impact Crater encompasses features that are expected to be present in a large complex impact crater (Fig. 2.3), but there are also some abnormalities (discussed in chapter 6.1.1). The features are characterized by a radial zonation pattern through the Mjølnir Impact Crater. The extent of these features may be related to the anomalously high collapse factor (ratio of apparent crater to the transient cavity diameter) of 2.6, well above the average for marine impact craters, which is 1.6 (Tsikalas et al., 2010b).

A short conceptual model for the evolution of the Mjølnir Impact Crater and the morphological elements is presented in this subchapter. The model is based on observations from this study and further correlated and discussed in relation to previous studies (Dypvik et al., 2004; Corseri et al., 2020). The model emphasizes on the changes caused by the impact, and subsequent events shaping the crater.

6.1.1 Impact

In the earliest Cretaceous the study area is thought to have been a stable section of the Bjarmeland Platform, characterized by a marine environment and deposition of horizontal strata (Hekkingen Formation) (Fig. 6.1A). The Mjølnir impact event caused a structural anomaly on the Bjarmeland Platform (ca. 142 Ma ± 2.6 Ma) (Dypvik et al., 1996). The impact introduced several characteristic features expected to be found in a marine complex impact crater according to Kenkmann et al. (2013), including a radial subdivision of the Mjølnir Impact Crater – an outer zone, annular depression and central high (Fig. 6.1B). The Impact

also altered the lower Jurassic-upper Permian stratigraphy, creating a zone of uplifted- and autochthonous breccia and the deposition of allochthonous breccia (Ragnarok Formation Unit II) (Fig.6.1B) (Dypvik et al., 2004). The outer boundary of the brecciated stratigraphy is considered to roughly coincide with the previously described disturbance zone (DZ). This includes an autochthonous brecciation of the Fuglen Formation – Snadd Formation interval at the outer zone of the Mjølnir Impact Crater, continuing inward to the annular depression where the brecciation includes collapsed megablocks reaching down to the Havert Formation (Fig 6.1B). The central high is most likely comprised of structurally uplifted autochthonous breccia (Dypvik et al., 2004). The highly fragmented autochthonous breccia is thought to be formed during the excavation and modification stages (chapter 2.2.1). Immediately after impact the allochthonous breccia was deposited, consisting of fallback ejecta and backwash material (Dypvik et al., 2004).

During the modification stage (chapter 2.2.1.3) of the Mjølnir Impact Crater, normal faults of the outer zone and rim faults were formed, most likely due to gravitational collapse during the transformation from the 16 km diameter transient crater into the final 40 km diameter crater form (Tsikalas et al., 1998b). The faults are identified in a concentric strike pattern all around the crater (Figs. 5.18-5.25). The outermost, are identified as rim faults, characterized by a listric fault slope (Figs. 5.20-5.22). These may merge into low-angle detachments in stratified targets, where gliding occur along bedding planes (Kenkmann et al., 2013). Evidence of a low-angle detachment has however proven hard to identify in the seismic data, but the presence of low angle décollement at the floor of the listric faults has been suggested by Tsikalas et al. (2010b). Inwards from the rim faults, in the periphery of the Mjølnir Impact Crater, the strata have been heavily faulted (Figs. 5.19-5.23). This heavily faulted zone corresponds to the previously recognized and termed “marginal fault zone” (Tsikalas et al., 2010a). The marginal fault zone and the outer zone display complex structural characteristics and deformation. This includes evidence of extensional forces articulated as horst and grabens, half-grabens and internally deformed reflectors (Figs. 5.18-5.25). The marginal fault zone consists of several normal faults forming the same circumferential pattern as the rim faults. The normal faults are seemingly centripetally directed, or directed outwards, forming rotated fault blocks and horst and graben structures. The horst and graben structures are most prominent in the eastern marginal fault zone but are also found in the northern and southern parts (Figs. 5.19-5.21). The western marginal fault zone comprises faults of less vertical

offset, forming rotated fault blocks, in contrast to the other areas (Figs. 5.22&6.1B). Usually, the periphery of terrestrial craters are characterized by step-like terraces, making the marginal fault zone an unusual feature of the Mjølnir Impact Crater (Tsikalas et al., 2010a). Complex craters are usually characterized by a raised crater rim adjacent to the rim faults (Fig. 2.3), this feature is absent from the Mjølnir Impact Crater, most likely due to erosion of the backwash following the impact (Tsikalas et al., 2010a).

6.1.2 Post-impact

In the post-impact succession wedge geometries were observed, interpreted as prograding sequences within the Cretaceous unit (Fig. 5.5). These represent mud-rich southeast and southwest prograding units, infilling the Barrents Sea from early Barremian to Albian (Midtkandal et al., 2019), covering the Mjølnir Impact Crater (Fig 6.2A). Corseri et al. (2020) propose that compressional events during Paleogene times caused structural uplift of the central high. These tectonic events are thought to have reactivated the steep normal faults located at the flanks of the central high (Figs. 5.23-5.25). Structurally lifting it from its original position, rising 35 m above the annular basin in the Albian, to its present position ~435 m above the rim level (Fig. 6.2B). The compression may also have reactivated other impact related faults, causing a vertical displacement of the post-impact stratigraphy (Hekkingen Formation-URU interval). The reactivation most likely included faults throughout the structure but is most visible in the faults of the outer zone and the rim faults. The internal reflections within the Cretaceous unit in the eastern and southern outer zone of the Mjølnir Impact Crater also show deformation that has a seemingly compressional nature (Figs. 5.23&6.2B), possibly caused by these Paleogene events.

The interpreted stratigraphy shows a trend of an overall southward dip within the study area. This is thought to be caused by early Cenozoic tectonism, tilting the Mesozoic and Paleozoic sequences of the Bjarmeland Platform (NPD, 2014). The tilted stratigraphy also includes the Mjølnir Impact Crater (Figs. 5.5&6.3). During the Cenozoic the study area was affected by uplift and erosion linked to pre-glacial fluvial and coastal erosion, and subsequent glacial erosion represented by the Upper Regional Unconformity (URU). The exhumation in the Cenozoic may also have reactivated faults, altered migration pathways, caused failure of seals, gas expansion and lifting source rock out of the oil and gas window (Ohm et al., 2008; Edmundson et al., 2019). The glacial deposits are represented by the Naust Formation (Fig

6.3). Depression 1-3 (Fig. 5.17) may also be included in the glacial deposits. Depression 1 is identified on the ultra-high-resolution P-cable data (Fig. 5.17) and is characterized by internal continuous reflections. These reflections may represent several hiatuses, stratigraphically located beneath URU. These hiatuses may be a result of deep glacial erosion or linked to the fluvial and coastal erosion of the early Cenozoic. The interpreted Naust Formation includes a lobe-shaped feature deposited over the central high. The relative placement of the lobe, and the fact that it is seemingly unaffected by the central high, may indicate that there has been little tectonic movement of the central structure through the Quarternary.

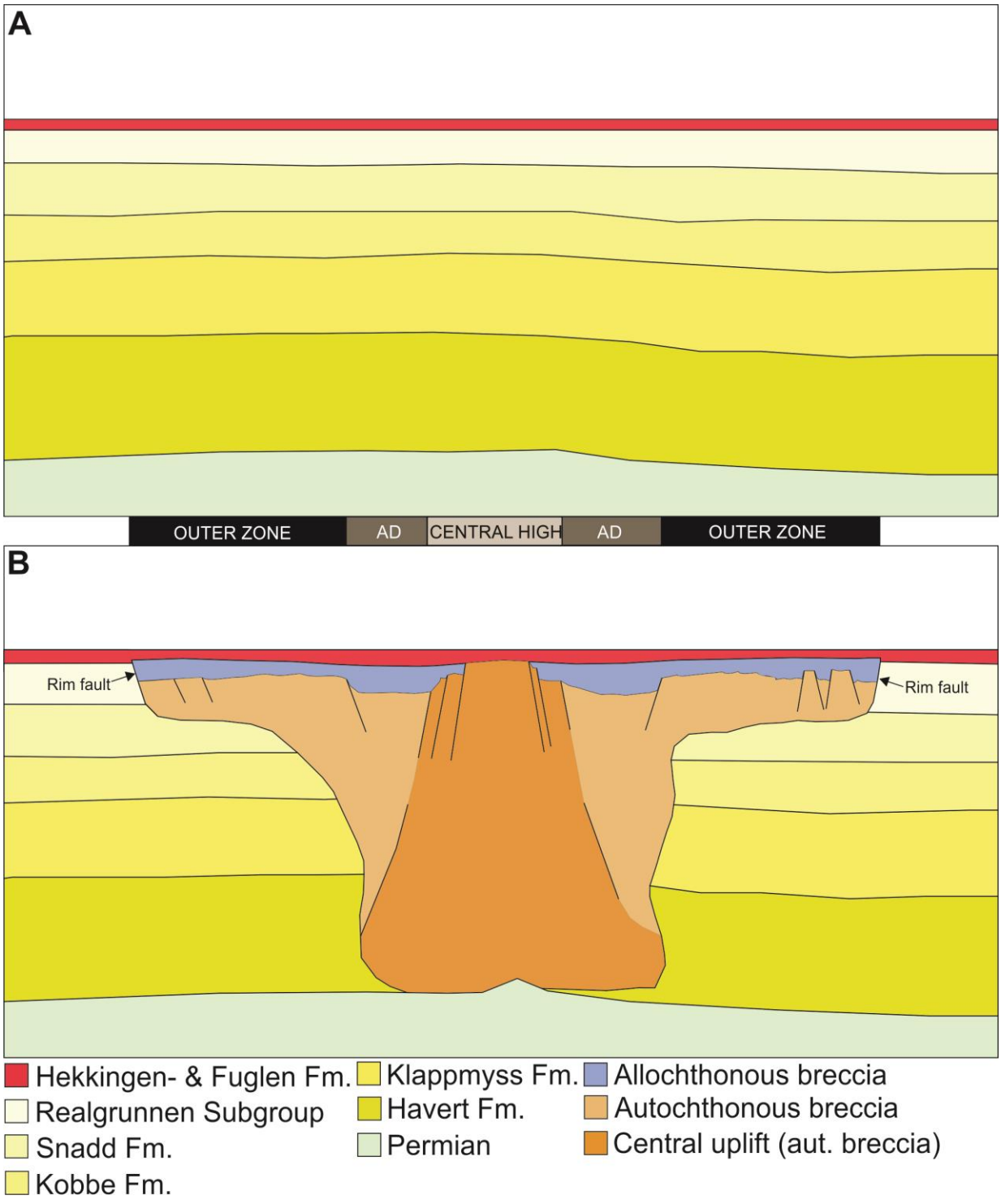

Figure 6.1: (A) Sketch showing the Mesozoic succession of the stable Bjarmeland Platform at the Jurassic-Cretaceous boundary prior to the Mjølnir impact event. (B) A simplified model the Mjølnir Impact Crater after the impact, with a marine deposition, represented by the Hekkingen Formation draping the original crater relief. The figure shows the radial zones – outer zone, annular depression (AD) and central high that formed during impact. The effects of the impact on target rock and deposited allochthonous breccia is also indicated, with the outer bounds roughly coinciding with the disturbance zone (DZ). The uplifted strata of Jurassic, Triassic and the uppermost Permian age. The model only shows parts of the faulting including rim faults, marginal fault zone, faults bounding the annular depression and faulting related to the central high. Partly based on Corseri et al. (2020)

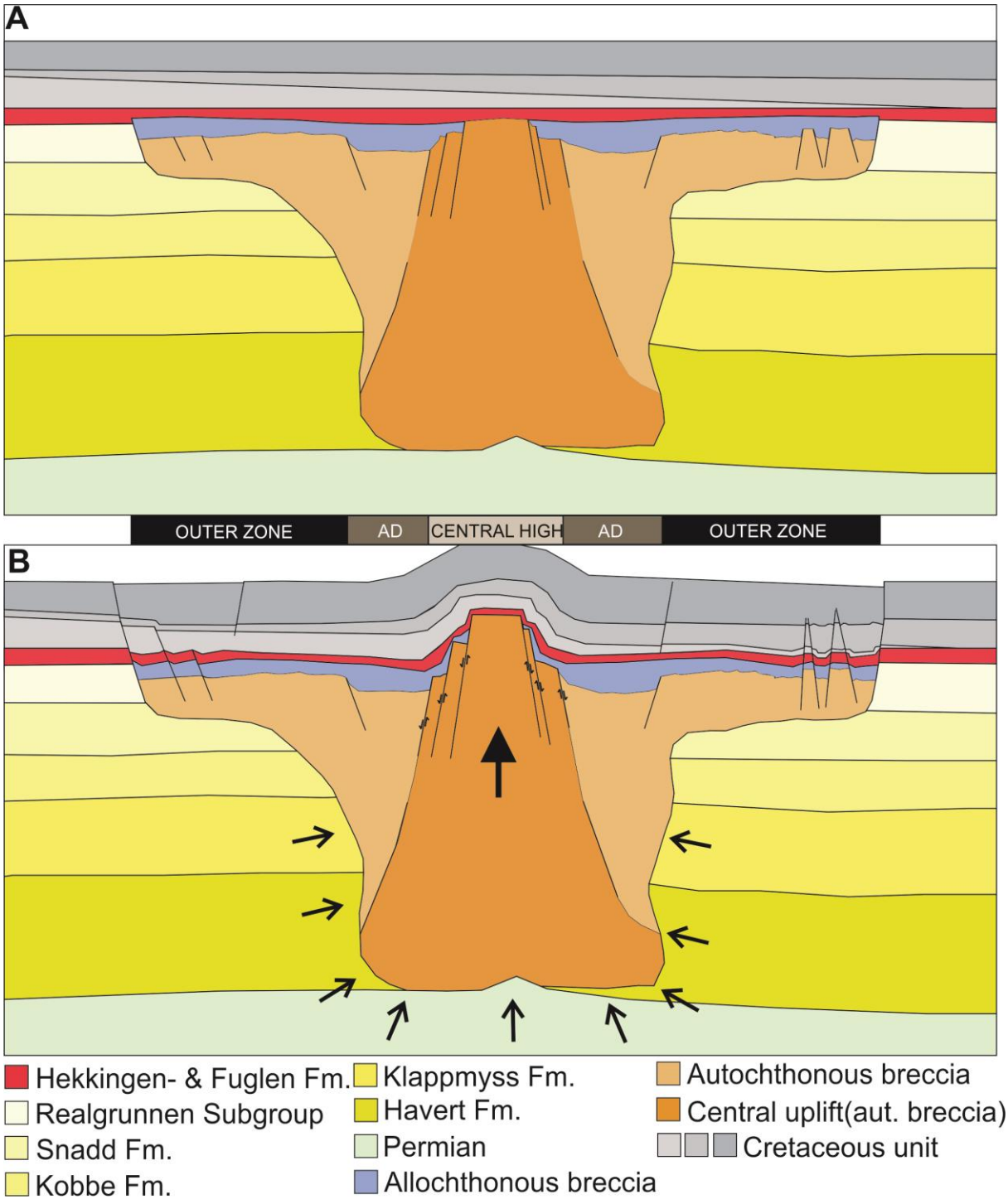

Figure 6.2: (A) Sketch showing the Mjølnir Impact Crater before the Albian Stage, where Lower Cretaceous prograding units infilling the Barents Sea and the Bjarmeland Platform from the northern (east and -west) uplifted area, thus giving them a wedge-shaped form. (B) Shows the structural uplift of the central high after regional tectonic compression in the post-Albian. These events are thought to have reactivated the steep-angled normal faults of the central high, and possibly other impact related faults (marginal fault zone, rim faults etc.) causing vertical displacement of the upper Jurassic (Hekkingen Fm.)-cretaceous unit interval. The compressional events may also have deformed internal reflections within the cretaceous unit in the horst graben structures of the marginal fault zone. Based on paper Corseri et al. (2020).

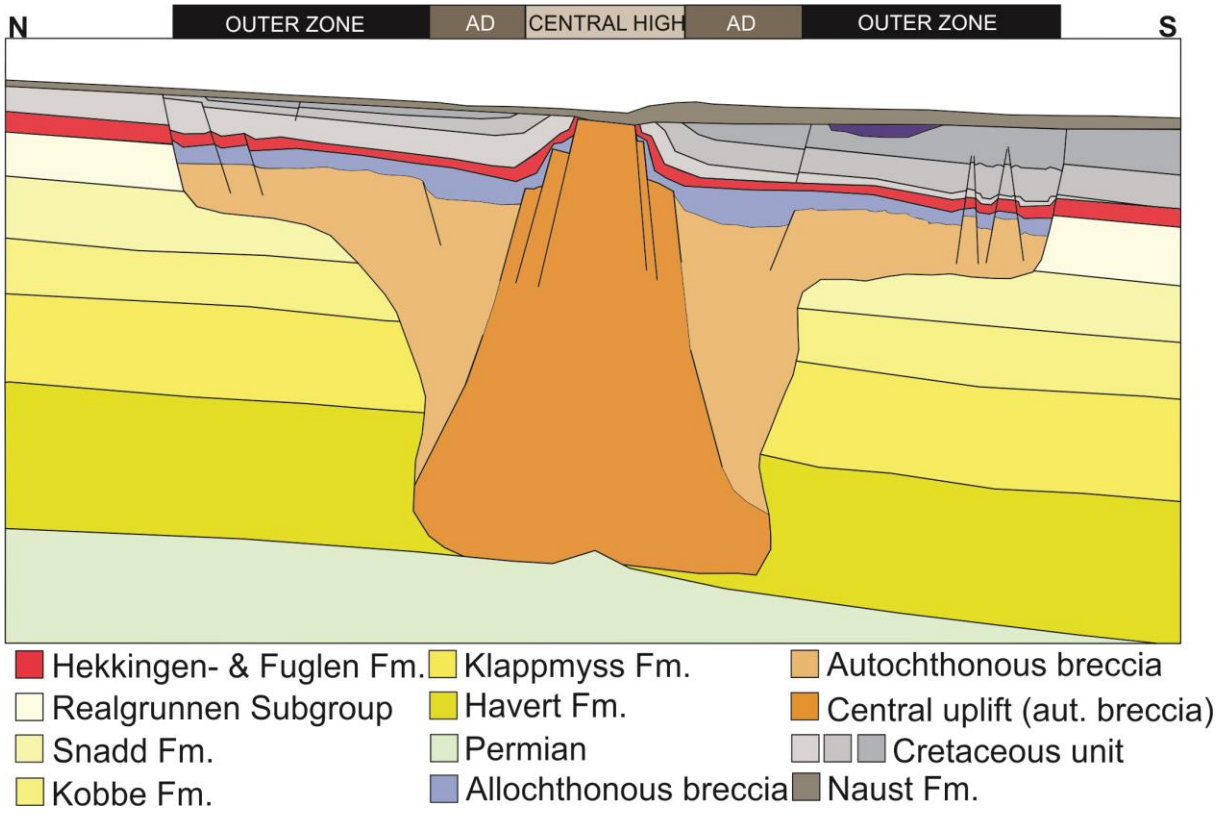

Figure 6.3: Sketch showing a model of the present Mjølnir Impact Crater following the early Cenozoic north-south tilt of the Bjarmeland Platform and the Cenozoic uplift and erosion. The model includes observed and interpreted features at their relative location within the crater. These features include the deposited Naust Formation and the lobe shaped deposit directly over the central high, a depression (purple) related to the interpreted URU, the characteristic outer zone (marginal fault zone) containing both horst and graben structures and rotated fault blocks.

6.2 Petroleum system assessment

A regional uplift of the Barents Sea during the late Mesozoic – Cenozoic has been documented by several authors (e.g. Vorren et al., 1991; Vagnes & Amundsen, 1993; Grogan et al., 2000; Smelror et al., 2009; Amantov & Fjeldskaar, 2018). The uplift is linked to pre-glacial fluvial and coastal erosion of the Barents Sea shelf (e.g. Richardsen et al., 1993; Lasabuda et al., 2018a; b). In addition to this the Barents Sea shelf was exposed to glaciation and erosion during the Late Pliocene and Pleistocene (Smelror et al., 2009). A compilation of erosion estimates from different methods show that a that a total of 1800-2300 m of sediment has been removed during the Cenozoic on the Bjarmeland Platform (Lasabuda, 2018). This eroded sediment package needs to be regarded when assessing the petroleum system. Erosion and uplift are known to have a significant impact on several elements in a functioning petroleum system; source rock, reservoir rock, cap rock, trap, migration and preservation (Doré & Jensen, 1996; Henriksen et al., 2011a). It is therefore important to understand the timing of uplift and exhumation estimates, to better understand the potential of a potential petroleum system and identify risk factors (Ohm et al., 2008; Baig et al., 2016).

6.2.1 Source rock

In order to understand the potential of the Mjølnir Impact Crater as a potential petroleum system, it is important to understand the potential source rock lithology, their maturity and how the Mjølnir impact event might have altered their potential.

In order to get a better understanding of the source rock potential in generating petroleum in the kitchen area of the study area, a simplified 1D maturation model has been implemented. The model uses the velocities calculated in Table 4.2 and the formation thicknesses was measured in petrel. An assumed geothermal gradient of 30^{o}C/km is used, based on regional trends from Khutorskoi et al. (2008). The uplift and erosion are also accounted for by adding a 2000m thick sediment package, thus obtaining an estimated thermal history of the source rock. The evaluated temperature point (TP1) (Fig. 6.4) is located downdip of the crater and is chosen in order to investigate the maturity of potential source rock formations that could charge the Mjølnir Impact Crater.

The maturation of a source rock is an irreversible process (Henriksen et al., 2011a). This implies that if a source rock is buried at a certain depth and exposed to higher temperature, the

kerogen might have been matured and generated petroleum if the temperatures were sufficient at maximum burial. Subsequent uplift of the source rock reduces the temperature it is exposed to, thus potentially ceasing the generation of petroleum. The uplift will not reverse the maturity parameters for the rock (Henriksen et al., 2011a). In the Barents Sea Shelf in general, mature source rocks have been observed shallower than their vitrinite reflectance measurements suggest. This indicates that the source rock has been buried deeper and exposed to higher temperatures at an earlier stage, and subsequently uplifted (Henriksen et al., 2011a).

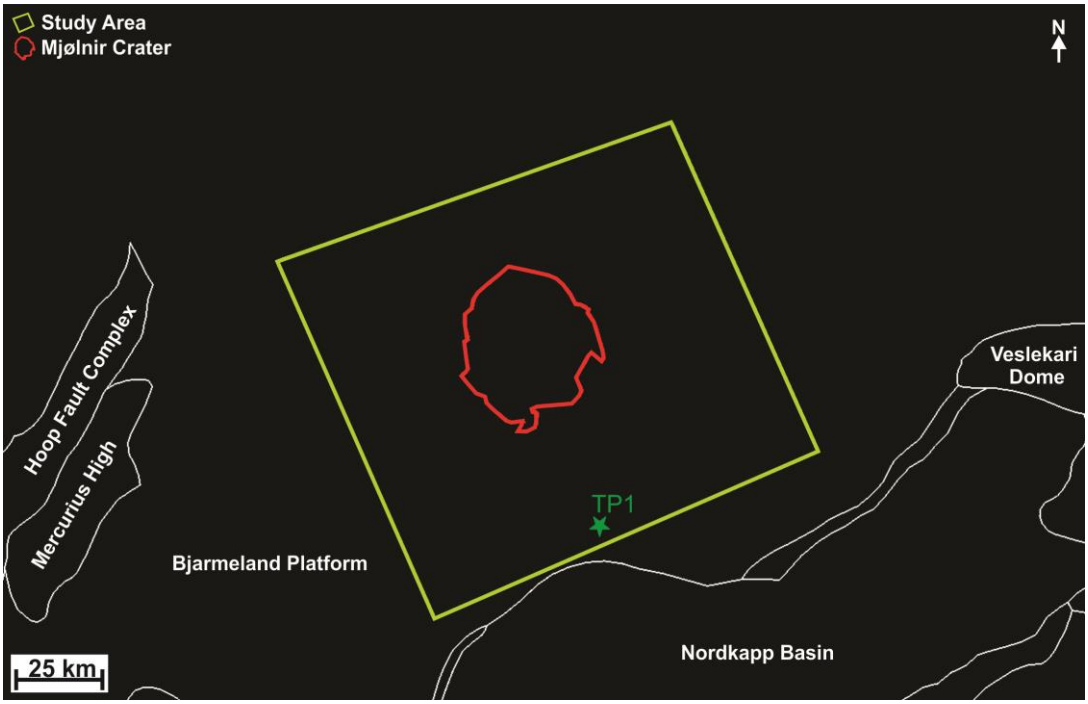

Figure 6.4: The figure shows the location of the modelled temperature point (TP1) in the southern parts of the study area, close to the Nordkapp Basin. Structural elements are from the NPD

Hekkingen Formation

The Upper Jurassic Hekkingen Formation represent the most prolific source rock for hydrocarbon in the Barents Sea, due to its generally high TOC content and its potential of generating hydrocarbons (Ohm et al., 2008; Worsley, 2008; Dypvik et al., 2010b). The Hekkingen Formation was also characterized by high gamma ray readings in well 7435/12-1 (Korpfjell), indicating elevated organic content (NPDfactpages, n.d.-c).

In temperature point 1 (TP1) the Hekkingen Formation has a calculated thickness of ~97 m, and its base is found at a depth of 765 m (Table 6.1). By adding a 2000m thick sediment package representing the net erosion, the maximum burial depth is 2765 meters. The maximum burial depth corresponds to a pre-uplift temperature of 83 ^{o}C. These calculations indicate that the Hekkingen Formation has previously been exposed to temperature conditions that are favorable for the generation of oil. The calculated temperatures correspond well with the oil-maturity of the Hekkingen Formation on the Bjarmeland Platform proposed by Ohm et al. (2008).

The Mjølnir impact event has been dated (142±2.6 Ma) as a contemporaneous event to the deposition of the Hekkingen Formation (Dypvik et al., 1996). This means that the lower parts of the Hekkingen Formation may have been highly affected by the Mjølnir Impact event, possibly as excavated material from the excavation stage. The Hekkingen Formation may also have been affected locally by the high temperatures associated with the Mjølnir Impact event. Soot particles found in the ejecta deposits (Sindre Bed) is suggested to have been produced by impact induced 20 min-long sea-floor fires in the exposed crater following the impact (Dypvik et al., 2010a). Dypvik et al. (2010a) suggests that the kerogen found within the Hekkingen Formation fueled the blazing fire and calculated that source rock equivalent to 30 million standard m^3 was lost. If so, the local source rock potential of the Hekkingen Formation may be reduced within the as the kerogen was combusted at the time of impact.

Steinkobbe Formation

The Steinkobbe Formation was first identified and defined by Mørk and Elvebakk (1999) based on cores from the Svalis Dome. Similar lithologies have been found and assigned to the Steinkobbe Formation on the Sentralbanken High in the northern Barents Sea (Lundschien et al., 2014). The Steinkobbe Formation has not been specifically mapped in this study, but it is time-equivalent to the Kobbe Formation and may constitute parts of it within the study area. Thus, the Kobbe Formation (Fig. 5.12A) is used as a basis for the 1D maturation modelling.

In TP1 the Kobbe Formation has a thickness of 456 m. and its base is found at a depth of 1896 m. By adding a 2000 m thick sediment package, the maximum burial of the formation is 3896 m. This corresponds to a temperature of 117 ^{o}C, placing the formation in conditions favorable for the generation of oil.

Lower Triassic formations

The Lower Triassic formations include the Havert- and Klappmyss formations. Henriksen et al. (2011b) suggest that the Lower Triassic formations hold source rock potential on the Bjarmeland Platform, indicating that these formations have a moderate risk in the study area due to thinning towards the east. The Havert- and Klappmyss Formation are mapped with high confidence within most of the study area. The Havert Formation has a calculated thickness ranging between 1248 and 1824 m (chapter 5.2.2.1), and the Klappmyss Formation ranges between 816 and 1104 m in the study area (chapter 5.2.2.2). The following maturity calculations use the same factors used for the calculations regarding the Hekkingen Formation.

In TP1 the Klappmyss Formation has a measured thickness of 974 m and its base is found at a depth of 2823 m. By adding the eroded sediment package, the maximum burial depth is 4823 m. This corresponds to a temperature of 145^{o}C, placing the formation in conditions favorable to gas generation at maximum burial (gas window).

In TP1 the Havert Formation has a measured thickness of 1728 m and its base is found at a depth of 4551 m. By adding the eroded sediment package, the maximum burial depth is 6551m. This corresponds to a temperature of 197^{o}C, placing the formation in the window for gas generation.

Table 6.1: The table shows the measured thicknesses of formations and subgroup (ms). An assumed internal velocity of 1800 m/s is used for the Naust Formation. Velocities for the Cretaceous unit to the Snadd Formation is presented in Table 4.2. The velocities for the Kobbe-, Klappmyss- and Havert formations was extracted from Ktenas et al. (2018)

Location	Formation /Subgroup	Measured thickness TWT (s)	Mean Formation velocity (m/s)	Formation thickness (m)	Present burial depth – base (m)	Maximum burial depth (pre uplift)	Thermal history (30 ºC/km)
TP1	Naust Formation	0.02 s	1800m/s	18 m			
	Cretaceous unit	0.555 s	2388 m/s	663 m			
	Hekkingen Formation	0.067 s	2518 m/s	84 m	765 m	2765 m	83 ºC
	Fuglen Formation	0.031 s	2584 m/s	40 m	805 m	2805 m	84 ºC
	Realgrunnen Subgroup	0.163 s	2902 m/s	237 m	1042 m	3042 m	91 ºC
	Snadd Formation	0.241 s	3324 m/s	401 m	1443 m	3443 m	103 ºC
	Kobbe Formation	0.240 s	3800 m/s	456 m	1896 m	3896 m	117 ºC
	Klappmyss Formation	0.385 s	4800 m/s	974 m	2823 m	4823 m	145 ºC
	Havert Formation	0.720 s	4800 m/s	1728 m	4551 m	6551 m	197 ºC

6.2.2 Migration

Several possibilities of secondary migration into the Mjølnir Impact Crater may be discussed.

The regional north-south tilt of the Bjarmeland Platform that was established by early Cenozoic tectonism (NPD, 2014), could possibly be an important factor with respect to lateral migration of hydrocarbons. The seismic data shows that the Mesozoic and Paleozoic sequences and the Mjølnir Impact Crater all deepen towards the south (Fig. 5.5-5.9). The southward tilt could potentially allow for higher temperature exposure of source rocks in the area south of the Mjølnir Impact Crater, thus a higher potential for shallower source rocks (Hekkingen Formation) to mature and generate petroleum. The deeper Nordkapp Basin directly to the south of the Mjølnir Crater could potentially represent an area in which petroleum is or has previously been generated. The tilted sequences of the Bjarmeland Platform may subsequently have acted as a migration pathway, in carrier beds along cap rocks, charging the Mjølnir Impact Crater.

Faults are regarded as the main vertical conduits for fluids in many basins around the world, especially deep-seated faults. This is because deeper stratigraphy is often consolidated or lithified, reducing the permeability of the formations (Ligtenberg, 2005). Deep seated faults associated with the Mjølnir impact event are interpreted below the annular depression (Fig. 5.25). These faults are thought to bound the collapsed sedimentary megablocks at either side. They may also act as conduits for hydrocarbon generated at deeper levels (Havert-, Klappmyss- and Steinkobbe formations), reaching shallower parts of the Mjølnir Impact Crater. Deep-seated faults outside the Mjølnir Impact Crater are also identified within the study area (Fig. 5.2). Figure 5.5 also shows a prominent fault located in the southern study area, which could potentially act as pathways for vertical migration of petroleum towards the Mjølnir Impact Crater.

6.2.3 Reservoir

Reservoir rocks in the Barents Sea occur at many stratigraphic levels, ageing from Paleozoic to Paleogene (Henriksen et al., 2011b). The Middle Triassic to Middle Jurassic lithostratigraphy (Kobbe- and Snadd formations and the Realgrunnen Subgroup) have previously proven to encompass reservoir rock. This is illustrated by Figure 6.4, showing discovery wells that have proven petroleum in the respective stratigraphy on and adjacent to the Bjarmeland Platform. The potential reservoir units of the Barents Sea are also affected by the Cenozoic uplift and erosion. The reservoir units have previously been buried deeper and exposed to higher temperature, causing diagenetic effects and reducing their reservoir quality (porosity). Thus, when predicting reservoir quality, the maximum burial needs to be considered (Henriksen et al., 2011a).

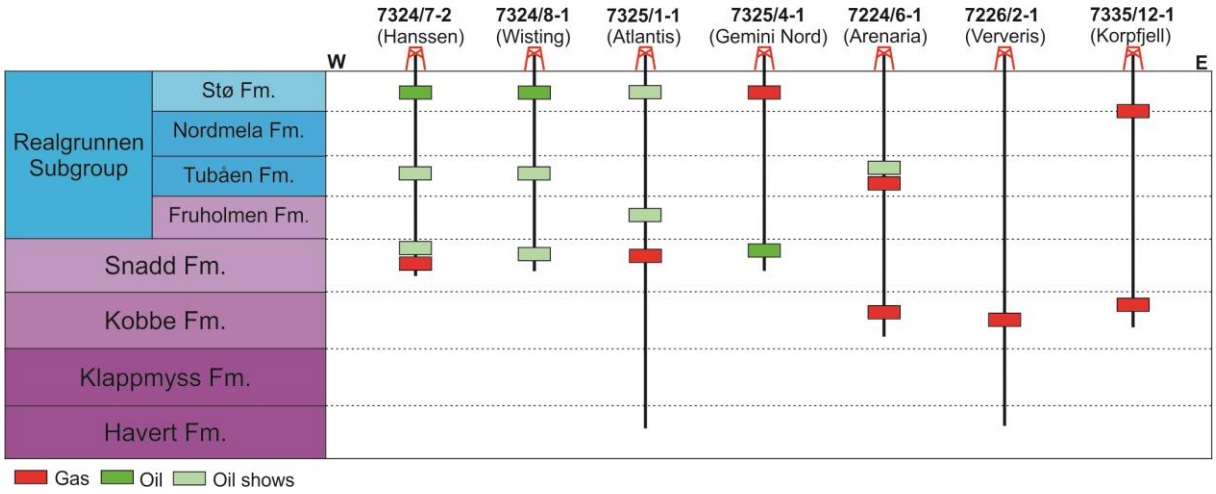

Figure 6.5: The figure displays discovery wells on the Bjarmeland Platform and one well from the Hoop Fault Complex (Atlantis) from west to east. The position is represented by latitude coordinates, longitude is not considered. All wells indicate the stratigraphic level in which petroleum has been discovered and oil shows. Vertical depth is not to scale. Figure created from information extracted from the NPDfactpages.

The Mjølnir impact event may have altered the properties of the target rock. With respect to the potential reservoir rocks located within the Mjølnir Impact Crater, their primary properties (porosity and permeability) may be affected. Tsikalas et al. (2010b) have formerly modeled the porosity anomalies within the disturbance zone (DZ), related to the effects of the Mjølnir impact event. The final porosity anomaly also included a reconstruction of the properties directly after impact, by introducing a decompaction factor to the present anomaly. The distribution of porosity change ranges from a reduction of -1% at the central high to an increase of 6.3% at the periphery. These estimations imply that the impact-induced fracturing

generated 13-33 km^3 of excess pore space in the periphery of the Mjølnir Impact Crater (i.e. outer zone), and reduced the pore space of the central crater by 6-13 km^3 (Tsikalas et al., 2010b). The generated pore space in the periphery (outer zone) enhances the porosity and permeability of the rock.

Kobbe Formation

The Kobbe Formation has been defined and mapped with high confidence within most of the study area. Within the defined annular depression and central high, the Kobbe Formation was however difficult to map, due to chaotic seismic reflections. This corresponds to the section that is interpreted to be affected by the Mjølnir impact event, marked by the disturbance zone (DZ). Hence, the Kobbe Formation is regarded to be included as a part of the autochthonous breccia within the annular basin and central high. The Kobbe Formation constitutes the primary reservoir of the Goliath field in the Hammerfest Basin. Coastal sandstones of the Kobbe Formation have also been penetrated in the Nordkapp Basin and on the southern Bjarmeland Platform (Lundschien et al., 2014).

Snadd Formation

The Snadd Formation is affected by the Mjølnir Impact event to a varying degree. The disturbance zone (DZ) extends from the top of the formation at the periphery of the Mjølnir Impact Crater, moving towards the annular depression, where the whole formation may be regarded as autochthonous breccia. The primary reservoir potential of the Snadd Formation is regarded as channelized sandy systems (NPD, 2014) and seemingly represents the best reservoir interval within the Triassic stratigraphy (Henriksen et al., 2011b). Figure 6.5 show both oil and gas discoveries made in sandstones within the Snadd Formation, in the Gemini Nord, Hanssen and Atlantis discoveries. The previously described ellipse-shaped high amplitudes within the Snadd Formation (chapter 5.2.2), are interpreted to represent these channelized sandstones. The lack of sufficient seismic data coverage did not allow lateral mapping of these channelized bodies. From the seismic sections, the majority of these sandstone bodies are visible outside of the Mjølnir Impact Crater and the defined disturbance zone (DZ), and not regarded as part of the structure. The presence of such channels in the annular depression and central high may be camouflaged by the chaotic seismic signal.

Realgrunnen Subgroup

The Late Triassic-Middle Jurassic Realgrunnen Subgroup (Fruholmen-, Tubåen-, Nordmela- and Stø formations) represent the main reservoirs in the Norwegian sector of the Barents Sea (Henriksen et al., 2011b). Figure 6.5 shows that most of the illustrated wells, excluding Ververis, have indications of fossil hydrocarbon columns or discoveries in the Realgrunnen Subgroup. The Realgrunnen Subgroup also constitute reservoir for producing fields in the Barents Sea – the Goliat field (Fruholmen Formation) and Snøhvit Field (Stø- and Nordmela formations). In the Snøhvit field the reservoir quality is considered fairly good, with porosity measurements as high as 20% and permeability at 700 mD (NPD, 2014).

The Realgrunnen Subgroup shows a thickness ranging between 116 and 320 m (Fig. 5.13A). The subgroup seems to be affected by the Mjølnir impact event throughout the crater. From the rim faults to the flanks of the central high (outer zone and annular basin) the formation is interpreted to be brecciated, thus classified as autochthonous breccia. This implies that the Mjølnir impact event may have improved the primary properties (porosity and permeability) of the subgroup within the crater, due to fracturing of the formation (i.e. increased porosity).

6.2.4 Trap, seal and preservation

The petroleum exploration wells on the Bjarmeland Platform (Fig. 6.5) have generally been drilled at the outer boundary, adjacent to other structural elements of the Barents Sea. The Mjølnir Impact Crater is a structural anomaly on the otherwise less structured Bjarmeland Platform and thus may be important regarding possible accumulation of hydrocarbons. Observations in the Mjølnir Impact Crater reveal several potential trapping structures, primarily classified as structural traps. The seismic data has revealed horst and graben structures (Fig. 5.19) and rotated fault blocks (Fig. 5.22) in the outer zone (marginal fault zone). These extensional features may structurally trap Jurassic sandstone (Realgrunnen Subgroup), especially in the horsts, where the sandstone is seemingly juxtaposed with the allochthonous breccia of the Ragnarok Formation Unit II in the adjacent grabens (Fig. 5.19). The listric rim faults may also constitute potential hydrocarbon traps, by vertically offsetting the strata. Similar listric rim fault patterns define the outermost boundary of the Avak structure (Alaska, USA), where three gas fields appear as a consequence of the impact event that created the structure. All three structural accumulations are located outside the Avak structure, but they are partly trapped by the outermost listric faults (rim faults) (Kirschner et

al., 1992). The observed amplitude anomaly (AA) 1 and 5 have a similar relative location to the crater as the gas fields in the Avak structure, making it an interesting analogue. When considering the structural features of the Mjølnir Impact Crater as potential traps, trap integrity and retention needs to be taken into account as the seismic data shows reactivation of several of the faults within the Mjølnir Impact Crater. The renewed activity along the fault-plane may cause fault-seal breach and hydrocarbon leakage from the trap (Edmundson et al., 2019).

The Hekkingen- and Fuglen formations constitute good sealing lithologies in the Barents Sea (NPD, 2014). The post-impact sedimentation of the Hekkingen Formation (Top Hekkingen – TD interval) drapes the whole Mjølnir Impact Crater, i.e. a favorable stratigraphic position as a sealing lithology for the structure. The Fuglen Formation is interpreted within the Mjølnir Impact Crater and could have potential as a cap rock for the underlying reservoir units in the Realgrunnen Subgroup. The bright spots and the related vertical zone of chaotic seismic of amplitude anomaly 6-8 may be interpreted as hydrocarbons vertically migrating out of the Mjølnir Impact Crater. The vertical zones of chaotic seismic could represent gas chimneys, created from gas migration through the Cretaceous unit (Figs. 5.32-5.33). The bright spots located above may represent shallow gas accumulations along URU, given that the Naust Formation represents a sealing lithology. These features may represent seal breach of the Hekkingen and Fuglen formations and subsequent tertiary migration. The vertical zones of chaotic seismic of AA6-AA8 may alternately be interpreted to represent disturbed seismic reflections due to bright spots located above, thus not representing the true geology of the subsurface.

The north-south tilt of the Bjarmeland Platform introduces a high variation in burial depth of the Mjølnir Impact Crater (Fig. 5.5). The post-impact sedimentation, represented by the Cretaceous unit, has a calculated thickness variation between ~870 m in the southern study area and ~0 m to the north (truncated by URU) (Fig. 5.14B). The thickness variation trend of the Cretaceous unit reflects the variation in burial depth of the Mjølnir Impact Crater, and the unit may be considered overburden for the structure. The overburden thickness affects the maximum hydrocarbon column that may be supported, in other words, as the overburden thickness increases, the maximum height that can be supported by the mechanical strength of the cap rock increases (Edmundson et al., 2019). The burial depth of the structure is also

crucial to consider with respect to biodegradation of hydrocarbons. Shallow accumulations of hydrocarbons may be affected by biodegradation by micro-organisms at lower temperatures (>60 ^{o}C) (Bjørlykke, 2010), introducing another risk-factor for reduced overburden thickness. Reservoirs that have been buried at greater depths (80-90 ^{o}C) may however be sterilized by the heat, not allowing for the recolonization of hydrocarbon degrading bacteria, even post uplift (Wilhelms et al., 2001). When considering the factors of overburden thickness and possible biodegradation, the southern Mjølnir Impact Crater may be considered more favorable for retaining and preserving accumulations of hydrocarbon, compared to the northern parts, characterized by less overburden.

The Red Wing Creek structure (Table 2.1) represent an impact structure that is being exploited for commercial hydrocarbons. The complex impact structure has proven a 490 m net pay column in the central uplift, due to structural repetition of the main reservoir formation (Grieve, 1997). The Red Wing Creek structure is however buried by 1,5 km of sediment, unlike the central high of the Mjølnir Impact Crater which is buried by ~50 meters of Quarternary deposits (till and sediment) (Dypvik et al., 2010c). The thin overburden covering the central high of the Mjølnir Impact Crater may limit its potential of retaining a hydrocarbon column.

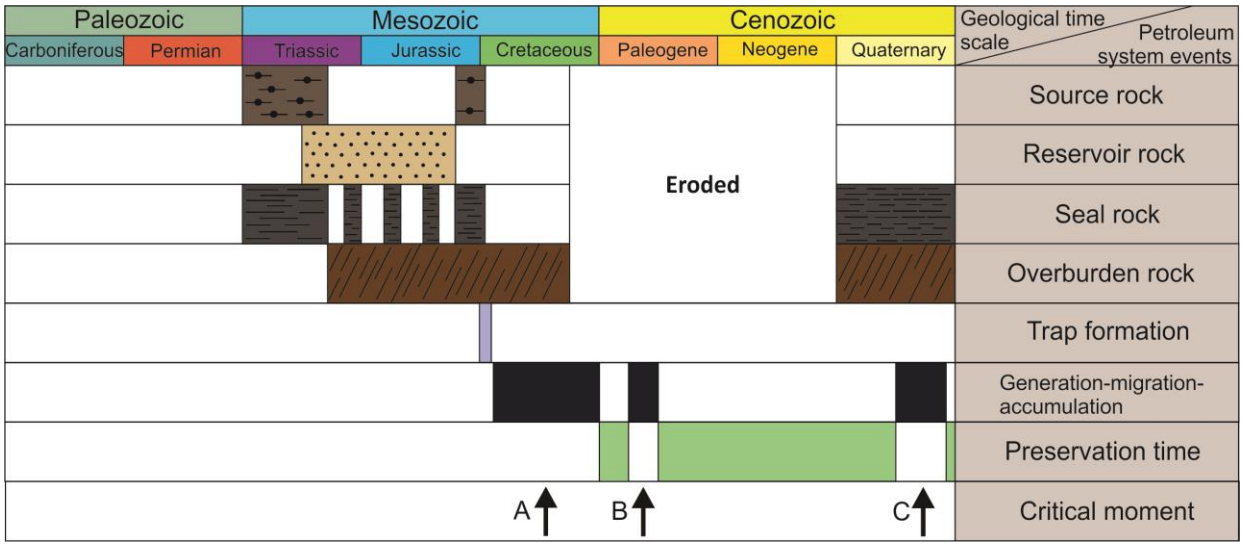

Figure 6.6: The figure shows a proposed Petroleum System Event Chart for the Mjølnir Impact Crater, indicating the time of source, reservoir, seal and overburden rock deposition. The timing of trap formation, generation, migration and accumulation is also shown. The trap formation is related to the faulting induced by the Mjølnir impact event. The critical moments (A-C) refers to several possible phases of generation, migration, remigration and accumulation: A) Burial of the Mjølnir Impact Crater, maturing the source rock (generation) and migration through deep-seated faults formed during impact. B) early Paleogene regional tectonic compression causing reactivation of faults and structurally lifting the central high and tilting of the Mesozoic and Paleozoic stratigraphy, possibly causing remigration into structural traps formed during the Mjølnir impact event. C) Migration and remigration into structural traps due to late Cenozoic uplift and erosion.

6.2.5 Hydrocarbon accumulations

A total of 5 amplitude anomalies (AA) have been identified in the Realgrunnen Subgroup within the study area (Figs. 5.27-5.32). AA1 and AA5 are located adjacent to the rim fault of the western and southern Mjølnir Impact Crater, respectively. AA2-4 are located in the southern crater (Fig. 5.26). These amplitude anomalies may represent accumulations of hydrocarbons, causing an increase in amplitude of the seismic reflection (i.e. bright spot). It is however important to keep in mind that such amplitude anomalies may be caused by lithological differences, or lateral variations of impact-related brecciation or disturbance of the stratigraphy.

Amplitude anomaly 2-4

The amplitude anomalies 2-4 are concentrated in the southeastern outer zone of the Mjølnir Impact Crater (Fig. 5.26). The increase in seismic amplitude may represent hydrocarbon accumulations structurally trapped in horsts of the outer zone (Figs. 5.28-5.29). Each anomaly is only visible on one seismic 2D line, and no apparent migration pathway into the horsts has been identified. There are however deeper faults underlying the outer zone, as seen on other seismic 2 lines (Fig. 5.25), and similar faulting could constitute a vertical migration conduit from underlying source rocks (Steinkobbe-, Klappmyss- and Havert Formation). The structural traps are juxtaposed with the allochthonous breccia of the Ragnarok Formation Unit II and overlain by the Fuglen Formation. The Fuglen formation has proven to constitute a sealing lithology (NPD, 2014), but for there to be an accumulation of hydrocarbons, the allochthonous breccia must also represent an impermeable lithology.

Amplitude anomaly 1

Amplitude anomaly 1 (AA1) is located at the platform-area just adjacent to an interpreted rimfault of the western Mjølnir Impact Crater (Fig. 5.26). The anomaly is only visible on one seismic 2D line (Fig. 5.27). AA1 is characterized by an amplitude shutoff with depth, creating a flat spot (Fig. 5.27). This could represent a gas-water-contact (GWC) or oil-water-contact (OWC) but may also be due to lithological differences. The interpreted fault underlying AA1 may function as a conduit for vertical migration of hydrocarbons from deeper laying reservoir rock or underlying source rocks and into the reservoir rock of the Realgrunnen Subgroup (Fig 6.7). The overlying vertical zone of chaotic seismic may represent tertiary migration from the reservoir, due to fault-seal breach, possibly tied to the reactivation of the rim fault (Fig. 6.7)

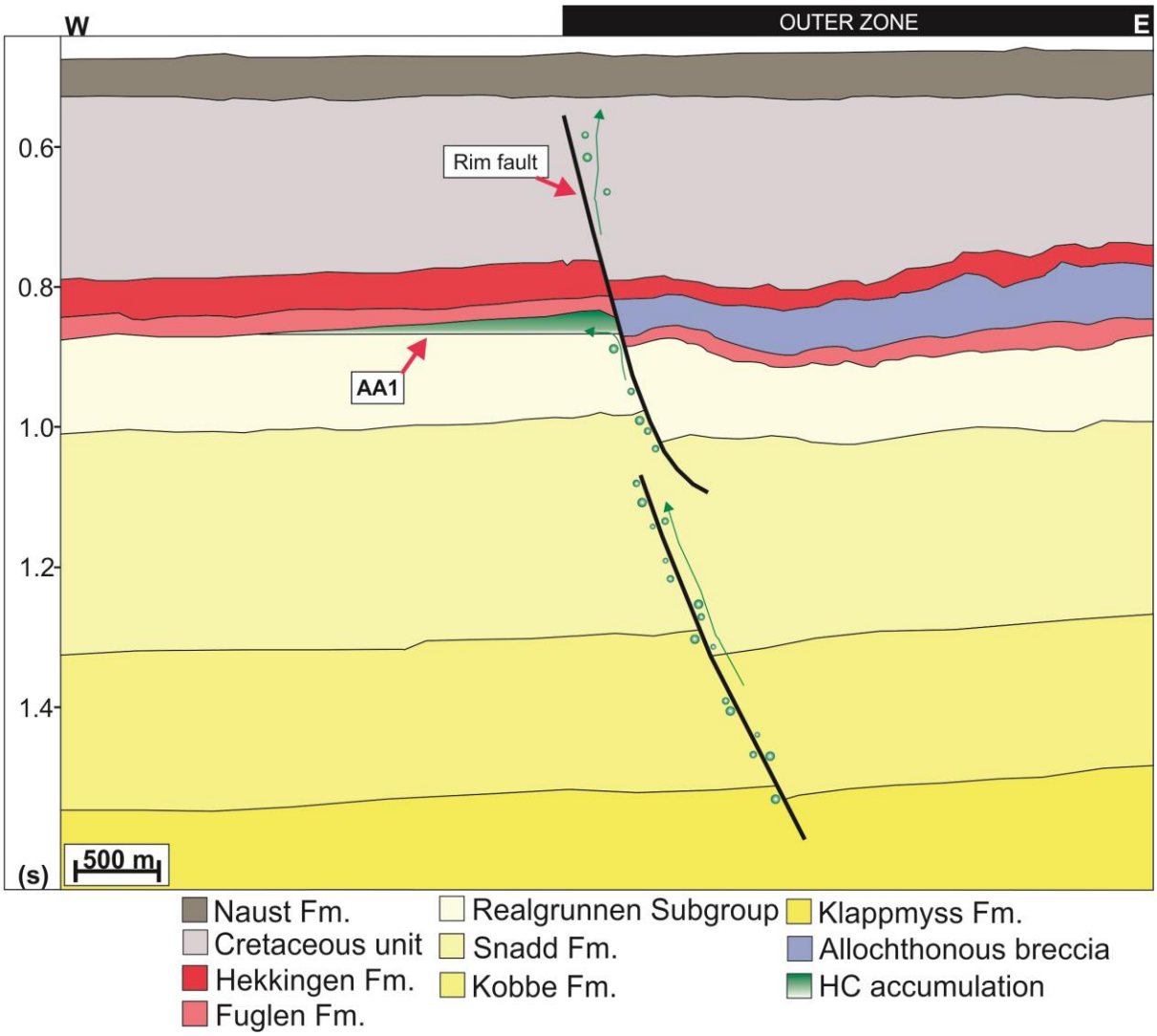

Figure 6.7: The sketch shows a model for amplitude anomaly 1 (Figs. 5.26-5.27) as a hydrocarbon (HC) accumulation (green). The accumulation is bounded by rim faults to the west. The deep-seated fault could possibly function as a conduit for HC migration (green arrow) from underlying source rocks, and into the structure. The previously described flat spot may represent an oil-water-contact or gas-water-contact.

Amplitude anomaly 5

Amplitude anomaly 5 is located at the Platform-area adjacent to the interpreted rim faults of the southern Mjølnir Impact Crater (Fig. 5.26). This bright spot and potential flat spot (Fig. 5.30) may be interpreted to represent change in pore fluids within porous rock of the Stø Formation. More specifically, gas- or light-oil saturation resulting in a stronger negative

amplitude of the reflection. By combining the three seismic 2D lines where AA5 is visible (Fig. 5.30-5.32) and the contour lines in the structural map of Top Stø horizon (Fig. 5.8B), a possible outline of the amplitude anomaly is established (Fig. 6.9). AA5 is seemingly structurally trapped by adjacent faults, including rim faults of the Mjølnir Impact Crater (Figs. 5.30-5.32). AA5 is overlain and juxtaposed by the Fuglen Formation, which may function as a sealing lithology for the trap (Fig. 6.8). The Avak structure may work as an analogue for this interpretation, as it includes three similarly located gas fields bounded by the rim faults of the structure (Kirschner et al., 1992). The relative location of AA5, at the southern margin of the Mjølnir Impact Crater, may be considered favorable, due to the thicker overburden and larger potential sealing capacity than other parts of the structure (chap. 6.2.4). Temperature calculations from TP1 also indicate that the Realgrunnen Subgroup has previously been exposed to higher temperatures (Table 6.1) that might have sterilized the reservoir, preventing biodegradation of potential hydrocarbon accumulations. The location of AA5 could also be favorable for lateral migration from the south (including the Nordkapp Basin), since the strata is dipping towards the south (Fig. 5.5). Since the potential trap is located outside of the Mjølnir Impact Crater, it is not considered to be largely affected by the increased porosity induced by the in-place brecciation of the Realgrunnen Subgroup.

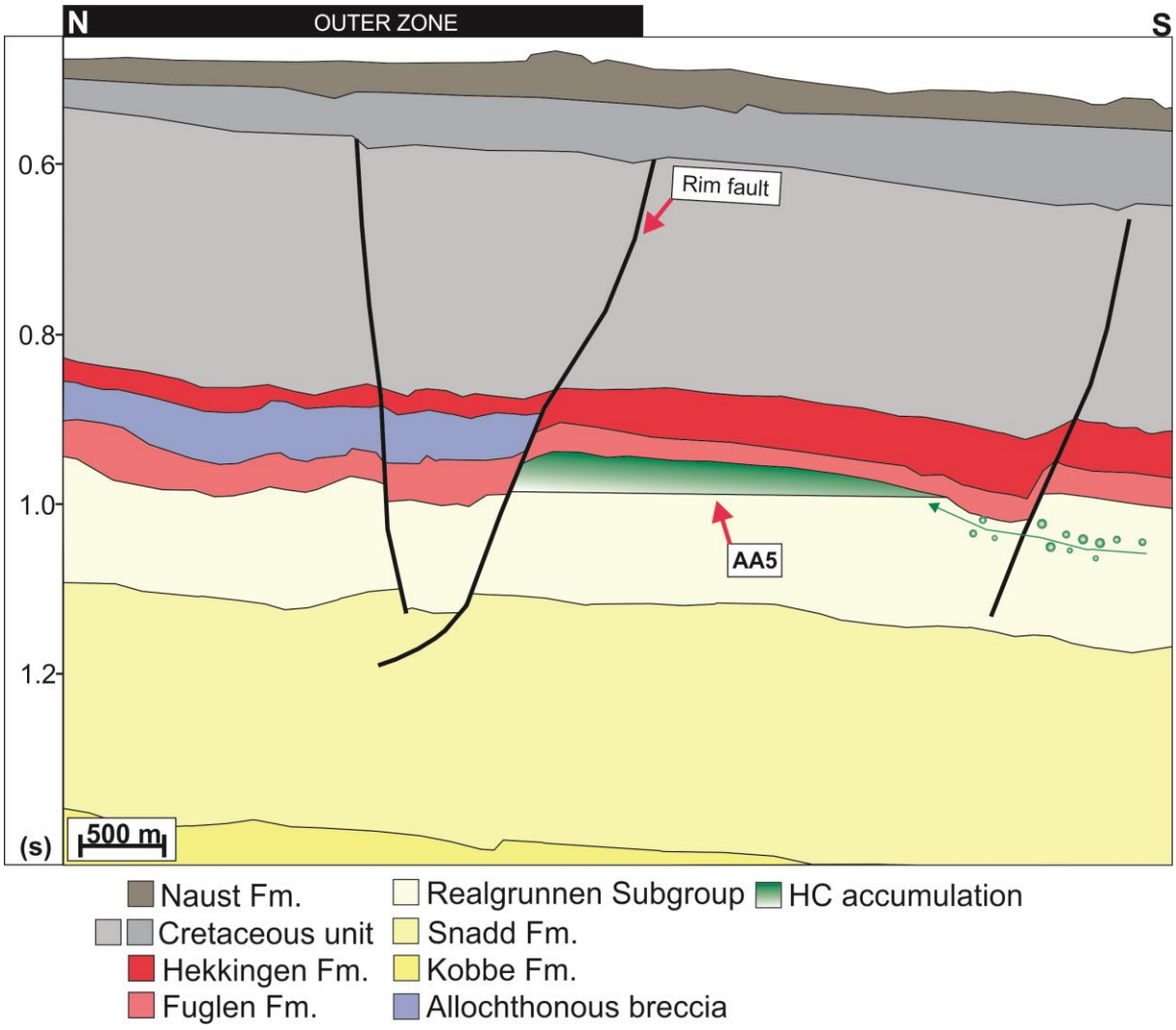

Figure 6.8: The sketch shows a model for amplitude anomaly 5 (Figs. 5.30-5.32) as a hydrocarbon (HC) accumulation (green). The accumulation is bounded by rim faults to the north and faulting at the Bjarmeland Platform to the south. The general north-south dip of the Bjarmeland Platform and Mjølnir Impact Crater makes lateral migration from the south a possibility (green arrow). The previously described flat spot may represent an oil-water-contact or gas-water-contact.

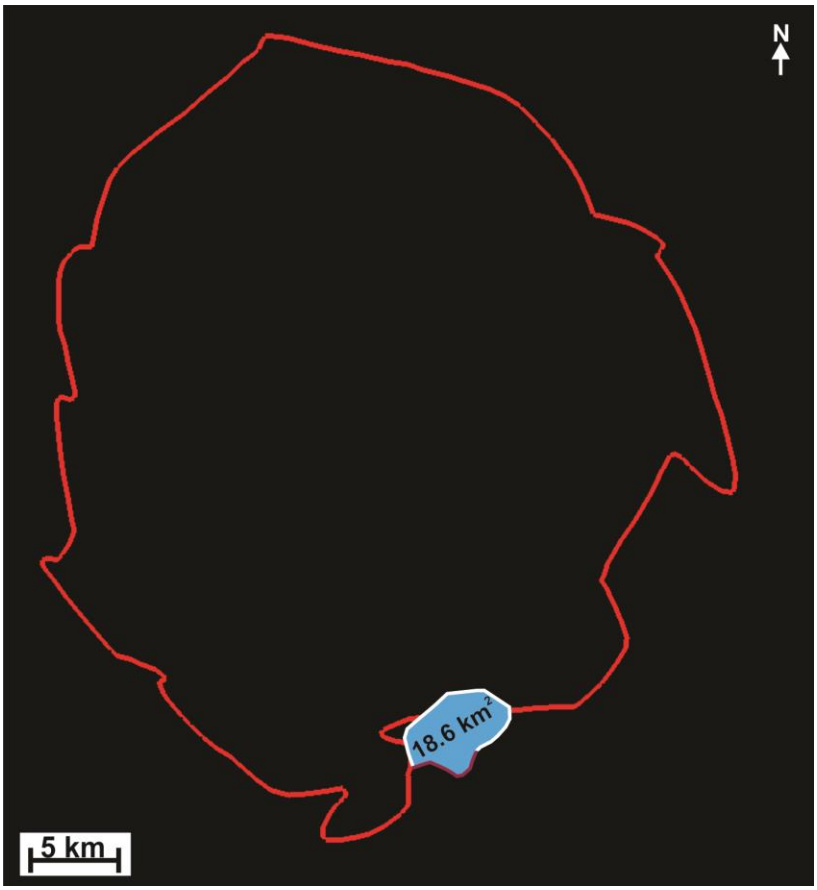

Figure 6.9: The figure shows the outline (structural closure) of AA5 (blue) at the southern margin of the Mjølnir Impact Crater, adjacent to rim faults towards the north. In this area, the rim faults do not coincide with the shapefile of the crater. The closure has been defined by mapped faults (white line, Figs. 5.30-5.32) and contour lines of the Top Stø horizon (purple line, Fig. 5.8B). The closure is somewhat uncertain due to the insufficient data coverage. The total closure is 18.6 km^2.

The established closure of the structure makes it possible to roughly calculate the potential in-place-hydrocarbons (Fig. 6.9). The volumetric calculations for original-oil-in-place (OOIP) is dependent on the gross rock volume (GRV), net-to-gross reservoir (N/G), porosity of the reservoir (ϕ), Saturation of oil (S_{oil}) and the oil formation volume factor (B_{oil}) ("Volumetrics," 2018). As shown in the following equation:

Equation 6.1 Original-oil-in-place

$$OOIP\ (m^3) = \frac{GRV * \frac{N}{G} * \phi * S_{oil}}{B_{oil}}$$

In order to obtain the gross rock volume, the drainage area (A) and thickness (t) of the reservoir interval must be obtained. The identified rough outline of the amplitude is calculated to 18.6 km^2, using the calculation tool in Petrel E&P software. It should however be mentioned that this outline is based on very sparse data coverage, introducing a source of error. The measured thickness of the amplitude varies between 20 ms and 35 ms (TWT). The lowest measured thickness corresponds to 30 m and is used for the following calculations. By using Equation 6.2 the GRV is found to be 0.558 km^3.

Equation 6.2 Gross rock volume

$$GRV = A * t$$

The reservoir rock is assumed to be of fairly good quality, but the previous burial and diagenesis has most likely reduced the porosity, as indicated for sandstone in Figure 2.6, and the porosity has not been increased due to brecciation (chapter 6.2.3). Taking this into account, an assumed porosity of 15% is used for the calculations. The Net-to-gross (N/G) (i.e. pay zone) is set to 0.5, meaning the calculations assumes that 50% of the total thickness (30meters) consists of reservoir rock. The oil-saturation (S_{oil}) is set to 0.7, which represents the volume fraction of the porosity that is filled with oil. Lastly, the oil formation volume factor, representing the change in oil volume between the reservoir conditions and surface conditions, is set to 1.3. This estimation is based on the relatively shallow position of the reservoir.

The calculated original-oil-in-place using the factors described above is 24,412,500 Sm^3, corresponding to 153.55 MMbbl.

7 Conclusions

The petroleum system potential and evolution of the Mjølnir Impact Crater have been studied using both conventional 2D seismic- and P-cable seismic data. The primary focus has been on identifying and evaluating source rock, migration, reservoir rock, trap and seal in and around the Mjølnir Impact Crater. The key findings of this study are summarized below.

- A simplified 1D maturation model within the fetch area of the crater structure has indicated potential oil generation for the Hekkingen- and Steinkobbe formations and gas generation for the Klappmyss- and Havert formations, at maximum burial.
- Deep-seated faults in the Mjølnir Impact Crater and on the Bjarmeland Platform may function as conduits for vertical migration from underlying source rocks. The southward dip of the stratigraphy also enables lateral migration from the south to potential structures associated with the crater.
- Multiple formations affected by the Mjølnir impact event may constitute reservoir rock (Kobbe- and Snadd formations and the Realgrunnen Subgroup). The porosity of these reservoir rocks may also be increased in the outer zone of the crater, due to brecciation. The Jurassic sandstones of the Realgrunnen Subgroup is proposed to represent the most important reservoirs in the study area. The possible reservoir rocks are at depths of 1000 meters and have seen maximum burial of 3000 meters, thus diagenetic effects are considered to be limited.
- The structural setting of the Mjølnir Impact Crater encompasses potential structural traps. The most important traps are likely to be horst and graben structures in the marginal fault zone and listric faults (rim faults) at the outer boundary of the crater. The faults have however been reactivated in connection to regional tectonic stresses and Cenozoic uplift and erosion (~2000 meters) events in the Barents Sea, which may cause leakage due to fault-seal breach.
- A series of amplitude anomalies (AA) have been identified in the study area, which may indicate the presence of hydrocarbons. Amplitude anomaly 2-4 are likely to represent hydrocarbon accumulations in the reservoir rock intervals of the Realgrunnen Subgroup, structurally trapped in horsts of the southern marginal fault zone. Amplitude anomaly 1 and 5 are likely to represent hydrocarbon accumulations in the reservoir rock of the Realgrunnen Subgroup, structurally trapped by faults of the

Mjølnir Impact Crater (rim faults) and the Bjarmeland Platform. Amplitude Anomaly 5 was calculated to potentially represent a volume of c. 153.55 MMbbl original-oil-in-place (OOIP). These amplitude anomalies are primarily concentrated to the southern Mjølnir Impact Crater, which is likely to be the most favorable section of the crater in terms of hydrocarbon potential, due to thicker overburden and effective sealing, and possibly more favorable migration pathways.

Future work

The data coverage (grid size) has given som constrains on the detailed interpretations of an impact structure characterized by such complex geology. Seismic 3D data would be a useful tool to gain a better understanding of the structural features of the crater and allow for more detailed assessment of the Mjølnir Impact Crater as a potential petroleum system. Petroleum 3D maturation modelling would test the different scenarios of the petroleum system proposed in this thesis. Sequential restoration exercise would also be important to future work to consider the complex effects of impact, Cenozoic uplift, erosion and tilt of the stratigraphy.

8 References

Amantov, A., & Fjeldskaar, W. (2018). Meso-Cenozoic exhumation and relevant isostatic process: The Barents and Kara shelves. Journal of Geodynamics, 118, 118-139. doi:10.1016/j.jog.2017.12.001

Andreassen, K., Nilssen, E., & Ødegaard, C. (2007). Analysis of shallow gas and fluid migration within the Plio-Pleistocene sedimentary succession of the SW Barents Sea continental margin using 3D seismic data. An International Journal of Marine Geology, 27(2), 155-171. doi:10.1007/s00367-007-0071-5

Badley, M. E. (1985). Practical seismic interpretation. Boston: International Human Resources Development Corporation.

Baig, I., Faleide, J. I., Jahren, J., & Mondol, N. H. (2016). Cenozoic exhumation on the southwestern Barents Shelf: Estimates and uncertainties constrained from compaction and thermal maturity analyses. Marine and Petroleum Geology, 73(C), 105-130. doi:10.1016/j.marpetgeo.2016.02.024

Barton, R., Bird, K., Hernández, J. G., Grajales-Nishimura, J. M., Murillo-Muñetón, G., Herber, B., Weimer, P., Koeberl, C., Neumaier, M., Schenk, O., & Stark, J. (2009). High-Impact Reservoirs. Oilfield Review, 21(4), 14-29.

Bjørlykke, K. (2010). Petroleum Geoscience : From Sedimentary Environments to Rock Physics.

Brown, A. R. (2004). Interpretation of three-dimensional seismic data (6th ed. ed. Vol. 42). Tulsa, Okla: American Association of Petroleum Geologists.

Buthman, D. B. (1997). Global Hydrocarbon Potential of Impact Structures. In K. S. Johnson & J. A. Campbell (Eds.), Ames Structure in Northwest Oklahoma and Similar Features: Origin and Petroelum Production (pp. 83-99): Oklahoma Geological Survey Circular 100.

Cavanagh, A., Di Primio, R., Scheck-Wenderoth, M., & Horsfield, B. (2006). Severity and timing of Cenozoic exhumation in the southwestern Barents Sea. J. Geol. Soc., 163, 761-774.

Corseri, R., Gac, S., Faleide, J. I., & Planke, S. (2020). The Tectonized central peak of the Mjølnir Impact Crater, Barents Sea. Journal of Structural Geology, 131. doi:https://doi.org/10.1016/j.jsg.2019.103953

Dalland, A., Worsley, D., & Ofstad, K. (1988). A Lithostrategraphic scheme for the Mesozoic and Cenozoic succession offshore mid- and northern Norway(Vol. 4).

Dallmann, W. K., Stratigrafisk komité for, S., & Norsk, p. (1999). Lithostratigraphic lexicon of Svalbard : review and recommendations for nomenclature use : Upper Palaeozoic to Quaternary bedrock. Tromsø: Norsk polarinstitutt.

Donofrio, R. (1998). North American impact structures hold giant field potential. Oil & Gas Journal, 96(19), 69-83.

Doré, A. G., & Jensen, L. N. (1996). The impact of late Cenozoic uplift and erosion on hydrocarbon exploration: offshore Norway and some other uplifted basins. Global and Planetary Change, 12(1), 415-436. doi:10.1016/0921-8181(95)00031-3

Dypvik, H., Gudlaugsson, S. T., Tsikalas, F., & Attrep, M. (1996). Mjolnir structure: An impact crater in the Barents Sea. Geology, 24(9), 779. doi:10.1130/0091-7613(1996)024<0779:MLSAIC>2.3.CO2

Dypvik, H., Mørk, A., Smelror, M., Sandbakken, P., Tsikalas, F., Vigran, J. O., Bremer, A., Nagy, J., Gabrielsen, R. H., Faleide, J. I., Bahiru, G. M., & Weiss, H. H. (2004). Impact breccia and ejecta from the Mjølnir crater in the Barents Sea - The Ragnarok Formation and Sindre Bed. Norsk geologisk tidsskrift, 84.

Dypvik, H., Smelror, M., Mørk, A., & Tsikalas, F. (2010a). Ejecta Geology. In H. Dypvik, F. Tsikalas, & M. Smelror (Eds.), The Mjølnir Impact Event and its Consequences (1st ed. 2010. ed., pp. 175-194). Berlin, Heidelberg: Springer Berlin Heidelberg: Imprint: Springer.

Dypvik, H., Smelror, M., Mørk, A., & Tsikalas, F. (2010b). Introduction. In H. Dypvik, F. Tsikalas, & M. Smelror (Eds.), The Mjølnir Impact Event and its Consequences (1st ed. 2010. ed., pp. 1-22). Berlin, Heidelberg: Springer Berlin Heidelberg: Imprint: Springer.

Dypvik, H., Smelror, M., Mørk, A., Werner, S. C., & Torsvik, T. H. (2010c). Impact Cratering and Post-impact Sedimentation. In H. Dypvik, F. Tsikalas, & M. Smelror (Eds.), The Mjølnir Impact Event and its Consequences (1st ed. 2010. ed., pp. 139-174). Berlin, Heidelberg: Springer Berlin Heidelberg: Imprint: Springer.

Dypvik, H., Tsikalas, F., & Smelror, M. (2010d). The Mjølnir Impact Event and its Consequences : Geology and Geophysics of a Late Jurassic/Early Cretaceous Marine Impact Event(1st ed. 2010. ed.).

Edmundson, I., Rotevatn, A., Davies, R., Yielding, G., & Broberg, K. (2019). Key controls on hydrocarbon retention and leakage from structural traps in the Hammerfest Basin, SW Barents Sea; implications for prospect analysis and risk assessment. Petroleum Geoscience. doi:10.1144/petgeo2019-094

Ehrenberg, S. N., & Nadeau, P. H. (2005). Sandstone vs. carbonate petroleum reservoirs; a global perspective on porosity-depth and porosity-permeability relationships. AAPG Bulletin, 89(4), 435-445. doi:10.1306/11230404071

EID. (2019). About the Earth Impact Database. Retrieved from http://www.passc.net/EarthImpactDatabase/New%20website_05-2018/Index.html

Faleide, J. I., Bjørlykke, K., & Gabrielsen, R. H. (2015). Geology of the norwegian continental shelf.

Faleide, J. I., Gudlaugsson, S. T., & Jacquart, G. (1984). Evolution of the western Barents Sea. Marine and Petroleum Geology, 1(2), 123,IN121,129,IN125,137-128,IN124,136,IN128,150. doi:10.1016/0264-8172(84)90082-5

Faleide, J. I., Solheim, A., Fiedler, A., Hjelstuen, B., Andersen, E., & Vanneste, K. (1996). Late Cenozoic evolution of the western Barents Sea-Svalbard continental margin. Glob. Planet. Change, 12(1-4), 53-74.

Faleide, J. I., Tsikalas, F., Breivik, A., Mjelde, R., Ritzmann, O., Engen, Ø., Wilsom, J., & Eldholm, O. (2008). Structure and evolution of the continental margin off Norway and Barents Sea. Episodes, 31, 82-91.

Faleide, J. I., Vågnes, E., & Gudlaugsson, S. T. (1993). Late Mesozoic-Cenozoic evolution of the south-western Barents Sea in a regional rift-shear tectonic setting. Marine and Petroleum Geology, 10(3), 186-214. doi:10.1016/0264-8172(93)90104-Z

Gabrielsen, R. H., Færseth, R. B., Jensen, L. N., Kalheim, J. E., & Riis, F. (1990). Structural elements of the Norwegian continental shelf, Part I: The Barents Sea Region. NPD-bulletin no 6.

Gernigon, L., Brönner, M., Roberts, D., Olesen, O., Nasuti, A., & Yamasaki, T. (2014). Crustal and basin evolution of the southwestern Barents Sea: From Caledonian orogeny to continental breakup. Tectonics, 33(4), 347-373. doi:10.1002/2013TC003439

Glørstad-Clark, E., Faleide, J. I., Lundschien, B. A., & Nystuen, J. P. (2010). Triassic seismic sequence stratigraphy and paleogeography of the western Barents Sea area. Marine and Petroleum Geology, 27(7), 1448-1475. doi:10.1016/j.marpetgeo.2010.02.008

Grieve, R. A. F. (1997). Terrestrial Impact Structures: Basic Characteristics and Economic Significance, with Emphasis on Hydrocarbon Production. In K. S. Johnson & J. A. Campbell (Eds.), Ames Structure in Northwest Oklahoma and Similar Features: Origin and Petroelum Production (pp. 3-17): Oklahoma Geological Survey Circular 100.

Grogan, P., Nyberg, K., Fotland, B., Myklebust, R., Dahlgren, S., Riis, F., Hannover, T. I. B. T. I. U., & Alfred-Wegener-Institut für Polar- und, M. (2000). Cretaceous Magmatism South and East of Svalbard: Evidence from Seismic Reflection and Magnetic Data. doi:10.2312/polarforschung.68.25

Gudlaugsson, S. T. (1993). Large impact crater in the Barents Sea. Geology, 21(4), 291-294.

Henriksen, E., Bjørnseth, H. M., Hals, T. K., Heide, T., Kiryukhina, T., Kløvjan, O. S., Larssen, G. B., Ryseth, A. E., Rønning, K., Sollid, K., & Stoupakova, A. (2011a). Chapter 17 Uplift and erosion of the greater Barents Sea: impact on prospectivity and petroleum systems. Geological Society, London, Memoirs, 35(1), 271-281. doi:10.1144/m35.17

Henriksen, E., Ryseth, A. E., Larssen, G. B., Heide, T., Rønning, K., Sollid, K., & Stoupakova, A. V. (2011b). Chapter 10 Tectonostratigraphy of the greater Barents Sea: implications for petroleum systems. Geological Society, London, Memoirs, 35(1), 163-195. doi:10.1144/m35.10

Jansa, L. F. (1993). Cometary impacts into ocean: their recognition and the threshold constraint for biological extinctions. Palaeogeography, Palaeoclimatology, Palaeoecology, 104(1), 271-286. doi:10.1016/0031-0182(93)90137-8

Kearey, P., Brooks, M., & Hill, I. (2002). An introduction to geophysical exploration (3rd ed. Vol. 4). Oxford: Wiley-Blackwell.

Kearey, P., & Brooks, M. H., I. (2002). An introduction to geophysical exploration (3rd ed. Vol. 4). Oxford: Wiley-Blackwell.

Kenkmann, T., Collins, G. S., & Wünnemann, K. (2013). The modification stage of crater formation. In G. R. Osinski & E. Pierazzo (Eds.), Impact Cratering: Processes and Products (pp. 60-75). Hoboken, N.J.: Wiley-Blackwell.

Khutorskoi, M., Viskunova, K., Podgornykh, L., Suprunenko, O., & Akhmedzyanov, V. (2008). A temperature model of the crust beneath the Barents Sea: Investigations along geotraverses. Geotectonics, 42(2), 125-136. doi:10.1134/S0016852108020039

Kirschner, C. E., Grantz, A., & Mullen, M. W. (1992). Impact origin of the Avak Structure, Arctic Alaska, and genesis of the Barrow gas fields. AAPG Bulletin, 76(5), 651-679. doi:10.1306/BDFF889E-1718-11D7-8645000102C1865D

Klausen, T. G., Mueller, R., Slama, J., Olaussen, S., Rismyhr, B., & Helland-Hansen, W. (2018a). Depositional history of a condensed shallow marine reservoir succession; stratigraphy and detrital zircon geochronology of the Jurassic Sto Formation, Barents Sea. Journal of the Geological Society of London, 175(1), 130-145. doi:10.1144/jgs2017-024

Klausen, T. G., Nyberg, B., & Helland-Hansen, W. (2019). The largest delta plain in Earth's history. Geology, 47(5), 470-474. doi:10.1130/G45507.1

Klausen, T. G., Ryseth, A. E., Helland-Hansen, W., Gawthorpe, R., & Laursen, I. (2015). Regional development and sequence stratigraphy of the Middle to Late Triassic Snadd Formation, Norwegian Barents Sea. Marine and Petroleum Geology, 62, 102-122. doi:10.1016/j.marpetgeo.2015.02.004

Klausen, T. G., Torland, J. A., Eide, C. H., Alaei, B., Olaussen, S., & Chiarella, D. (2018b). Clinoform development and topset evolution in a mud‐rich delta ‐the Middle Triassic Kobbe Formation, Norwegian Barents Sea. Sedimentology, 65(4), 1132-1169. doi:10.1111/sed.12417

Klitzke, P., Faleide, J. I., Scheck-Wenderoth, M., & Sippel, J. (2015). A lithosphere-scale structural model of the Barents Sea and Kara Sea region. Solid Earth, 6(1), 153. doi:10.5194/se-6-153-2015

Ktenas, D., Meisingset, I., Henriksen, E., & Nielsen, J. (2018). Estimation of net apparent erosion in the SW Barents Sea by applying velocity inversion analysis. Petroleum Geoscience, 25(2), 169-187. doi:10.1144/petgeo2018-002

Larssen, G. B., Elvebakk, G., Henriksen, L. B., Kristensen, S.-E., Samuelsberg, T. J., Svånå, T. A., Stemmerik, L., & Worsley, D. (2002). Upper Palaeozoic lithostratigraphy of the Southern Norwegian Barents Sea. Norwegian Petroleum Directorate Bulletin no. 9.

Lasabuda, A. (2018). Cenozoic tectonosedimentary development and erosion estimates for the Barents Sea continental margin, Norwegian Arctic. UiT The Arctic University of Norway, Faculty of Science and Technology, Department of Geosciences, Tromsø.

Lasabuda, A., Laberg, J. S., Knutsen, S.-M., & Høgseth, G. (2018a). Early to middle Cenozoic paleoenvironment and erosion estimates of the southwestern Barents Sea: Insights from a regional mass-balance approach. Marine and Petroleum Geology, 96, 501-521. doi:10.1016/j.marpetgeo.2018.05.039

Lasabuda, A., Laberg, J. S., Knutsen, S.-M., & Safronova, P. (2018b). Cenozoic tectonostratigraphy and pre-glacial erosion: A mass-balance study of the northwestern Barents Sea margin.

Leith, T. L., Weiss, H. M., Mørk, A., århus, N., Elvebakk, G., Embry, A. F., Brooks, P. W., Stewart, K. R., Pchelina, T. M., Bro, E. G., Verba, M. L.,

Danyushevskaya, A., & Borisov, A. V. (1993). Mesozoic hydrocarbon source-rocks of the Arctic region (Vol. 2).

Ligtenberg, J. H. (2005). Detection of fluid migration pathways in seismic data: implications for fault seal analysis. Basin Research, 17(1), 141-153. doi:10.1111/j.1365-2117.2005.00258.x

Løseth, H., Gading, M., & Wensaas, L. (2009). Hydrocarbon leakage interpreted on seismic data. Marine and Petroleum Geology, 26(7), 1304-1319. doi:10.1016/j.marpetgeo.2008.09.008

Lundschien, B. A., Høy, T., & Mørk, A. (2014). Triassic hydrocarbon potential in the Northern Barents Sea; integrating Svalbard and stratigraphic core data. NPD Bulletin, 11, 3-20.

Magoon, L. B., & Dow, W. G. (1994). The petroleum system. In L. B. Magoon & W. G. Dow (Eds.), The Petroleum system-From Source to Trap: AAPG Memoir 60 (pp. 3-24).

Melosh, H. J. (2013). The Contact and Compression Stage of Impact Cratering. In R. G. P. Osinski, Elisabetta (Ed.), Impact Cratering: Processes and Products (pp. 32-42). Hoboken, N.J.: Wiley-Blackwell.

Midtkandal, I., Faleide, J. I., Faleide, T. S., Serck, C. S., Planke, S., Corseri, R., Dimitriou, M., & Nystuen, J. P. (2019). Lower Cretaceous Barents Sea strata: epicontinental basin configuration, timing, correlation and depositional dynamics. 157(3), 458-476. doi:10.1017/S0016756819000918

Mørk, A., Dallmann, W. K., Dypvik, H., Johannessen, E. P., Larsen, G. B., Nagy, J., Nøttvedt, A., Olaussen, S., Pcelina, T. M., & Worsley, D. (1999). Mesozoic Lithostratigraphy. In W. K. Dallmann (Ed.), Lithostratigraphic Lexicon of Svalbard: Upper Palaeozoic to Quaternary Bedrock (pp. 127-214). Tromsø: Norwegian Polar Institute.

Mørk, A., & Elvebakk, G. (1999). Lithological description of subcropping Lower and Middle Triasic rocks from the Svalis Dome, Barents Sea. Polar Research, 18(1), 83-104. doi:10.1111/j.1751-8369.1999.tb00278.x

Mørk, A., Embry, A., & Weitschat, W. (1989). Triassic transgressive-regressive cycles in the Sverdrup Basin, Svalbard and the Barents Shelf. In Correlation in hydrocrabon exploration (pp. 113-130). Dordrecht: Springer.

Nanda, N. C. (2016). Seismic Data Interpretation and Evaluation for Hydrocarbon Exploration and Production : A Practitioner's Guide(1st ed. 2016. ed.).

NPD. (2014). Compiled CO_2 atlas for the Norwegian Continental Shelf.

NPDfactpages. (n.d.-a). Snadd Fm. Retrieved from https://factpages.npd.no/en/strat/pageview/litho/formations/150

NPDfactpages. (n.d.-b). Wellbore 7226/11-1. Retrieved from https://factpages.npd.no/no/wellbore/pageview/exploration/all/1177

NPDfactpages. (n.d.-c). Wellbore 7435/12-1. Retrieved from https://factpages.npd.no/nb-no/wellbore/pageview/exploration/all/8228

Ohm, S. E., Karlsen, D. A., & Austin, T. J. F. (2008). Geochemically driven exploration models in uplifted areas: Examples from the Norwegian Barents Sea. AAPG Bulletin, 92(9), 1191-1223. doi:10.1306/06180808028

Okeefe, J. D., & Ahrens, T. J. (1982). Impact of an asteroid or comet in the ocean and extinction of terrestrial life - NASA-CR-169086. In.

Olaussen, S., Dalland, A., Gloppen, T. G., & Johannessen, E. (1984). Depositional environment and diagenesis of Jurassic reservoir sandstones in the eastern part of Tromsø I area. In Petroleum Geology of the North European Margin (pp. 61-79). Dordrecht: Springer.

Osinski, G. R., Grieve, R. A. F., & Tornabene, L. L. (2013). Excavation and Impact Ejecta Emplacement. In R. G. P. Osinski, Elisabetta (Ed.), Impact Cratering: Processes and Products (pp. 43-59). Hoboken, N.J.: Wiley-Blackwell.

Richardsen, G., Vorren, T. O., & Tørudbakken, B. O. (1993). Post-Early Cretaceous uplift and erosion in the southern Barents Sea ; a discussion based on analysis of seismic interval velocities. Norsk geologisk tidsskrift, 73, 3-20.

Riis, F., Lundschien, B. A., Høy, T., Mørk, A., & Mørk, M. B. E. (2008). Evolution of the Triassic shelf in the northern Barents Sea region. Polar Research: Special Issue: The Boreal Triassic, 27(3), 318-338. doi:10.1111/j.1751-8369.2008.00086.x

Rossi, V. M., Olaussen, S., Staine, I. N., & Gennaro, M. (2020). Development of the Middle Triassic Kobbe Formation shelf-margin prism and transgressive-regressive cycles on the shelf (Hammerfest Basin, SW Barents Sea). Marine and Petroleum Geology, 111, 868-885. doi:10.1016/j.marpetgeo.2019.08.043

Ryseth, A. (2014). Sedimentation at the Jurassic-Triassic boundary, south-west Barents Sea: Indication of climate change. In A. W. Martinius, R. Ravnas, J. A. Howell, R. J. Steel, & J. P. Wonham (Eds.), From depositional systems to sedimentary successions on the Norwegian Continental Margin (pp. 187-214).

Ryseth, A., Augustson, J. H., Charnock, M., Haugerud, O., Knutsen, S.-M., Midboe, P. S., Opsal, J. G., & Sundsbo, G. (2003). Cenozoic stratigraphy and evolution of the Sorvestsnaget Basin, southwestern Barents Sea. Norsk geologisk tidsskrift, 83(2), 107-130.

Selley, R. C., & Sonnenberg, S. A. (2015). Elements of petroleum geology (3rd ed. ed.). San Diego, Calif: Academic Press.

Sheriff, R. E. (2002). Encyclopedic Dictionary of Applied Geophysics (4th ed.). Tulsa, OK: Society of Exploration Geophysicists

Shuvalov, V., Dypvik, H., & Tsikalas, F. (2002). Numerical simulations of the Mjølnir marine impact crater. Journal of Geophysical Research: Planets, 107(E7), 1-1-1-13. doi:10.1029/2001JE001698

Shuvalov, V., Dypvik, H., & Tsikalas, F. (2010). The Impact Dynamics. In H. Dypvik, F. Tsikalas, & M. Smelror (Eds.), The Mjølnir Impact Event and its Consequences (1st ed. 2010. ed., pp. 195-210). Berlin, Heidelberg: Springer Berlin Heidelberg: Imprint: Springer.

Smelror, M., Basov, V. A., & NGU. (2009). Atlas : geological history of the Barents Sea. Trondheim: Geological Survey of Norway.

Smelror, M., Dypvik, H., & Mørk, A. (2002). Phytoplankton blooms in the Jurassic-Cretaceous boundary beds of the Barents Sea possibly induced by the Mjølnir impact. In Geological and Biological Effects of Impact Events (pp. 69-81). Berlin, Heidelberg: Springer.

Smelror, M., Kelly, S., Dypvik, H., Mørk, A., Nagy, J., & Tsikalas, F. (2001). Mjølnir (Barents Sea) meteorite impact offers a Volgian-Ryazanian boundary marker. Newsletters on Stratigraphy, 38, 129-140.

Sømme, T. O., Dore, A. G., Lundin, E. R., & Torudbakken, B. O. (2018). Triassic-Paleogene paleogeography for the Arctic; implications for sediment routing and basin fill. AAPG Bulletin, 102(12), 2481-2517. doi:10.1306/05111817254

Stemmerik, L., & Worsley, D. (2005). 30 years on - Arctic Upper Palaeozoic stratigraphy, depositional evolution and hydrocarbon prospectivity. Norw. J. Geol., 85(1-2), 151-168.

Talwani, M., & Eldholm, O. (1977). Evolution of the Norwegian-Greenland Sea. Geological Society of America Bulletin, 88(7), 969-999. doi:10.1130/0016-7606(1977)88<969:EOTNS>2.0.CO2

Tiab, D., & Donaldson, E. C. (2015). Petrophysics : theory and practice of measuring reservoir rock and fluid transport properties(4th ed. ed.).

Tsikalas, F., Faleide, J. I., Gudlaugsson, S. T., & Eldholm, O. (2010a). Impact Structure and Morphology. In H. Dypvik, F. Tsikalas, & M. Smelror (Eds.), The Mjølnir Impact Event and its Consequences (1st ed. 2010. ed., pp. 47-74). Berlin, Heidelberg: Springer Berlin Heidelberg: Imprint: Springer.

Tsikalas, F., Faleide, J. I., Werner, S. C., Torsvik, T. H., Gudlaugsson, S. T., & Eldholm, O. (2010b). Impact Geophysics and Modelling. In H. Dypvik, F. Tsikalas, & M. Smelror (Eds.), The Mjølnir Impact Event and its Consequences (1st ed. 2010. ed., pp. 75-138). Berlin, Heidelberg: Springer Berlin Heidelberg: Imprint: Springer.

Tsikalas, F., Gudlaugsson, S. T., Eldholm, O., & Faleide, J. I. (1998a). Integrated geophysical analysis supporting the impact origin of the Mjølnir structure, Barents Sea. Tectonophysics, 289(4), 257-280. doi:10.1016/S0040-1951(97)00234-5

Tsikalas, F., Gudlaugsson, S. T., & Faleide, J. I. (1998b). The anatomy of a buried complex impact structure: The Mjølnir Structure, Barents Sea. Journal of Geophysical Research: Solid Earth, 103(B12), 30469-30483. doi:10.1029/97JB03389

Tsikalas, F., Gudlaugsson, S. T., & Faleide, J. I. (1998c). Collapse, infilling, and postimpact deformation at the Mjolnir impact structure, Barents Sea. Geological Society of America. Geological Society of America Bulletin, 110(5), 537-552. doi:10.1130/0016-7606(1998)110<0537:CIAPDA>2.3.CO2

Vagnes, E., & Amundsen, H. E. F. (1993). Late Cenozoic uplift and volcanism on Spitsbergen: caused by mantle convection? Geology, 21(3), 251-254.

Veeken, P. P. (2007). Seismic Stratigraphy, Basin Analysis and Reservoir Characterisation (Vol. 37): Elsevier.

Veeken, P. P. (2013). Seismic Stratigraphy and Depositional Facies Models. Burlington: Elsevier Science.

Volumetrics. (2018). SEG wiki. Retrieved from https://wiki.seg.org/wiki/Volumetrics#Original_Oil-In-Place:.5B2.5D

Vorren, T. O., Richardsen, G., Knutsen, S.-M., & Henriksen, E. (1991). Cenozoic erosion and sedimentation in the western Barents Sea. Marine and Petroleum Geology, 8(3), 317-340. doi:10.1016/0264-8172(91)90086-G

Wilhelms, A., Larter, S. R., Head, I., Farrimond, P., Di-Primio, R., & Zwach, C. (2001). Biodegradation of oil in uplifted basins prevented by deep-burial sterilization. Nature, 411(6841), 1034. doi:10.1038/35082535

Worsley, D. (2008). The post-Caledonian development of Svalbard and the western Barents Sea. Polar Research, 27(3), 298-317. doi:10.1111/j.1751-8369.2008.00085.x

Yeseul, K. (2018). Numerical analysis of sedimentary compaction. 지질학회지, 54(6), 631-640. doi:10.14770/jgsk.2018.54.6.631

9 Appendices

9.1 Appendix 1 – Seismic velocities

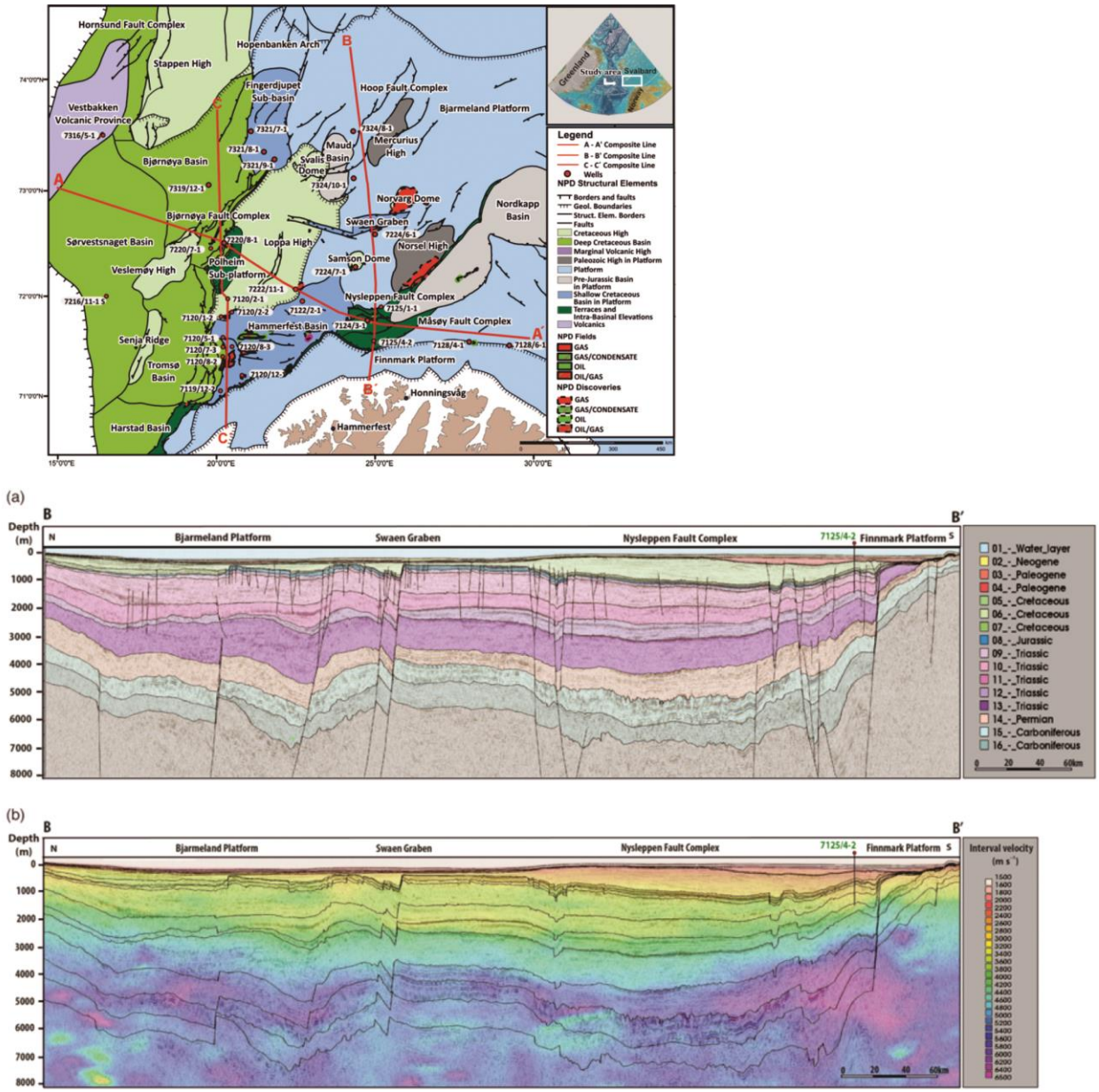

Figure 9.1: Seismic velocities of the Bjarmeland Platform from Ktenas et al. (2018)

9.2 Appendix 2 – Figures and seismic lines

Table 9.1: Name of the seismic lines used in this study.

Figure	Name of seismic line
4.4A	SS1302-126
4.4B	SS1302-035
4.50	NBR14-362688
5.2	NBR14-362688 & NBR14-145076
5.3	NBR14-145076
5.4	NBR14-362688
5.5	NBR14-266837
5.17a	TGS15002-HR15-2D-BS05-FINAL-MIG
5.17b	NBR14-266837
5.17c	NBR14-362688
5.18	NBR14-148000
5.19	NBR14-145787
5.20	NBR14-266837
5.21	NBR14-266837
5.22	NBR14-145787
5.23	TGS15002-HR15-2D-BS05-FINAL-MIG
5.24	TGS15002-HR15-2D-BS05-FINAL-MIG
5.25	NBR14-362688
5.27	NBR14-147482
5.28	NBR14-362688
5.29	NBR14-266837
5.30	NBR14-361497
5.31	SS1302-110-1
5.32	SS1301-055
5.33	NBR14-145787
5.34	NBR14-265769